Capsules with submicron shells: production, stability, and leakage behavior

THÈSE N^{O} 9075 (2018)

PRÉSENTÉE LE 17 DÉCEMBRE 2018

À LA FACULTÉ DES SCIENCES ET TECHNIQUES DE L'INGÉNIEUR

LABORATOIRE DE LA MATIÈRE MOLLE

PROGRAMME DOCTORAL EN SCIENCE ET GÉNIE DES MATÉRIAUX

ÉCOLE POLYTECHNIQUE FÉDÉRALE DE LAUSANNE

POUR L'OBTENTION DU GRADE DE DOCTEUR ÈS SCIENCES

PAR

Antoine Claude Jean VIAN

acceptée sur proposition du jury:

Prof. A. Fontcuberta i Morral, présidente du jury
Prof. E. Amstad, directrice de thèse
Prof. P. Garsteki, rapporteur
Prof. P. Fischer, rapporteur
Prof. F. Gallaire, rapporteur

ÉCOLE POLYTECHNIQUE
FÉDÉRALE DE LAUSANNE
Suisse
2018

" On peut rater une expérience mille fois
On peut rater mille expériences une fois
Mais on ne peut pas rater mille expériences mille fois"

***Adapted from* La cité de la peur**
Les nuls

Acknowledgements

I want to thank everyone that helped in the achievement of this PhD thesis, the list is long and probably incomplete :

- Of course I want to start with Esther. when we started we were only two PhDs, and seeing the lab growing more and more warm my heart. Esther was always here when needed, she was very reactive and helped a lot. She pushed me and drove me to get better every time. She is an amazing supervisor and I am proud to be the first PhD to graduate from this lab.

- Thanks to the member of the jury and the thesis committee for the stimulating discussions and their nice feedbacks.

- Gianluca and I were the first PhD in the lab. When we arrived the lab was practically empty, it took some time to have everything functional but it was a thrilling and rewarding experience and I am glad that we could do it together. Thanks for your friendship and all the discussion scientific or not that we had.

- I also want to thank Mathias, Huachuan, Jui-Chia, Johan, Bjoern, Michael, Alvaro, Aysu, Armend, Amin and all the member of the lab for their help and support. Especially to Mathias and Du for their help in sample imaging with SEM and TEM. Going to work in the lab everyday with smile is not given to everyone and that is thanks to you guys. You made the atmosphere in this lab so special and so pleasant, I have no doubt it will continue long after I am gone.

- All the master students I supervised, especially Raphaelle, Baptiste and Valentine.

- A special thank to Mercedes our secretary not only for help with administrative formalities but also for her naturally positive and cheerful attitude. All the MX staff, Chrystelle, Samia, ...

- Thanks to all the collaborators: Francois for your support and help, Omar, Pelin and Tung.

- Warm thanks to the entire IMX community and EPFL university.

- I adress special thanks to my family for their presence and their help. I want especially to thank my brother Sebastien which discussion was central for the development of a Matlab code to monitor the permeability of the capsules.

- Finally I cannot thank enough my wife Marie who was always there for me throughout this PhD. Her support and attentions made this thesis possible and there is a lot of her personal touch in this manuscript.

ABSTRACT

Capsules are often employed to prolong the shelf-life of active ingredients such as many drugs, food additives, or cosmetic substances because they delay their oxidation or prevent interactions with molecules contained in the surrounding. If designed properly, these capsules allow close control over the timing and location of the release of active ingredients. To take advantage of these features, capsules must possess shells whose thickness and composition are well-defined. A promising route to fabricate such capsules is the use of microfluidic devices to produce double emulsion drops that are used as templates to form the capsules. Additionnally, those double emulsions are also used as vehicles for active materials. However, current microfluidic techniques typically produce double emulsions with inhomogeneous shells, thereby negatively affecting the release kinetics of the encapsulants. A solution to this problem is to produce double emulsions with extremely thin shells to reduce their inhomogeneity. However a controllable production remains a challenge. This manuscript provides a novel strategy to controllably produce double emulsions that can be used as template to form capsules with submicron shell thicknesses.

We introduce new microfluidics techniques to controllably reduce the shell thickness of double emulsions to values below a micrometer. We present a simple process that squeezes primary double emulsions through a constriction, thereby removing the vast majority of the oil initially contained in the shell. This technique allows the controllable production of double emulsions with shells as thin as 330 nm. To increase the throughput of the production of double emulsions with thin shells, we developed a second microfluidic device, the aspiration device. We show that we can produce shell thicknesses down to 240 nm with a 10 times higher throughput than obtained with the squeezing process. We also demonstrate that the resulting double emulsion shell thickness only depends on the fluid flow rates but not on the shell thickness of injected primary double emulsions such that this device enables processing polydisperse double emulsion drops into double emulsions with well defined thin shells. We characterize the permeability of double emulsions drops and show that the release rate of encapsulants decreases with decreasing shell thickness We demonstrate that the permeability of drops with submicron shells is decreased by at least one order of magnitude compared to that of primary double emulsions. Thus these thin shell double emulsions open up new opportunities to use them for high throughput screening assays that require a high precision. Finally we convert double emulsions into capsules with thin homogeneous solid shells and show that they display a low permeability and a high mechanical stability.

Keywords: *microcapsules, microfluidics, double emulsions, thin shells, submicrometer shells, triggered release, capsule permeability.*

RÉSUMÉ

En général, les capsules sont employées pour prolonger la durée de vie des substances actives utilisées dans les produits pharmaceutiques, agroalimentaires et cosmétiques, car elle retardent leur oxydation ou empéchent les interactions avec d'autres molécules externes. Si ces capsules sont conçues de manière appropriées, elle peuvent également permettre de contrôler le temps et le lieu de libération des substances actives. Pour profiter de ces propriétés, l'épaisseur et la composition de leurs membrane doit ître trés finement contrôlée. L'utilisation de double émulsions produite gâce à la microfluidique est une technique prometteuse pour former ce type de capsule. De plus ces double émulsions sont capables également de transporter des substances actives. Cependant les techniques actuelles de microfluidique ne permettent que de fabriquer des gouttes en double émulsion avec des membranes d'épaisseur inhomogènes, ce qui affecte la cinétique de libération des substances de la capsule. Une solution serait de produire des double émulsions avec des membranes de très fine épaisseur pour réduire leur inhomogénéité. Cependant la production controllée de ce type de double émulsions reste un défi. Ce travail de thèse présente une nouvelle stratégie pour produire des doubles émulsions qui peuvent être utilisées pour former des capsules dont la membrane est inférieure à un micron d'épaisseur.

Dans ce manuscrit nous introduisons de nouvelles technique de microfluidique pour controller l'épaisseur de la membrane. La première technique consiste à forcer les double émulsions à franchir une constriction, ce processus permet d' élimine une grande partie de l'huile contenue initialement dans la membrane et par conséquent réduit l'épaisseur de cette dernière. Grâce à cette technique nous pouvons obtenir de manière reproductible des gouttes avec des membranes de 330 nm d'épaisseur. Afin d'augmenter le débit de production des double émulsions avec des fines membranes, nous avons développé une nouvelle puce microfluidique. Nous démontrons que cette puce nous permet d'obtenir des gouttes dont l'épaisseur de la membrane est inférieure à 240 nm et d'augmenter d'un facteur 10 le débit par rapport au processus de constriction. De plus, nous établissons que l'épaisseur finale de la membrane ne dépend que du débit des fluides injectés dand la puce mais est indépendante de l'épaisseur initiale de la membrane des double émulsion initialement injectées. Ainsi cette puce peut traiter des double émulsions dépaisseur de membrane différente et les transformer en double émulsions d'épaisseur contrôlée et très fine. Nous caractérisóns la perméabilité des double émulsions et montróns que le vitesse de libération des encapsulants diminue avec la finesse de la membrane. Par conséquent, ces double émulsion avec des membranes très fines ouvrent de nouvelles perspectives d'applications dans les tests de tri à haut débit qui demandent une grande précision. Enfin nous utilisons ces doubles émulsions pour former des capsules avec une fine membrane solide qui présentent une faible perméabilité et une grande stabilité mécanique.

Mots-clés: *microcapsules, microfluidique, double émulsions, fine membrane, membrane sub-micrométriques, libération contrôlée, perméabilité des capsules.*

FOREWORD

This project is devoted to the formation of mechanically stable capsules with thin shells using double emulsions as template. In particular, we focus on the formation of double emulsions with submicron shells using microfluidics. This manuscript presents the work that was done in the scope of this thesis and is divided in 6 chapters:

- **Chapter 1** is a general introduction that sets the framework of this thesis: we first describe the fundamentals of emulsions and their stabilization. We introduce microfluidics as a powerful tool to precisely control the dimensions of emulsion drops. We summarize methods to convert double emulsion drops into capsules and how the permeability of these capsules can be tuned. Finally we point towards the problematic of heterogeneity of double emulsions shell thicknesses and mention possibilities to overcome these difficulties.

- The experimental techniques used in this project can be found in **Chapter 2**. In particular we present the microfluidic double emulsion device, that is used to produce primary double emulsion drops.

- A first approach to form double emulsions with submicron thick shells is presented in **Chapter 3**. Primary double emulsion drops are squeezed through a constriction to remove the oil from its shell. This chapter is an adaptation of the previously published paper presented in Reference [1].

- To increase the throughput of the production of double emulsions with thin shells, we introduce in **Chapter 4** a new microfluidic device, the aspiration device. The device consists of a main channel that is intersected by many microchannels that aspirate the oil from the shell of the double emulsion drops. This chapter is an adaptation of the previously published paper presented in Reference [2].

- **Chapter 5** focuses on the influence of the shell thickness of double emulsions on their permeability. We show that the permeability of double emulsions can be decreased by at least an order of magnitude if the shell thickness is reduced to values below 1 μm. This chapter is adapted from the currently under review paper presented in Reference [3].

- In **Chapter 6** we employ double emulsion drops with thin shells to produce rigid mechanically stable capsules that have a very low footprint. Furthermore we show that the permeability of those capsules is similar to those of model capsules with a much higher footprint. This chapter is adapted from the paper currently in refereed proceedings presented in Reference [4].

Contents

1 Emulsions as template for encapsulation **2**

1.1 Emulsions: Basic concepts . . . 3

1.1.1 Type of emulsions . . . 3

1.1.2 Stabilization of emulsions . . . 4

1.2 Drops as templates to produce capsules . . . 6

1.2.1 Microcapsules from single emulsion templates . . . 6

1.2.2 Microcapsules made from double emulsion templates . . . 6

1.2.3 Release mechanisms . . . 7

1.2.4 Controlling release kinetics . . . 11

1.3 Microfluidics . . . 12

1.3.1 Fluid behavior at microscale . . . 12

1.3.2 Electric circuit analogy . . . 13

1.3.3 Drop-based microfluidics . . . 14

1.3.4 Device fabrication . . . 16

1.3.5 Production of double emulsions with microfluidics . . . 17

1.3.6 Characterization of double emulsion drops . . . 19

1.3.7 Submicron shell double emulsion drops . . . 21

2 Material and methods **24**

2.1 Surfactant . . . 25

2.2 Double emulsion device fabrication . . . 25

2.3 Surface treatment of double emulsion device . . . 26

2.4 Composition of W/O/W double emulsions . . . 26

2.5 Quantification of the shell thickness and measurement accuracy . . . 27

2.6 Accuracy of the drop radius measurement . . . 28

2.7 Accuracy of the shell thickness measurement . . . 29

2.8 Viscosity measurments . . . 30

3 Reduction of shell thickness of double emulsions using microfluidics **32**

3.1 Abstract . . . 33

3.2 Introduction . . . 34

3.3 Materials and methods . . . 35
3.3.1 Device fabrication and dimensions . . . 35
3.3.2 Operation of the squeezing device and drop collection . . . 35
3.3.3 Energy required to separate a double emulsion drop into two drops . . . 36
3.4 Results and discussion . . . 37
3.4.1 Device operation . . . 37
3.4.2 Interfacial energy associated with drop splitting . . . 38
3.4.3 Minimal velocity required to split a drop . . . 41
3.4.4 Efficiency of the removal as a function of the velocity in the constriction . 42
3.4.5 Influence of the constriction geometry . . . 44
3.4.6 Influence of the shell of primary double emulsions . . . 46
3.5 Conclusions . . . 47

4 Scalable production of double emulsion drops with thin shells 48
4.1 Abstract . . . 49
4.2 Introduction . . . 49
4.3 Material and methods . . . 51
4.3.1 Device fabrication . . . 51
4.3.2 Quantification of drop velocity in the main channel . . . 51
4.3.3 Modelling . . . 52
4.4 Results and discussions . . . 55
4.4.1 Operation of the aspiration device . . . 55
4.4.2 Influence of fluids flow rate on device operation . . . 57
4.4.3 Influence of the number of microchannels on removal efficiency . . . 63
4.4.4 Influence of primary double emulsions shell thicknesses . . . 64
4.4.5 Influence of the oil phase . . . 65
4.5 Conclusion . . . 67

5 Submicron shell double emulsion drops for screening assays 68
5.1 Abstract . . . 69
5.2 Introduction . . . 69
5.3 Material and methods . . . 70
5.3.1 Production of double emulsions . . . 70
5.3.2 Production of submicron shell double emulsions . . . 70
5.3.3 Leakage measurements . . . 71
5.3.4 Custom made MATLAB image analysis . . . 71
5.4 Results . . . 72
5.5 Discussion . . . 75
5.6 Conclusion . . . 76

6 Mechano-responsive microcapsules with thin, homogeneous shells 78
6.1 Abstract . . . 79
6.2 Introduction . . . 80
6.3 Materials and methods . . . 81
6.3.1 Double emulsion composition . . . 81
6.3.2 Microcapsule fabrication . . . 82
6.3.3 Imaging . . . 82
6.3.4 Quantification of capsule footprint . . . 82
6.3.5 Quantification of the permeability of capsules . . . 82
6.3.6 Calculation of cumulative leakage . . . 83
6.4 Results and discussions . . . 83
6.4.1 Production of capsules with thin shells . . . 83
6.4.2 Mechanical stability of capsules . . . 87
6.4.3 Permeability of capsules . . . 90
6.5 Conclusions . . . 92

7 Conclusion and Outlook 94

Appendices 98

A Force-responsive polymersomes inspired by the marine bioluminescence of dinoflagellates 99

B Abbreviations 101

C Notations 103

D Curriculum Vitae 105

List of figures 108

Bibliography 109

Chapter 1

Emulsions as template for encapsulation

In this chapter, fundamental principles of emulsions are described. Moreover, techniques to use emulsion drops as templates for capsule production and a discussion about the latest capsules enabling controlled release of reagents are presented. Additionnally, microfluidic techniques are introduced as powerful tools to produce drops with controllable dimensions.

Contents

1.1 Emulsions: Basic concepts 3
1.1.1 Type of emulsions 3
1.1.2 Stabilization of emulsions 4
1.2 Drops as templates to produce capsules 6
1.2.1 Microcapsules from single emulsion templates 6
1.2.2 Microcapsules made from double emulsion templates 6
1.2.3 Release mechanisms 7
1.2.4 Controlling release kinetics 11
1.3 Microfluidics 12
1.3.1 Fluid behavior at microscale 12
1.3.2 Electric circuit analogy 13
1.3.3 Drop-based microfluidics 14
1.3.4 Device fabrication 16
1.3.5 Production of double emulsions with microfluidics 17
1.3.6 Characterization of double emulsion drops 19
1.3.7 Submicron shell double emulsion drops 21

1.1 Emulsions: Basic concepts

1.1.1 Type of emulsions

An emulsion is a dispersion made out of two or more immiscible liquids. In a two-phase emulsion (*i.e.* single emulsion), drops composed of one liquid are dispersed in another liquid, the continuous phase. For example, single emulsions can consist of water-in-oil (W/O), or oil-in-water (O/W) drops, as schematically presented in Figure 1.1A and B.

Additionally emulsion droplets can also themselves embed other emulsion droplets and are thus known as multiple emulsions. For example, water-in-oil-in-water (W/O/W) double emulsion drops are composed of an inner aqueous drop embedded in another larger oil drop that is itself dispersed in a continuous aqueous phase, as seen in Figure 1.1C. These multiple emulsions are usually obtained through a two step emulsification process in which a primary emulsion is re-dispersed in an external phase.

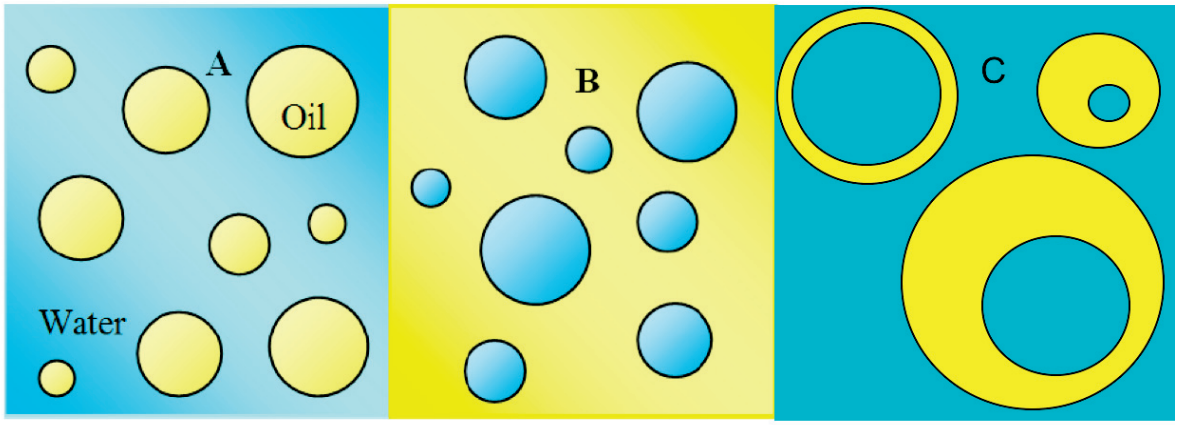

Figure 1.1: Schematic illustration of (**A**) oil-in-water (O/W) emulsions, (**B**) water-in-oil (W/O) emulsions. Illustration adapted from [5] (**C**) Illustration of water-in-oil-in-water (W/O/W) double emulsion drops

1.1.2 Stabilization of emulsions

From a thermodynamic point of view, most emulsions are systems that are out of equilibrium because the formation of drops and thus the formation of new interface costs energy. Indeed in a liquid phase, molecules are interacting with their neighbors. When all the molecules are identical, these interactions are balanced. At an interface of a droplet, the molecules of the dispersed phase are in contact with molecules from the continuous phase and consequently, their interactions are not optimized to minimize their energy. It results in a surface energy or surface tension, γ, which expresses the energy cost of a particular interface. When an emulsion is created from two separate phases, this cost is payed by the work of a vigorous mixing of the two phase system. This mixing transfers mechanical energy to the system that can be used to generate new interfaces and thus promote droplet formation (this is what is happenning when preparing a salad dressing for example).

After an emulsion is formed, it tends to go back to its equilibrium state through coalescence of drops. Indeed when two drop merge, they reduce their surface by ΔA and therefore save interfacial energy by $\Delta G_\gamma = \gamma \Delta A$. This results in an increase of the average drop diameter and a decrease of the number of drops in the emulsion

However this evolution can be kinetically prevented by using surfactants that increase the lifetime of emulsions. Surfactants are amphiphilic molecules that preferentially arrange at the liquid-liquid interface, as exemplified in Figure 1.2A. Once adsorbed, they significantly lower the interfacial tension γ. Therefore, the energy difference between a state in which drops are separated and the one in which they are merged, ΔG_γ, is reduced, thereby increasing the kinetic stability of the emulsions. Additionally they add Marangoni stresses that help to prevent the coalescence [6].

Alternatively interfaces can also be stabilized by solid particles, resulting in pickering emulsions [7–9]. Colloidal particles that have an affinity for both phases assemble at the interphase, as schematically presented in Figure 1.2B. Therefore they reduce the interfacial surface ΔA, thereby lowering ΔG_γ, and thus stabilizing the drop [8]. However the adsorption of such particles at the interface is slower than that of surfactant molecules because their size is usually much larger. Therefore pickering emulsions are not suitable for systems that demand rapid stabilization.

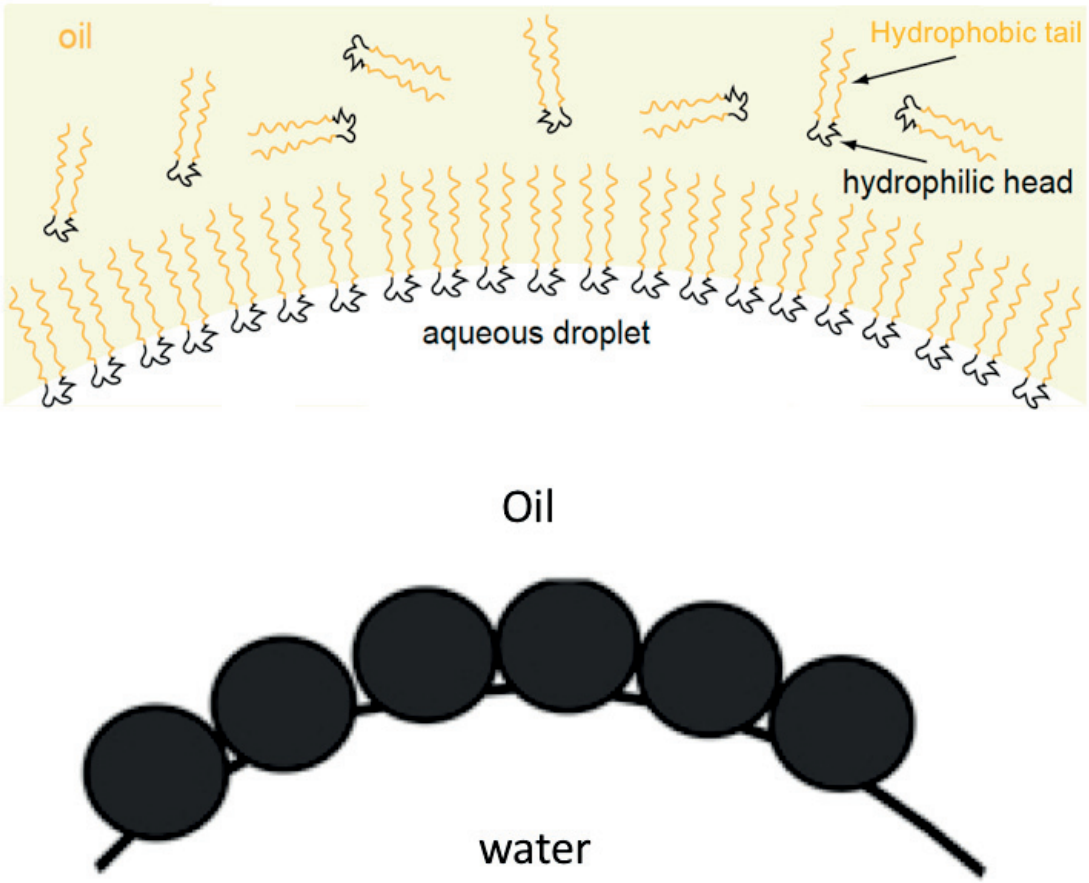

Figure 1.2: (**A**) Schematic illustration of a tri-block surfactant adsorbed at the interface of an aqueous droplet in oil. Figure adapted from [10]. (**B**) Schematic illustration of an O/W interface stabilized with nanoparticles. Figure adapted from [8]

These stabilized emulsions drops are often used as templates to form microcapsules for a wide range of applications including encapsulation of food additives [11–15], cosmetic products [16–20], drug delivery systems [21–24] or for fluorescence activated cell sorting (FACS) [25–29].

1.2 Drops as templates to produce capsules

1.2.1 Microcapsules from single emulsion templates

Microcapsules are 1-100s micrometer sized spheres with solid shells and hollow cores. They are widely used as carriers of actives substances for a large variety of applications including pharmacy [30, 31], food [32, 33], cosmetics [34], fragrances [35] and agriculture [36].

These capsules can be produced from single emulsion drops if one of the reagents used for solidification is soluble in both phases. In this configuration, one of the reagents diffuses from one phase into the other phase. For example, capsules are produced from an aqueous drop containing alginate in the core and CaI_2 in the oil phase. Ca^{2+} ions penetrate into the aqueous core of a drop, thereby preferentially crosslinking alginate located in the vicinity of the drop interface as schematically shown in Figure 1.3A. As more and more calcium ions diffuse further into the drop, the shell thickness of the forming capsule increases. To stop the gelation process the drop is then redispersed in a Ca^{2+}-free continuous phase, resulting in a capsule with an alginate based shell and liquid core [37], as shown in Figure 1.3B and C.

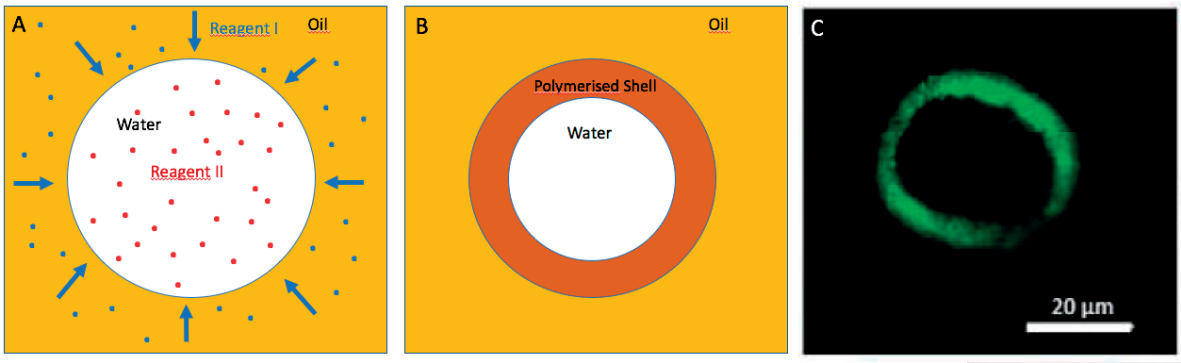

Figure 1.3: Formation of a capsule from a single emulsion water in oil drop. (**A**) Schematic representation of a reagent loaded into the aqueous core. (**B**) Schematic presentation of the formed capsule. (**C**) Fluorescent micrographs of capsules whose shell is composed of ionically crosslinked alginate (adapted from [37]).

However this process limits the number of capsule materials that can be used because one of the components needs to be soluble in both phases. Therefore, alternative techniques to form capsules that offer more choice in the composition of the shell are usually preferred.

1.2.2 Microcapsules made from double emulsion templates

Double emulsion drops are attractive templates to produce capsules made from a wide range of materials. They are drops composed of one phase within drops composed of another phase and their stability is directly correlated to the interfacial tensions between the different phases [38].

These drops are often used as templates to form capsules through solidification of their shells [39]. This can be achieved, for example, through solvent evaporation [40–42] or polymerization [43–45].

If solidified through evaporation of the solvent, the middle fluid consists of a volatile solvent that has some solubility in the continuous phase. This fluid encompasses polymers or colloids that form the shell upon solvent evaporation. As the solvent partitions into the outer phase, the solutes precipitate in the shell of the double emulsion drop. The solvent can either completely partition into the continuous phase or if it is composed of a mixture of different solvents, one of the solvent partitions whereas the other solvent dewets and forms a single emulsion drop that separates from the capsule [46]. Capsules with extremely thin shell thicknesses (down to the dimensions of a surfactant bilayer) can be formed with this technique [47, 48]. However the number of solvents that can be used is limited and the most commonly used ones are toxic, thereby excluding biological applications.

Capsules with a much wider range of shell compositions can be formed if they contain chemically reactive substances that can be solidified. For example, a monomer solution of ethoxylated trimethylolpropane triacrylate (ETPTA) resin and 2-hydroxy-2-methyl-1-phenyl-1-propanone that is added as a photoinitiatior is used as the middle phase of double emulsion drops. The shell can subsequently be rapidly polymerized simply through exposure to UV-light, thus transforming the shell of double emulsion drops into a solid network [49]. Therefore the dimensions of the shell of the capsules are directly related to that of the double emulsion templates.

To summarize, solvent evaporation enables the formation of capsules with extremely thin shells capsules but can only be used with a limited number of solvents that are generally toxic. The polymerization process offer more versatility in terms of shell materials and their shell size is directly related to the one of the double emulsion template. The shell composition is a key parameter to control the release of encapsulants with a trigger.

1.2.3 Release mechanisms

The composition of the shell the capsules is key to control the release of encapsulants from capsules. Multiple release triggers are available, here we present three main types: temperature, solvents and mechanical stress.

Temperature induced release

Temperature can be an interesting stimulus for applications in drug delivery for example. Polymers that remain solid at room temperature but can melt at body temperature are attractive materials to form capsules for biological applications. To fabricate the capsule, the polymer needs to be heated above its melting temperature and then be cooled down and solidified after double emulsions are produced [24, 50]. For example parrafin has a melting temperature T_m around

43 °C. A capsule with a parrafin shell can release an encapsulated dye in less than 5 min when heated above this temperature, as seen in Figure 1.4A.

Another attractive possibility to fabricate temperature responsive capsules is the use of temperature responsive polymers, such as poly[N-isopropylacrylamide] (PNIPAM). Crosslinked PNIPAM is hydrated at room temperature. If the temperature is increased above the lower critical solution temperature (LCST), which is for the PNIPAM around $T_c = 32$ °C in the absence of salts, the hydrogen bonds between the hydrophilic amine chains are broken, and the polymer undergoes a reversible phase transition into a collapsed dehydrated state [51]. This change in conformation of the polymer changes the permeability of the capsules, thereby enabling release of the encapsulant, as exemplified in Figure 1.4B. This technique is interesting since the transformation is reversible, hence the process can be used for repeated triggered release.

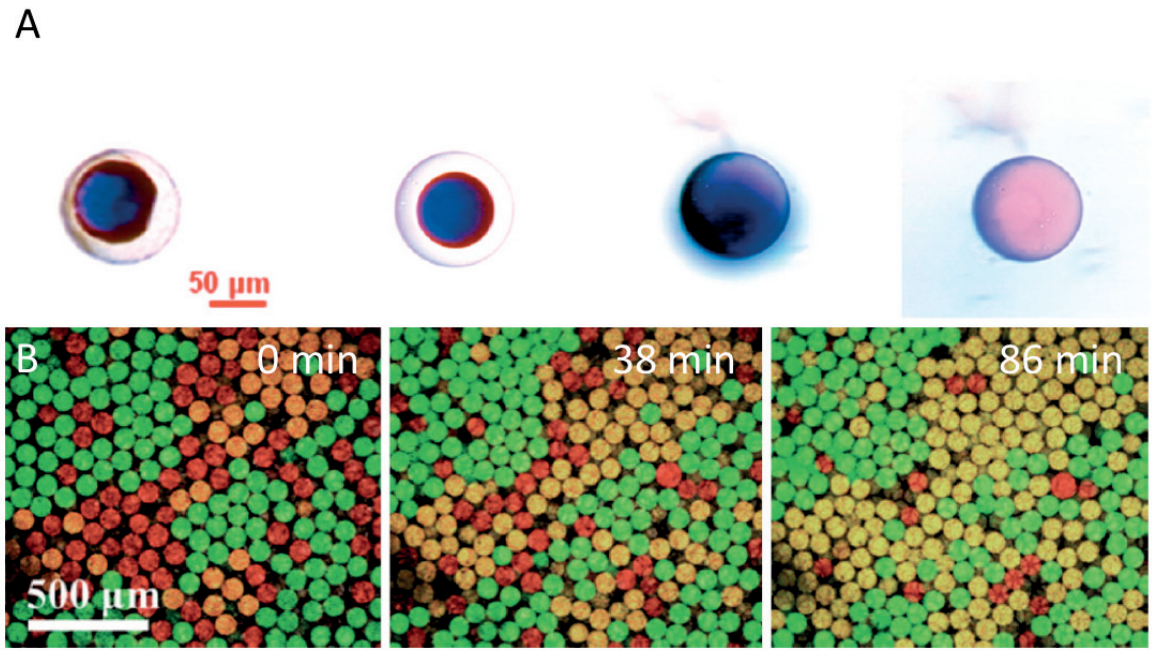

Figure 1.4: Temperature induced release. (**A**) Microcapsules composed of paraffin shells encapsulating toluidine blue. The shell becomes liquid when heated to 45 °C (second frame), this enables the inner core to coalesce with the outermost phase (third frame). The encapsulated dye is almost entirely released after five minutes of heating, (fourth frame). The figure is adapted from [24]. (**B**) Confocal fluorescent micrograph of a mixture of capsules incubated at 40 °C over time. Capsules in green and yellow are composed of Poly(ethylenglycol)-b-Poly(lactic acid) (PEG-b-PLA) which is insensitive to changes in temperature. Capsule in red have a PEG-b-PLA shell comprising 5 wt% of PNIPAM-b-(Poly(lactic glyco acid) (PNIPAM-b-PLGA). Only the capsules containing PNIPAM-b-PLGA in their shell release their content. The micrograph is adapted from [52]

Chemically triggered release

Another important stimulus used to trigger release are chemical reactions. For example Polystyrene (PS) goes from a solid to a liquid state once in contact with hydrocarbon oils [47]. This behavior can be exploited to produce oil-sensitive capsules. When polystyrene capsules migrate towards an oil-water interface, the portion of the capsules in contact with the oil degrades such that encapsulants are released, as seen in Figure 1.5A.

Additionally this approach can prove useful for detection of contaminants in water such as fluorides [53]. Polymers such as poly(phthaldehyde) (PPHA) were functionalized with a fluoride responsive end-cap. Upon exposure to fluoride, the bond between the polymer and the end cap is broken and the entire molecule depolymerises quickly. Hence microcapsules with 1.8 μm thick shells composed of PPHA functionalized molecules release their contents within three days when exposed to as little as 50 mM of fluoride, as shown in Figure 1.5B

A parameter that is experimentally often easy to vary is the pH, rendering it an attractive external stimulus. To render capsules pH responsive, they must be composed of or contain a pH responsive polymer. For example, capsules made of an ionic diblock copolymer of Poly(acrylic acid) and Poly(methylmetacrylate) (PAA-b-PMMA) become permeable if pH $>$ 7 because the polymer starts dissolving at this pH. Hence, when the pH is raised above this threshold, encapsulants are released in less than 15 min, as seen in Figure 1.5C. By tuning the polymer the capsule shell is made of it is possible to obtain different pH thresholds for release. These capsules are interesting for pharmaceutical applications. For example, depending on the pH in the digestive system they would release their payload to specific areas.

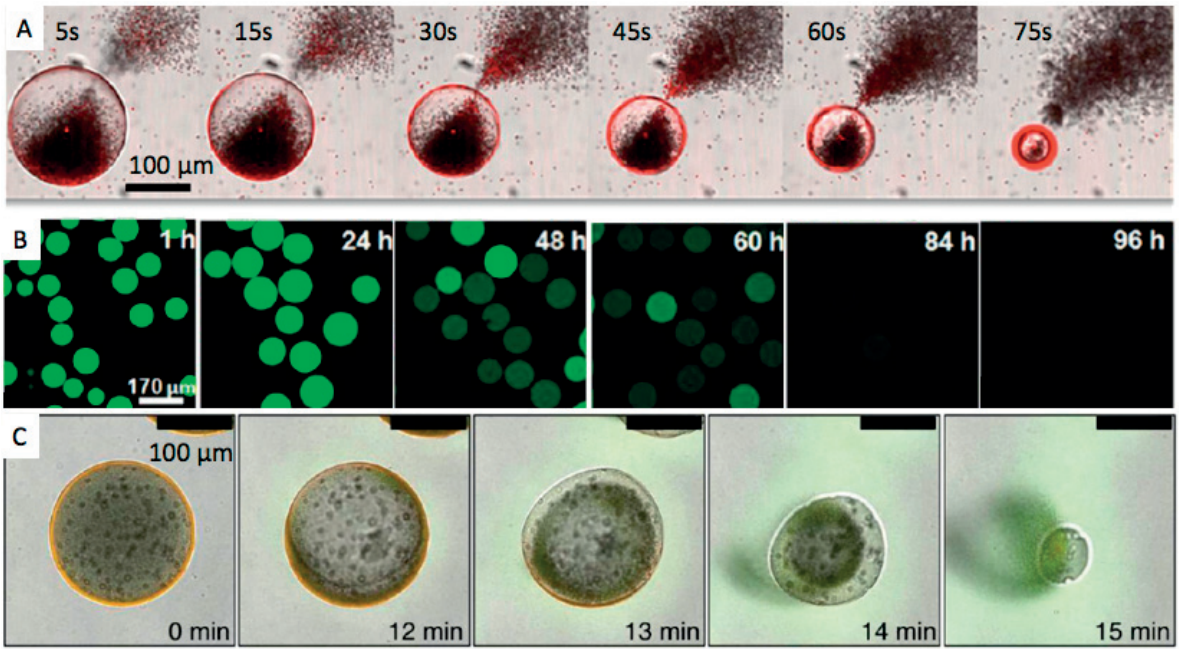

Figure 1.5: Triggered encapsulant release. (**A**) Timelapse confocal microscopy images showing the release kinetics of a PS capsule loaded with microparticles in contact with toluene. The figure is adapted from [47]. (**B**) Timelapse fluorescent micrographs of fluorescent dye release from PPHA microcapsules exposed to an aqueous solution containing 50 mM fluoride. Adapted from [53] (**C**) Timelapse confocal microscopy images showing release of a green dye encapsulated in a pH responsive PAA-b-PMMA capsule. The capsule also encapsulates polystyrene microparticles used as tracers (grey). Time 0 corresponds to the time when the pH of the surrounding solution is shifted to 9. The micrograph is adapted from [54]

Mechano-responsive capsules

Externally imposed stress is also an interesting route to controllably release payload. The earliest application of mechano-responsive capsules was in carbonless copy paper to encapsulate and release the colorless ink upon exposure to pressure. Capsules completely coat the surface of a sheet of paper, only releasing the encapsulated ink at locations that were strongly compressed by a pen [55]. The threshold pressure when capsules rupture depends in parts on the shell composition [56]. For example, PS capsules have brittle shells and hence are more prone to rupture if sheared than polystyrene-polyisoprene-polystyrene (PS-PIP-PS) microcapsules that have more ductile shells and are therefore more deformable [47]. When both types of microcapsules of diameter 110 μm are introduced in a channel with a 70 μm constriction, PS capsules rupture in the constriction whereas (PS-PIP-PS) remain intact, as seen in Figures 1.6A and B.

Shear responsive capsule are also useful for self-healing applications where they are embedded in a matrix material [57]. When the material is subjected to a stress above a threshold, capsules release the encapsulated agents that heal defects thereby strengthening the matrix. For example healing in glassy epoxy using epoxy/amine self-healing systems were developed. Microcapsules containing epoxy monomers and amine hardeners are used as self-healing agents in an epoxy

matrix. They are produced from double emulsions used as templates. Their shells contain an acrylate mixture (2-phenoxyethyl acrylate and 1,6-hexanediol diacrylate 50:50 ratio), and a photoinitiator [58]. They are subsequently cured to form the capsule shell through UV exposure for 5 min. The epoxy microcapsules contain Epon 828 in their cores. The amine microcapsules contain triethylentetramine (TETA) in their core that serves as a hardener. The capsules are embedded in a bisphenol, a diglicidyl ether resin (Epon 828), that is cured with diethylenetriamine in a 100:12 ratio. The epoxy matrix contains 10 wt% of microcapsules loaded with epoxy and 1.8 wt% of microcapsules loaded with amines. The matrix material is then cracked with a rasor blade and cured at 35°C for 48 h. The addition of amine and epoxy microcapsules enabled a 100% healing efficiency of the material tested in tension at 5 μ/s [59]. Healing efficiency is calculated as the ratio of the peak load for the healed material over that of the virgin material.

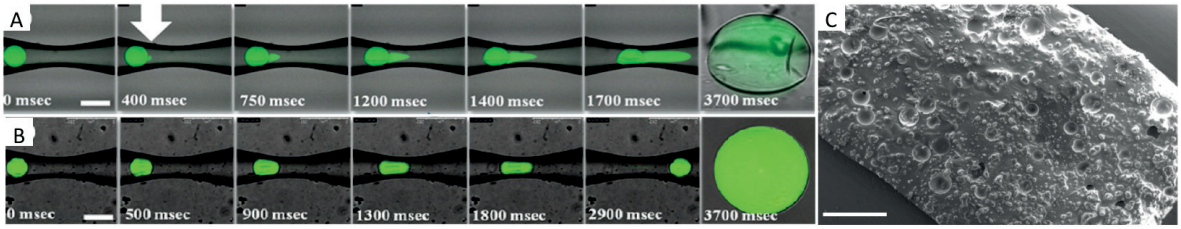

Figure 1.6: Mechano-responsive capsules. Superimposed optical and fluorescent micrographs of 110 μm diameter (**A**) PS and (**B**) PS-PIP-PS capsules that are pushed through a 70 μm diameter constriction. Micrograph adapted from [47]. (**C**) SEM image of epoxy and hardener microcapsules with polyacrylate shells embedded in an epoxy matrix. The capsules impart self-healing properties to the epoxy matrix. The image is taken from [59]. Scale bars are 100 μm.

To summarize, three main triggers that are commonly used depending on the application include: temperature, chemical, and mechanical stimuli. The kinetic of this release strongly depends on the capsule dimensions.

1.2.4 Controlling release kinetics

In the examples described in the previous Section 1.2.3, the time necessary to release content depends sensitively on the shell thickness of capsules. For example, for capsules composed of PAA-b-PMMA that are produced from evaporation of the oil shell a double emulsion template (See section 1.2.2), the release time increases with increasing shell thickness for microcapsules, as exemplified by the data shown in Figure 1.7 [54].

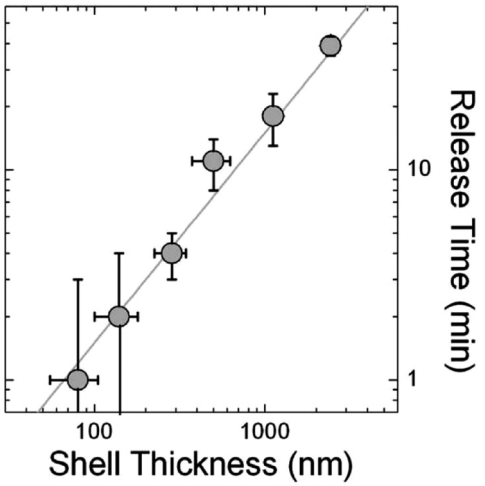

Figure 1.7: Time delay before encapsulated fluorescent dye is released as a function of the shell thickness for pH-responsive microcapsules. The vertical error bar corresponds to the standard deviation in the measured release time, horizontal deviation corresponds to the standard deviation on shell thickness in each batch. Reproduced from [54].

Therefore a close control over the dimensions of the microcapsules is crucial to precisely tune the release rate of encapsulants from the microcapsules. Capsules with well-defined shell thicknesses can be produced from monodisperse drop templates thanks to microfluidic techniques.

1.3 Microfluidics

1.3.1 Fluid behavior at microscale

Microfluidics describes the manipulation of small amounts of fluids (10^{-9} to 10^{-18} L) using channels with dimensions ranging from tens to hundreds of micrometers [60]. At this length scale, inertial forces are less important than viscous forces such that Reynolds numbers are small (Re < 1), and flows are usually laminar. Consequently, when two fluids streams come together in a microchannel, they flow parallel to each other, with minimal turbulences. This so called co-flow phenomenon can be visually observed, as shown in Figure 1.8.

Since flows are laminar, diffusion is the main mixing mechanism. This opens up new opportunities to control temporally and spatially the concentration of molecules within a microfluidic channel. Experiments conducted with microfluidic devices enable the use of smaller sample volumes and require less reagents while offering fast and accurate detection. For example, focusing of a stream of fluid with microfluidic devices was used for on-chip cytometry where cells are counted and observed individually. In this experiment, cells diluted in bulk are accelerated and focused in a narrow stream corresponding to their diameter [61].

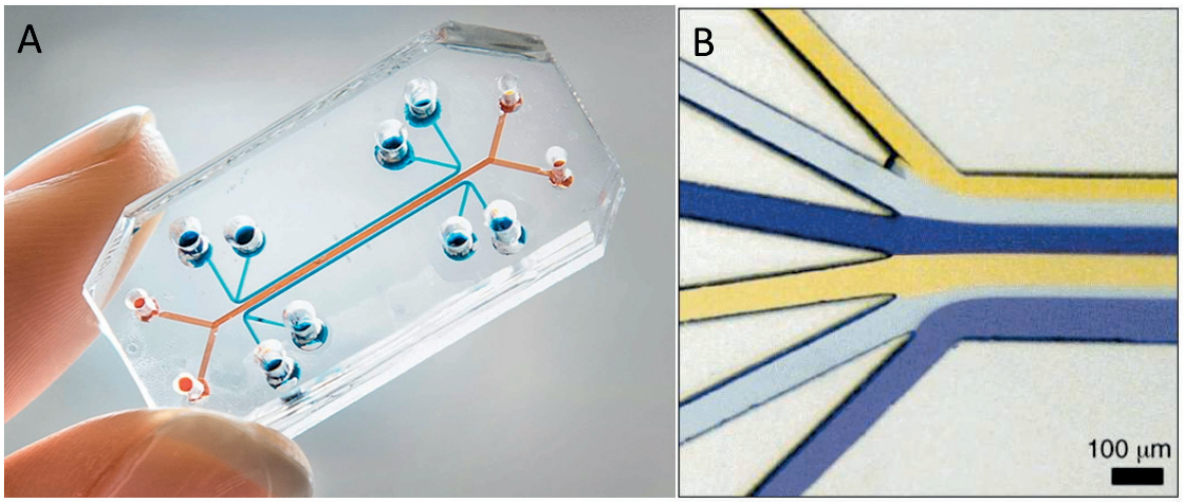

Figure 1.8: Microfluidic co-flow devices (**A**) Photograph of microfluidic device used as an intestinal organ-on-chip device. Image taken from [62] (**B**) Optical microscopy image of multiple colored streams co-flowing through a microfluidic channel. Image taken from [63]

At the scale used and because the flow is not turbulent, fluid flows can be controlled and guided precisely in microfluidic channels. The behavior of fluid flows is predictible and governed by simple equations.

1.3.2 Electric circuit analogy

In channels with stationary conditions and at low Reynolds numbers, when the flow is laminar, the Navier-Stokes equation can be simplified to link the pressure to the flow rate in the fluid. These conditions are known as Poiseuille flow conditions, in which a linear relationship between pressure drop ΔP in a channel and flow rate Q exists:

$$\Delta P = R_H Q \tag{1.1}$$

Where R_H is defined as the hydrodynamic resistance that can be calculated from the geometrical characteristics of the channel and the viscosity of the fluid [64]. For a straight channel with a rectangular cross section it corresponds to:

$$R_H = \frac{12\eta L}{1 - 0.63(h/w)} \frac{1}{h^3 w} \tag{1.2}$$

here η corresponds to the dynamic viscosity of the fluid, L the length of the channel, h is the smallest dimension of the channel cross-section while w is the largest dimension.

By analogy, in electric circuits exists also a simple linear relationship between the voltage difference ΔV and intensity I , $\Delta V = RI$, here R is an electrical resistance. Both systems have linear relations, such that an analogy between the two equations can be made: R corresponds to R_H, I to Q and ΔV to ΔP. The resemblance between the two equations allowed the use

of electronic equivalent systems to calculate the fluid flows in microchannels, as exemplified in Figure 1.9 [65].

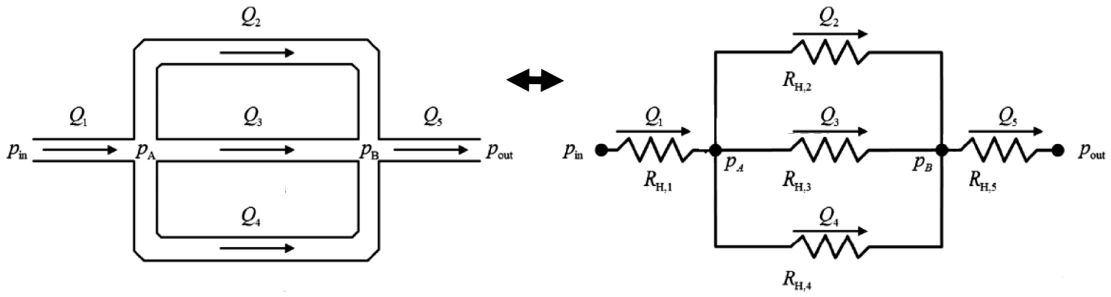

Figure 1.9: Example of electric circuit model describing the fluid flow in a simple microfluidic device with parallelized channel. Q_i corresponds to the flow rate in each channel section i. The pressure at the beginning of the channel is noted p_{in}, at node A, p_A, at node B, p_B, and p_{out} at the output. Each channel section can be characterized by its hydrodynamic resistance $R_{H,i}$ and its flow rate, Q_i. The Figure is adapted from [65].

Since the flow is laminar, a simple analogy to electric circuits helps to determine fluid flows within channels. In addition the laminar flow regime enables manipulation of multiphase flows and in particular the controlled generation of monodisperse droplets.

1.3.3 Drop-based microfluidics

This specific field of microfluidics emerged in the beginning of the new millennium and enabled the production of monodisperse droplets [66]. The main applications of drop based microfluidics are in the field of biology where they can be used as individual reactor chambers for biological materials. They are used to characterize cells on a single cell level [67, 68], for conducting directed evolution of enzymes [69, 70], single cell transcriptomics [71, 72], drug screening [73, 74], or biomarker analysis [75–77]. These platforms are convenient for a fast and cheap detection of biological reactions. In directed evolution for example, the cost of operation can be reduced from 15 millions USD to less than 4 USD while the time for one experiment can be reduced from 2 years to just 7 hours for the same screening experiment [78].

In microfluidic devices drops are formed at a junction where two immiscible fluids meet. Different junction geometries exist but the most often used ones are T-junctions and flow-focussing geometries. If larger quantities of drops must be produced, step emulsification geometries are often employed. A T-junction is the simplest geometry to form drops: the break up of a fluid stream that is injected in the junction is induced by the shearing of a second fluid that flows orthogonally to the first one, as seen in Figure 1.10A. In flow-focussing junctions, two immiscible phases are injected in a microchannel at a constant flow-rate [66]. In this configuration, a first phase is injected into the junction and sheared off from two sides by a second phase, thus forming the drops in an output channel, as seen in Figure 1.10B [79]. The size of the drops produced

with such devices depends on the dimensions of the channel and the relative flow rates used to inject the different fluids. Depending on the flow rate, two types of regimes can be obtained: dripping and jetting. In the dripping regime, drops form at the junction. By contrast, in the jetting regime, drops form downstream the junction. In this case, a jet forms that breaks drops through Rayleigh Plateau instabilities [80]. Flow rates can be adjusted using syringe or pressure driven pumps. For example drops of 100 μm diameter can be produced with a frequency up to 10 kHz [81]. Alternatively the production of drops through step emulsification reduces the dependance of the drop size on flow rates. In this configuration, a step change at the junction between the two phases is introduced, leading to the production of drops through changes in the surface curvature. Before the step, the inner phase is compressed so that the curvature in z-direction of the inner fluid is high whereas after the junction, the curvature in z-direction is smaller because the fluid is less constrained , as seen in Figure 1.10C [82]. Since the Laplace pressure is proportional to the curvature, the fluid is driven out of the nozzle by the pressure gradient. The production rate with one nozzle is around 45 Hz but these nozzles can be easily parallelized [83].

Increasing the drop production frequency necessitates to parallelize junctions. Parallelization of flow-focussing and T-junction devices is tedious because of the high dependance of the drop size on the fluid flow rates. Hence this demands a precise control over the injection rate in each paralleled nozzles, which is difficult to achieve. By contrast, in step emulsification devices the size of the drops depends mainly on the geometry of the channel. Hence the reduced dependance of the drop size on the fluid flow rates facilitates a controllable parallelization of multiple junctions [83].

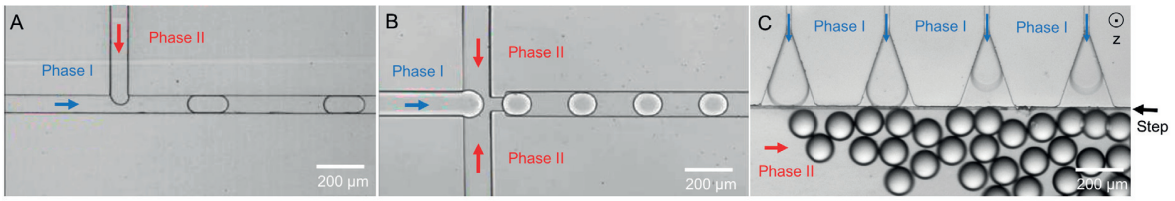

Figure 1.10: Optical microscopy images of the drop production with microfluidic devices. Drop production in a (**A**) T-junction and (**B**) in a flow focussing device. (**C**) Device with multiple stations of step emulsification drop makers.

To summarize, all devices enable the production of tens of micron sized drops with a very narrow size distribution. Flow focussing and T-junction microfluidic devices offer close control over the drop size by varying the fluid flow rates but drop production rates are limited. By contrast, step emulsification techniques enable higher drop production rates because the drop size is mainly dependant on the channel geometries. However, they offer less flexibility for the production of double emulsion drops.

1.3.4 Device fabrication

The size of the drops produced with microfluidics is strongly influenced by the channel geometry. Hence a precise control over the dimensions of microfluidic devices is necessary. Multiple techniques exist for the production of droplet microfluidic devices. In this introduction we focus on two main techniques used to fabricate the devices that are based on glass capillaries and polymer resins.

Glass is chemically inert to a large variety of solvents. Hence glass capillary microfluidics allow the production of drops made from a wider range of solvent solutions. The dimensions of the capillaries can be adjusted by heating them and pulling them controllably to the desired diameter [80]. For drop production, a tapered circular capillary is coaxially introduced from the left into a bigger square capillary. A first phase flows through the inner circular capillary, while the second phase flows in the interstice between the first capillary and the outer capillary, as shown in Figure 1.11A. When the two fluids meet, drops form in the second capillary. The size of the drops depends on the dimensions of the orifice of the first capillary and the relative fluid flow rates. The capillary technology is convenient because the devices are chemically inert such that a large variety of solvents can be processed. However, capillaries are manually aligned such that there do not exist two identical devices, hence compromising the reproducibility of experiments [84].

The production of microfluidic channels is much more reproducible if they are fabricated through soft lithography techniques [60]. Soft lithography is often used to produce poly(dimethylsiloxane) PDMS devices. The process can be divided in three main steps. The first step consists of the fabrication of a pattern containing the negative channels using photo lithography [85, 86]. A layer of photosensitive resin with the desired thickness is spin coated onto a wafer. This resin is exposed to UV through a mask to transfer the pattern from the mask onto the photoresist. The uncrosslinked resin is removed, resulting in a master composed of crosslinked resin composed of the negative channels contained on the wafer, as shown in Figure 1.11B. In a second step, PDMS is cast on the master and cured by heating at 60°C. The resulting patterned PDMS piece can be removed from the master, as shown Figure 1.11C. The PDMS piece is exposed to oxygen plasma for subsequent bonding with a glass slide or another PDMS piece. The production of PDMS devices is more reproducible because masters are employed. However, unlike glass capillaries, PDMS devices swell when put in contact with most organic solvents [87]. To overcome this limitation, it is possible to coat the surface with parylene to form a chemically inert protective layer, hence enabling the use of a wider range of solvents [88].

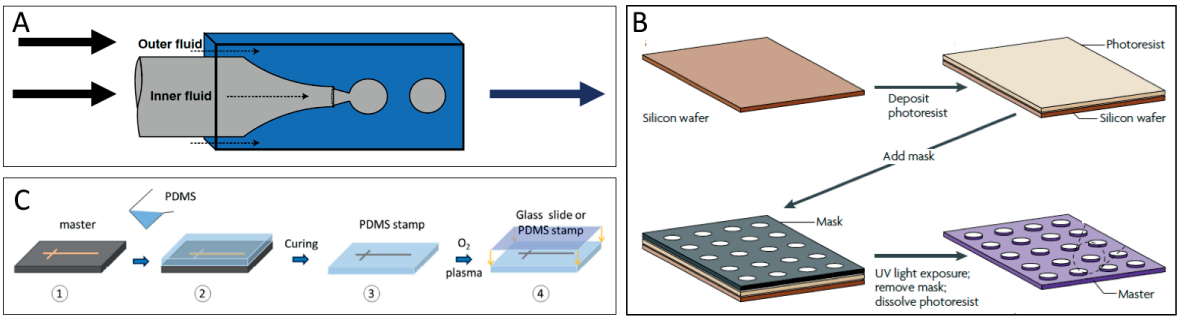

Figure 1.11: (**A**) Schematic illustration of a co-flow glass microcapillary device. Image taken from [84] (**B**) Schematic illustration of the photolitography process. Step 1: Deposition of photoresist on silicon wafer. Step 2: UV illumination through mask to transfer pattern onto the photoresist. Step 3: Removal of uncrosslinked photoresist. Adapted from [89](**B**) PDMS microfluidic devices prepared using soft lithography. Step 1: preparation of the master with photolitography. Step 2: casting of PDMS onto the master. Step 3: curing and removal of the PDMS stamp. Step 4: exposure to an oxygen plasma to bond the device to a glass slide or an another PDMS stamp.

To summarize, glass capillary devices are made of glass tubes compatible with a large variety of solvents but they only allow access to a limited number of junction geometries. By contrast, PDMS devices are more versatile in terms of geometrical shapes that can be produced but the number of solvents that can be processed is much smaller, even if a protective layer is added. Nevertheless, the PDMS device fabrication is a cheap and fast process that has become more and more accessible and is now even used in industrial applications (Capsum, Fluidigm Corporation, RainDance Technologies).

1.3.5 Production of double emulsions with microfluidics

Double emulsion drops used as templates for capsule production enable a higher versatility in terms of shell materials that can be used (see Section 1.2.2). Additionally, control over their shell thickness and therefore the kinetics of the release of encapsulants can be gained if they are produced with microfluidic devices. Glass capillary devices as well as PDMS based microfluidic devices are great tools to precisely tune the dimensions of the double emulsions [39].

For the production of double emulsions with glass capillaries, unlike in the single emulsion case (see section 1.3.4), an additional circular capillary is inserted coaxially from the right side of the square capillary. An inner aqueous phase is injected through the left cylindrical capillary. The middle oil phase is injected through the interstice between the left cylindrical smaller and larger square capillary. The outer phase is injected through the interstice between the smaller right capillary and the larger square capillary and embeds the co-flowing inner aqueous and middle oil phases, as shown in Figure 1.12A. The three fluids are then hydrodynamically focused in the right cylindrical capillary in which the co-flowing inner and middle oil phases break up to form monodisperse W/O/W double emulsions that flow through the collection capillary, as

seen in Figure 1.12F. The double emulsions formed with glass capillary devices have typically diameters ranging from 20 to 200 μm and an average shell thickness that varies from 3 to 20 μm, as demonstrated in Figure 1.12B-E [39]. The diameter can be controlled with the size of the orifice as well as with the relative flow rates of the inner phase, Q_i, middle phase, Q_m and outer phase Q_o [90]. When Q_m is decreased, the shell thickness of double emulsions also decreases proportionally [84]. However the manual alignment of the two capillaries in a larger one can prove to be a tedious task and the reproducibility of the fabrication of these devices is hence limited.

The fabrication of PDMS devices is much more reproducible because they are made from a master [91]. In one type of these devices, the inner and middle phases co-flow before they are processed into double emulsions through shearing by an outer phase, as shown in Figure 1.12G. The range of diameters and shell thicknesses of double emulsions obtained with this PDMS devices is similar to the one obtained with glass capillary devices.

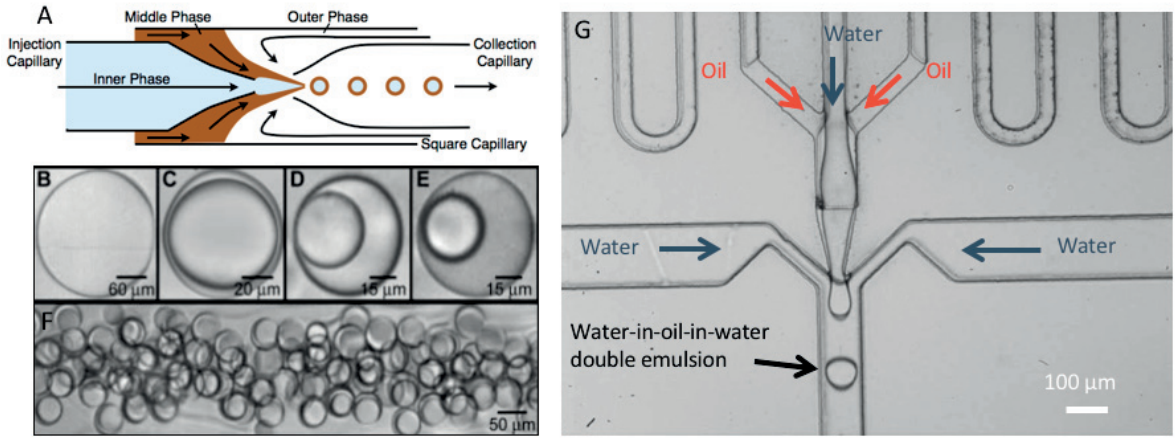

Figure 1.12: Production of double emulsions in microfluidic devices. (**A**) Schematic illlustration of a coaxial microcapillary device. The round injection and collection capillaries are coaxially aligned within a larger square capillary. The co-flowing inner and middle phases are focused within the collection capillary by the outer phase that breaks them into double emulsion drops (**B** to **E**) Double emulsion drops with shell thickness ranging from 3 to 20 μm (**F**) Double emulsion drops flowing through the collection tube. Figures are adapted from [84]. (**G**) Double emulsions produced with PDMS devices. Water and oil phases co-flow before they are broken into (W/O/W) double emulsions.

Double emulsions produced with those techniques have well-defined dimensions, hence the development of reliable techniques to characterize their shells is necessary to use them as templates for capsules.

1.3.6 Characterization of double emulsion drops

When the shell thickness of double emulsion drops is of the order of a few microns, direct measurements of the shell thickness using optical microscopy is not possible because their dimensions fall below the resolution limit of these microscopes. Two main indirect techniques can be used for the measurement of double emulsion shells: compression and rupturing.

The shell thickness can be indirectly measured through compression of the double emulsions in the vertical direction by constricting them between two microscope glass slides, thereby forcing them to expand horizontally, as illustrated in Figure 1.13A [91]. The resultant shape of the compressed emulsion is a spheroid with the same volume than non deformed double emulsion drops. By volume conservation between the two states one obtains:

$$t_s = R\Big[1 - \Big(\frac{r_c}{R_c}\Big)^{2/3}\Big] \tag{1.3}$$

where t_s is the shell thickness of the drop, R is the actual radius of the outer drop of the double emulsions, and R_c and r_c are the radius of the outer and inner drops of the double emulsions in the compressed situation, respectively, as shown in Figure 1.13B. This method can be used for double emulsion with shell thickness ranging from 2 to 10 μm.

If the shell is very thin (*e.g* less than one micron) the only remaining technique to measure the shell thickness is rupturing of the drops. When the double emulsion ruptures, it leaves behind an oil drop with the same volume as the volume of the oil contained in the shell, as seen in Figure 1.13C and D. Knowing the outer diameter of the double emulsion drop, R, and of the ruptured droplet, r, one obtains by volume conservation:

$$\frac{4}{3}\pi R^3 - \frac{4}{3}\pi(R - t_s)^3 = \frac{4}{3}\pi r^3 \tag{1.4}$$

Therefore the shell thickness can be determined using:

$$t_s = R - (R^3 - r^3)^{1/3} \tag{1.5}$$

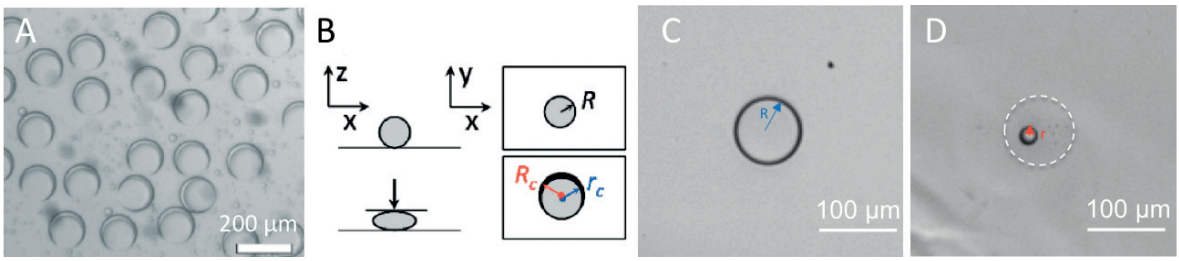

Figure 1.13: Techniques for measuring the shell thickness of double emulsions. (**A**) Optical microscopy image of double emulsion drops compressed between two glass slides. (**B**) Schematic representation of a double emulsion at rest and compressed on a xz plan (left) and on a xy plan (right). Images adapted from [91]. (**C**) Optical microscopy image of a double emulsion at rest with a radius R. (**D**) Resulting oil drop after the double emulsion drop ruptured with a radius r.

These techniques reveal an average measurement of the shell thickness from double emulsions as defined in Figure 1.14A. However most often, there is a density mismatch between the oil phase and the water phase. For example if fluorinated oils are used to form W/O/W double emulsions, the oil is denser than the two aqueous phases. Hence the lighter inner water core of the double emulsion tends to rise to the top of the outer oil drop resulting in an offset between the centers of the aqueous inner drop and the outer oil drop. Hence the oil shell is thinner on the top side and thicker at the bottom of the double emulsion drop, as schematically described in Figure 1.14B. [92, 93]. This motion of the internal aqueous drop toward the top side can destabilize the drop at the thinnest part of its shell and leads to its rupturing.

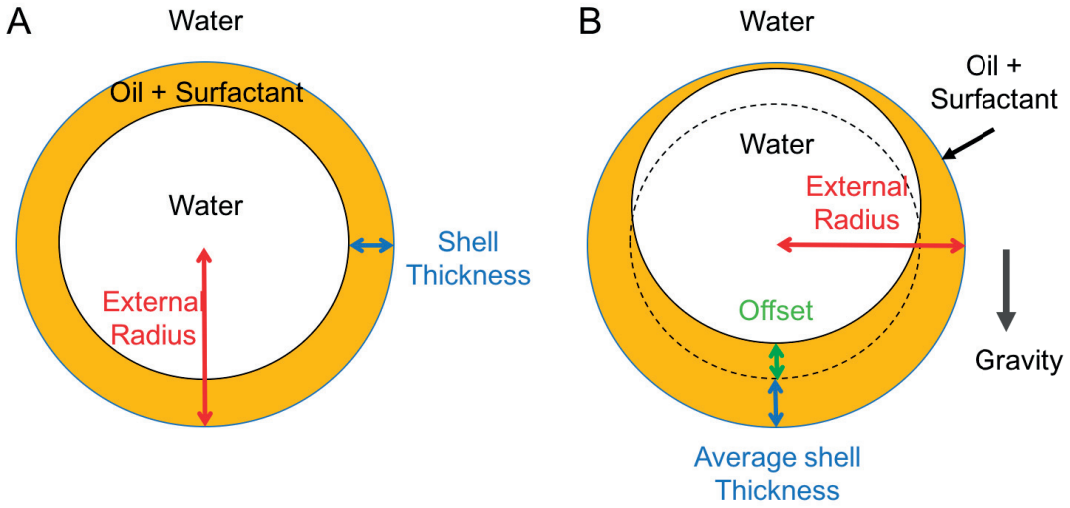

Figure 1.14: Schematic representation of inhomogeneity in the shell thicknesses of double emulsions (**A**) Illustration of a double emulsion drop with its external radius and shell thickness. (**B**) A double emulsion composed of fluids with different densities under the influence of gravity. The density difference causes an offset between the core and the outer drop.

Therefore when double emulsion drops are used as templates for capsules, most often their shell thickness is heterogeneous. This heterogeneity changes the release rate of the capsules.

1.3.7 Submicron shell double emulsion drops

The offset between the center of the inner and outer drop can destabilize a double emulsion droplet and influence the release kinetics of the capsule. A possibility to overcome this problem is to increase the confinement of the oil phase thereby increasing the viscous resistance to the movement of the smaller inner drop within the larger oil drop [94]. This so called "lubrication effect" increases the lifetime, stability, and homogeneity of double emulsion drops. Hence it is highly desirable to form double emulsion templates with an extremely thin shell, less than a micrometer thick. However, forming double emulsion drops with shell thicknesses below one micrometer is challenging and requires special microfluidics devices.

Double emulsions with submicron-sized shells can be produced with special glass capillary devices that contain three round capillaries inserted into a rectangular capillary. The left circular capillary is used to inject the middle phase while the inner aqueous phase is injected through the additional small capillary. The outer phase flows in the interstice between the left capillary and the square capillary. Drops are collected in the outer right capillary, as seen in Figure 1.15A.

Double emulsion drops are produced in two steps. In the left circular capillary, the inner aqueous phase is broken into water in oil plugs by operating the device in the dripping regime, as shown in Figure 1.15B. Those plugs are surrounded by a thin layer of oil and broken into drops by the outer aqueous phase. This two step emulsification can produce double emulsions with shell thickness as small as 800 nm [95]. However the control over the shell thickness is limited because the first and last double emulsion drops that form from each plug have thicker shells, as illustrated in Figure 1.15C. Moreover two plugs are separated by oil. When this oil reaches the 2^{nd} junction, oil in water single emulsion drops form. Additionnally the thickness of the submicron shell drops weakly depends on Q_m but rather on the thickness of the lubrication film present between the capillary and the aqueous plug that is dependent on the wettability of the glass capillary.

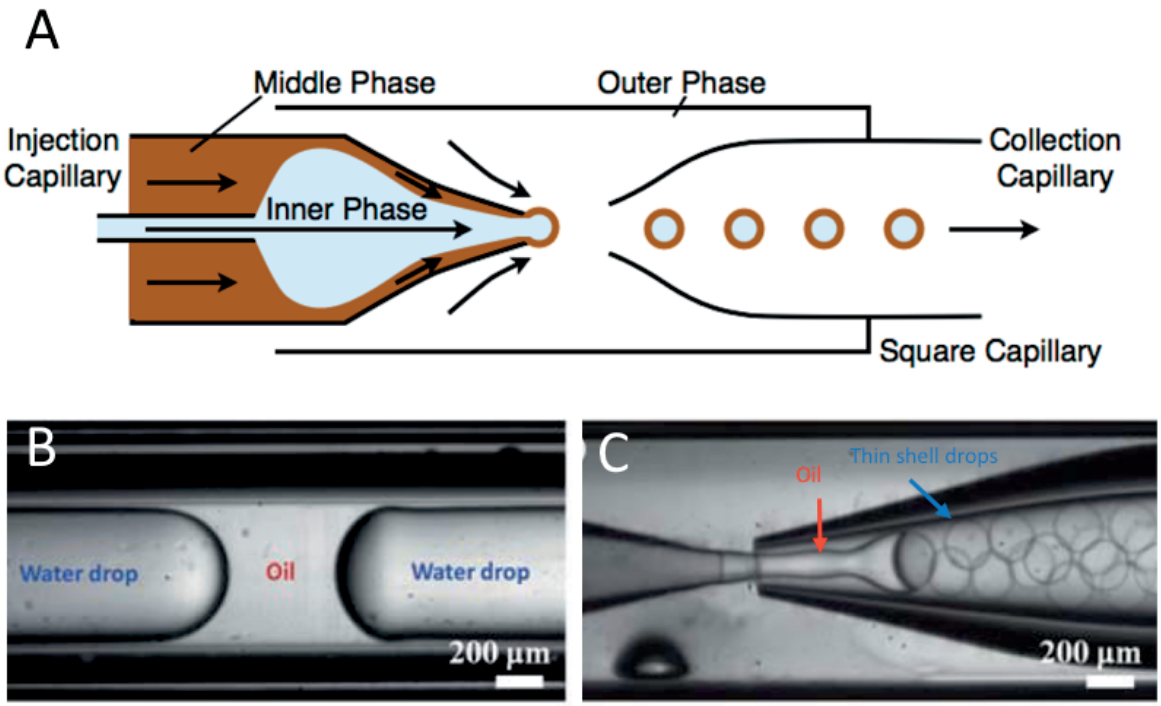

Figure 1.15: Production of double emulsions with thin shells in glass capillary devices.(**A**) Schematic illustration of the coaxial microcapillary device that enables production of double emulsions with thin shells. An inner capillary is inserted into the left capillary. The aqueous phase is injected into this capillary forming a plug in the left capillary. The middle oil phase is injected between the small capillary and the left capillary. The outer aqueous phase is injected in between the left circular capillary and the external larger square capillary. Drops are collected in the right circular capillary. (**B**) Optical microscopy image of the plug formation within the left capillary.(**C**) Optical microscopy image of the formation of double emulsions with thin shells in a microfluidic glass capillary device. One can observe the formation of a drop with a thicker shell at the end of a plug. Image are adapted from [95].

However the fabrication and operation of these glass capillary devices is complicated and thus they are rarely used. Therefore a stable, controllable production of submicron double emulsion droplets still remains a challenge to be met.

Chapter 2

Material and methods

In this chapter we detail the PDMS microfluidic device and the fluids used to form primary double emulsion drops. Moreover, we describe the methods used to characterize the double emulsion drop dimensions. We detail the resolution that is given by the experimental setup for the determination of the radius and the shell thickness. Finally we describe a way to change the middle phase viscosity of double emulsion drops without changing the interfacial tension by adding a more viscous component to the oil phase.

Contents

2.1 Surfactant 25
2.2 Double emulsion device fabrication 25
2.3 Surface treatment of double emulsion device 26
2.4 Composition of W/O/W double emulsions 26
2.5 Quantification of the shell thickness and measurement accuracy 27
2.6 Accuracy of the drop radius measurement 28
2.7 Accuracy of the shell thickness measurement 29
2.8 Viscosity measurments 30

2.1 Surfactant

Throughout this work, we stabilize water/fluorinated oil emulsions using a triblock copolymer composed of two fluorophilic Krytox^{TM} blocks interspaced by a hydrophilic PEG block. The surfactant was synthesized as described previously and is diluted in a fluorinated oil (3M^{TM} Novec^{TM} HFE7500) [96, 97]. This system is commonly used in biological applications since the fluorinated oil has remarkable properties such as high oxygen solubility [96].

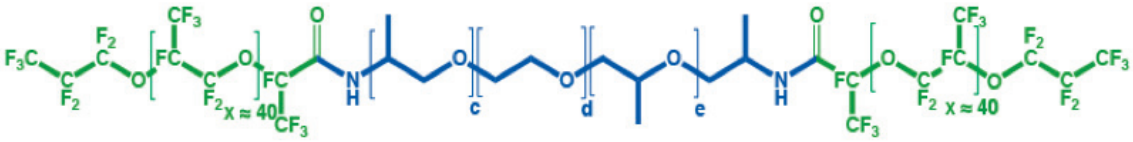

Figure 2.1: Chemical structure of the surfactant used in the experiments, in this thesis c+e = 6 and d = 12.5.

2.2 Double emulsion device fabrication

We fabricate all the microfluidic devices from PDMS (Dow Corning, USA) using soft lithography, as previously presented in Section 1.3.4 [85, 86]. W/O/W double emulsion drops with shell thicknesses ranging from 4 to 15 μm are formed using PDMS based microfluidic devices [91]. They are composed of two main junctions, in the first one the inner phase and middle phase co-flow. At the level of a second, three dimensional (3D) junction, the outer phase breaks this co-flow into double emulsion drops (see Section 1.3.5). This device is composed of 3D microchannels with variable heights, as illustrated in Figures 2.2 A and B. Besides the height, the width

of the channels vary: upstream the second junction where the drop is formed, the channel width is 20 μm, while the outlet channel is 100 μm wide. The outer phase is injected laterally with an angle of 45°.

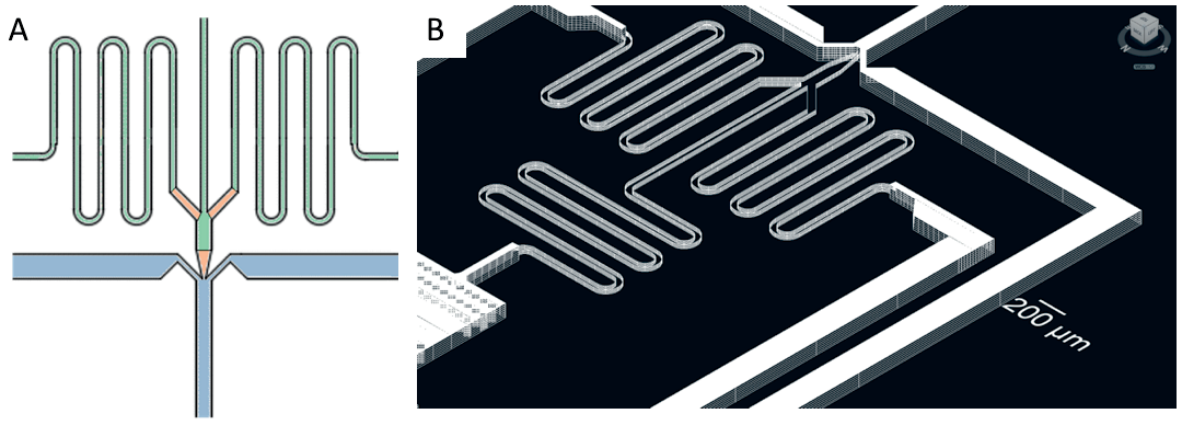

Figure 2.2: Schematic illustration of the double emulsion device. (**A**) The colors of the schematic represents the different height of the device: the green microchannels are 80 μm tall, the orange microchannels 40 μm tall and the blue microchannels 120 μm tall. (**B**) 3D representation of the device.

2.3 Surface treatment of double emulsion device

To produce double emulsions the different sections of the microfluidic device must be surface treated differently. The PDMS device was activated with 1M NaOH solution that was kept in the channels for 10 min before it was removed with compressed air. The difference in hydrodynamic resistance between the output channels and the inlet channels created by the S-shape of the inner phase and middle phase injection channels enables us to selectively only surface treat part of the device. To render the main channel downstream the 3D junction hydrophilic (blue section in Figure 2.2A), we treated it with an aqueous solution containing 2 wt% polydiallyldimethylammonium chloride (Sigma-Aldrich, USA). To render the injection channels fluorophilic (orange and green section of Figure 2.2A), we treated them with an HFE-based solution containing 2 wt% of trichloro(1H,1H,2H,2H-perfluorooctyl)silane (Sigma-Aldrich, USA). The solutions were kept in the channels for 30 min before the channels were dried with compressed air.

2.4 Composition of W/O/W double emulsions

As an innermost phase, we employ an aqueous solution containing 20 wt% PEG (Mw = 6 kDa); PEG is added to increase the viscosity of the inner phase, thereby facilitating the assembly of double emulsion drops. The middle phase is composed of a perfluorinated oil, HFE7500, containing 3 wt% of a triblock surfactant that has two perfluorinated blocks that are

separated by a PEG-based block, as presented in Section 2.1 [96, 97]. The outermost aqueous phase contains 10 wt% partially hydrolyzed poly(vinyl alcohol) (PVA) (Mw = 13-23 kDa).

2.5 Quantification of the shell thickness and measurement accuracy

We cannot quantify the shell thickness directly from optical microscopy images of double emulsions because it is at or below the resolution limit, as previously described in Section 1.3.6. To quantify the shell thickness, t_s, we measure the outer radius of the double emulsion drop, R, using optical microscopy. We subsequently rupture the drop by adding isopropanol to the outer phase and measure the radius of the resulting oil drop, r [1]. By volume conservation we obtain:

$$t_s = R - (R^3 - r^3)^{1/3} \tag{2.1}$$

Isopropanol has a limited solubility in the fluorinated oil. To test if its presence significantly influences our measurements, we quantify the shell thickness by compressing double emulsion drops with a glass slide and measuring the resulting shell thickness, by analogy to the method that has previously been employed to quantify shell thicknesses of double emulsion drops [91]. While this method works well for shell thicknesses above 1 μm, we cannot quantify shell thicknesses below this value. However, we employ this method to test the accuracy of the first method that involves the use of isopropanol on double emulsion drops with shell thicknesses well above 1 μm. To further test the accuracy of our method, we calculate the shell thickness from the measured drop generation frequency and the known fluid flow rate of the middle phase: when formed with a microfluidic double emulsion device, the amount of oil in a double emulsion drop is proportional to the flow rate of the middle phase, Q_m, divided by the frequency of formation of the drops, f. By volume conservation, we obtain

$$t_s = R - (R^3 - (\frac{Q_m}{f})^3)^{1/3} \tag{2.2}$$

here Q_m is varied from 600 μL/h to 900 μL/h. The shell thicknesses obtained with all three methods are in excellent agreement, as shown in Figure 2.3, indicating that the presence of isopropanol does not significantly influence the calculated shell thickness.

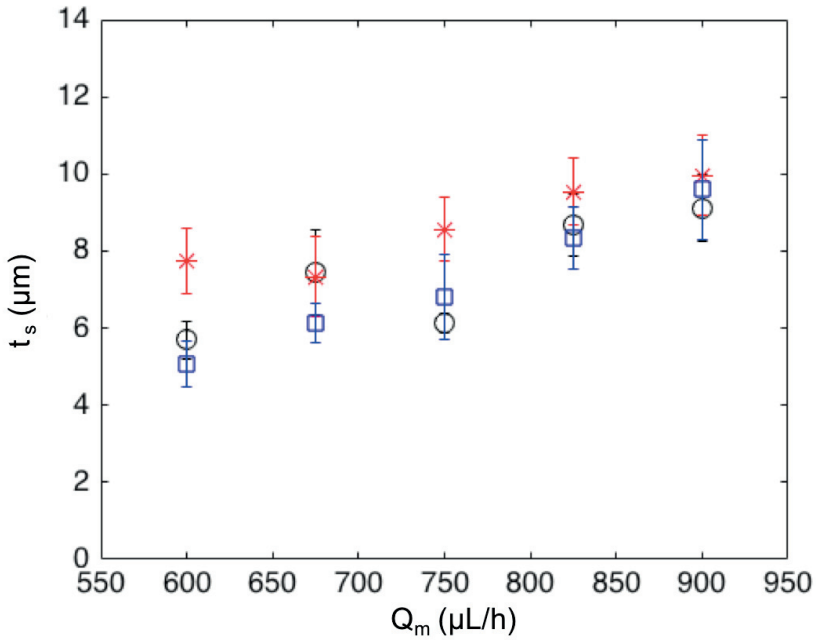

Figure 2.3: Shell thickness of double emulsion drops, t_s, as a function of the flow rate of the middle phase of the microfluidic double emulsion device, Q_m, determined using the known drop generation frequency and flow rate of the middle phase, ($\star$), compression using a glass slide ($\circ$), and using isopropanol to rupture the drops ($\square$).

Because the use of isopropanol to rupture double emulsions is the most sensitive method to determine shell thicknesses, we use this method to determine all shell thicknesses throughout this thesis.

2.6 Accuracy of the drop radius measurement

In this manuscript, all measurements of drops dimensions are repeated on at least 20 different drops to calculate standard deviations. But this experimental precision is limited by the experimental error determined by measurement tools.

To quantify the drop radius, we acquire images with pixel sizes of 0.5×0.5 μm^2 such that the resolution limit on these images is 1 μm. To increase the accuracy of our measurements, we quantify the total area, A, of the drops and obtain a measurement error of the area of $\Delta A \simeq 1$ μm^2. We calculate the upper and lower limit of the drop area, A^+, and A^-, using: $A^+ = \pi(R + \Delta R)^2$ and $A^- = \pi(R + \Delta R)^2$; here R is the mean radius (around 50 μm) and ΔR the given error of the measurement. Hence, we obtain:

$$A^+ - A^- = 2\Delta A = \pi[(R + \Delta R)^2 - (R - \Delta R)^2] \tag{2.3}$$

$$2\Delta A = \pi R^2 \left[\left(1 + \frac{\Delta R}{R} \right)^2 - \left(1 - \frac{\Delta R}{R} \right)^2 \right] \tag{2.4}$$

$$2\Delta A = \pi R^2 \left[\left(1 + 2\frac{\Delta R}{R} + \left(\frac{\Delta R}{R} \right)^2 \right) - \left(1 + 2\frac{\Delta R}{R} + \left(\frac{\Delta R}{R} \right)^2 \right) \right] \tag{2.5}$$

$$\Delta R = \frac{1}{2\pi} \left[\frac{\Delta A}{R} \right] \tag{2.6}$$

Therefore $\Delta R \simeq 0.05$ μm. Hence, using this technique, we can obtain a resolution of 0.1 μm instead of 1 μm that is achieved through a direct quantification from optical micrographs.

2.7 Accuracy of the shell thickness measurement

Using optical microscopy images and volume conservation, we determine the shell thickness, t_s, as detailed in Section 1.3.6 using:

$$t_s = R - (R^3 - r^3)^{1/3} \tag{2.7}$$

The largest error in quantifying t_s comes from the measurement of R. To determine this error, we quantify an upper and lower limit for the shell thickness t_s^+ and t_s^-, by adding and subtracting the measurement error of R, ΔR:

$$t_s^+ = R + \Delta R - [R + \Delta R)^3 - r^3]^{1/3} \tag{2.8}$$

$$t_s^- = R - \Delta R - [(R - \Delta R)^3 - r^3]^{1/3} \tag{2.9}$$

Hence the maximum error on the measurement for the shell thickness is determined by:

$$\Delta t_s = t_s^+ - t_s^- = 2\Delta R - [(R + \Delta R)^3 - r^3]^{1/3} - [(R - \Delta R)^3 - r^3]^{1/3} \tag{2.10}$$

$$\Delta t_s = 2\Delta R - R \left\{ \left[\left(1 + \frac{\Delta R}{R} \right)^3 - \left(\frac{r}{R} \right)^3 \right]^{1/3} - \left[\left(1 - \frac{\Delta R}{R} \right)^3 - \left(\frac{r}{R} \right)^3 \right]^{1/3} \right\} \tag{2.11}$$

$$\begin{aligned} \Delta t_s = 2\Delta R - R \Bigg\{ & \left[1 + 3\frac{\Delta R}{R} + 3\left(\frac{\Delta R}{R} \right)^2 + \left(\frac{\Delta R}{R} \right)^3 - \left(\frac{r}{R} \right)^3 \right]^{1/3} \\ & - \left[1 - 3\frac{\Delta R}{R} + 3\left(\frac{\Delta R}{R} \right)^2 - \left(\frac{\Delta R}{R} \right)^3 - \left(\frac{r}{R} \right)^3 \right]^{1/3} \Bigg\} \end{aligned} \tag{2.12}$$

If we consider $\frac{\Delta R}{R} << 1$ and $(\frac{r}{R})^3 << 1$ we can adapt the formula:

$$\Delta t_s = 2\Delta R - R\Bigg\{\Bigg[1-\left(\frac{r}{R}\right)^3+\frac{1}{3}\Bigg(3\frac{\Delta R}{R}+3\left(\frac{\Delta R}{R}\right)^2+\left(\frac{\Delta R}{R}\right)^3\Bigg)\Bigg] \\ -\Bigg[1-\left(\frac{r}{R}\right)^3+\frac{1}{3}\Bigg(-3\frac{\Delta R}{R}+3\left(\frac{\Delta R}{R}\right)^2-\left(\frac{\Delta R}{R}\right)^3\Bigg)\Bigg]+\theta\Bigg(\left(\frac{\Delta R}{R}\right)^3\Bigg)\Bigg\} \tag{2.13}$$

$$\Delta t_s = 2\Delta R - R\Bigg\{2\frac{\Delta R}{R}+2\left(\frac{\Delta R}{R}\right)^3+\theta\Bigg(\left(\frac{\Delta R}{R}\right)^3\Bigg)\Bigg\} \tag{2.14}$$

$$\frac{\Delta t_s}{R} = -2\left(\frac{\Delta R}{R}\right)^3+\theta\Bigg(\left(\frac{\Delta R}{R}\right)^3\Bigg) \tag{2.15}$$

In our case, double emulsions with thin shells typically have dimensions of $R \simeq 50$ μm, $\Delta R \simeq 1$ μm and $r \simeq 15$ μm. Hence the assumptions $\frac{\Delta R}{R} \simeq 0.02 << 1$ and $\left(\frac{r}{R}\right)^3 \simeq 0.06 << 1$ hold and we obtain $\Delta t_s \simeq 2$ nm. The resolution can therefore be estimated to be around 10 nm which is well below the resolution limit of an optical microscope.

2.8 Viscosity measurments

To change the viscosity of the middle oil phase of double emulsions without changing the interfacial tension we add Krytox^{TM} GPL to the fluorinated oil phase. The viscosity of the oil is quantified with a DHR3 Rheometer using the coaxial cylinder geometry (TA Instrument). We vary the shear rate from 0.1 to 100 $s^{-}1$, keeping the strain constant at 1%, measurements are performed with a rheometer (TA instruments DHR3).

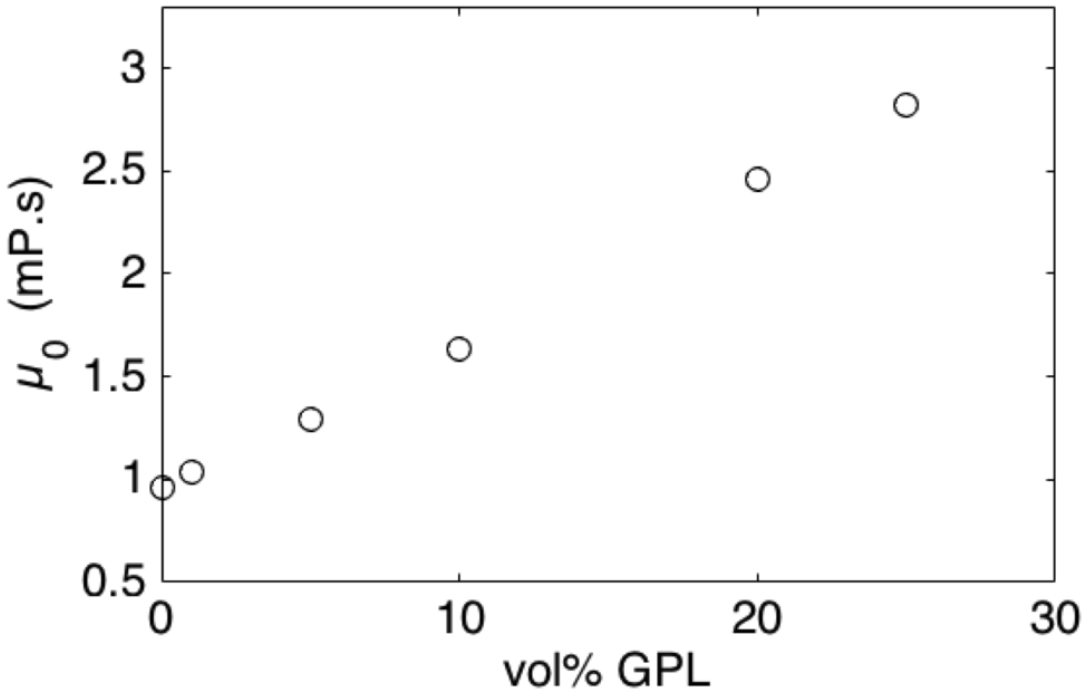

Figure 2.4: Viscosity of the middle phase, μ_0 as a function of the volume percentage of GPL added to the initial HFE7500 phase.

Chapter 3

Reduction of shell thickness of double emulsions using microfluidics

Antoine Vian, Valentine Favrod and Esther Amstad

In this chapter, a simple technique to obtain double emulsion drops with submicrometer thick shells is demonstrated. It consists of a microfluidic channel that encompasses a constriction, as a primary double emulsion drop travels through the constriction, it is deformed and a single emulsion oil drop detached from the shell of the double emulsion. The pinch off process of the oil drop is explained and key parameters affecting this pinch off behaviour are tested.

This chapter is adapted from the paper entitled **"Reducing the shell thickness of double emulsions using microfluidics"**, authored by Antoine Vian, Valentine Favrod and Esther Amstad, published in *Microfluidics and Nanofluidics*, in 2016, volume 20, pages 1-9 [1].

Contents

3.1 Abstract 33
3.2 Introduction 34
3.3 Materials and methods 35
3.3.1 Device fabrication and dimensions 35
3.3.2 Operation of the squeezing device and drop collection 35
3.3.3 Energy required to separate a double emulsion drop into two drops 36
3.4 Results and discussion 37
3.4.1 Device operation 37
3.4.2 Interfacial energy associated with drop splitting 38
3.4.3 Minimal velocity required to split a drop 41
3.4.4 Efficiency of the removal as a function of the velocity in the constriction 42
3.4.5 Influence of the constriction geometry 44
3.4.6 Influence of the shell of primary double emulsions 46
3.5 Conclusions 47

3.1 Abstract

Double emulsion drops are well-suited templates to produce capsules whose dimensions can be conveniently tuned by adjusting those of the drops. To closely control the release kinetics of encapsulants, the composition and thickness of the capsule shell must be precisely tuned; this is greatly facilitated if the shell is homogeneous in its composition and thickness. However, the densities of the two drops that form the double emulsions are often different, resulting in an offset of the two drop centers and therefore in an inhomogeneous shell thickness. This difficulty can be overcome if the shell is made very thin. Unfortunately, a controlled fabrication of double emulsions with thin shells is difficult. In this chapter, we present a microfluidic squeezing device that removes up to 93 vol% of the oil from the shell of W/O/W double emulsions. This is achieved by strongly deforming drops; this deformation increases their interfacial energy to sufficiently high values to cause splitting of double emulsions into double emulsions with a much thinner shell and a single emulsion oil drop. Therefore, we can reduce the shell thickness of the double emulsion down to 330 nm. Because this method does not rely on solvent evaporation, any type of oil can be removed. Therefore, it constitutes a new way to produce double emulsions with very thin shells that can be converted into thin-shell capsules made of a broad range of materials.

3.2 Introduction

A capsule can be made from a double emulsion drop, which is a drop contained in a second, larger drop made of an immiscible liquid that is dispersed in a third fluid [39]. Drops of a well-defined structure can be produced using microfluidics because this technique offers an excellent control over the fluid flow. This tight control allows tuning the diameter and shell thickness of double emulsions by adjusting the device geometry and fluid flow rates as demonstrated in Section 1.3.5 [84, 98, 99]. The diameters of these double emulsion drops can be conveniently varied between 20 and 200 μm, whereas their shell thicknesses typically range from 10 to 40 μm [39, 46, 100]. However, in many cases, the densities of the inner and outer drops are different such that their centers are offset [93, 101]. If such drops are converted into capsules, their shell thickness varies, hampering good control over the release kinetics of encapsulants [93]. This difficulty can be overcome if the shell is made very thin such that the offset of the two centers is minimal, as detailed in Section 1.3.7.

Reduction in the shell thickness brings an additional benefit: It makes double emulsions more stable against rupture. Rupture of double emulsion drops is typically caused by the coalescence of the innermost aqueous drop with the continuous aqueous phase. For this coalescence to occur, the innermost drop must move toward one of the interfaces between the outer oil drop and the continuous aqueous phase; this movement requires flow of fluid contained in the double emulsion shell [95]. The hydrodynamic resistance that impedes this fluid flow increases with decreasing shell thickness [102], and if the shell is sufficiently thin, the hydrodynamic resistance becomes so high that only minimal fluid flow occurs. As a result, double emulsions with thin shells have a lower propensity to coalesce. Unfortunately, it is very difficult to make double emulsion drops with shell thicknesses below 5 μm using microfluidics. It can be achieved by employing special glass capillary devices that are designed to make double emulsion drops with thin shells, as detailed in Section 1.3.7 [95, 103, 104]. However, the fabrication of these devices is difficult as different tapered glass capillaries must be manually precisely aligned. To overcome this difficulty, microfluidic devices that rely on the same assembly principle but can be fabricated using soft lithography have been developed; their fabrication requires only minimal alignment which facilitates their production (See Section 1.3.4) [91]. However, these devices can only make double emulsions with shell thicknesses down to 2.5 μm. This thickness can be reduced if their shells contain volatile oils that have some solubility in the outer phase, such that they slowly dissolve and evaporate from the liquid air interface [46, 105]. However, there are only very few solvent mixtures that fulfill all requirements such that they can be removed through evaporation, and these usually contain toxic solvents such as chloroform or toluene, which prevents most biomedical applications [106, 107]. Alternatively, up to 30 vol% of the solvent can be removed from the shell by pushing double emulsions through constrictions [91, 108]. This method does not impose any requirements on the solvent choice, thereby also allowing removal of biocompatible

solvents that have no solubility in the aqueous phase whatsoever. However, the amount of oil that can be removed is very limited. Hence, techniques that enable efficient and controlled removal of a wide range of solvents from double emulsion shells remain to be established. Such techniques would facilitate the production of double emulsion drops with thin shells, thereby broadening their use as templates to make thin-shell capsules composed of a wide variety of materials.

In this chapter, we introduce a microfluidic squeezing device that enables removal of up to 93 vol% of the oil contained in shells of W/O/W double emulsion drops. This is achieved by strongly deforming double emulsion drops such that their interfacial energy becomes so high that the leading end, which only contains oil, of the drop pinches off. Therefore, the double emulsion drop is split into a double emulsion drop with a much thinner shell and a single emulsion drop. The shell thickness of the resulting double emulsion drop can be conveniently controlled with the constriction geometry or the fluid flow rates. This technique constitutes a facile route to controllably reduce the thickness of shells of double emulsion drops after they have been formed without changing the composition of either the shell or the surrounding media.

3.3 Materials and methods

3.3.1 Device fabrication and dimensions

We fabricate the microfluidic squeezing device from PDMS using soft lithography, as detailed in Section 1.3.4 [85, 86]. It consists of one inlet that leads into a 100-μm-wide channel which is confined on a length of 190 μm to form a constriction whose width varies between 20 and 40 μm, before it opens up again to 100 μm.

3.3.2 Operation of the squeezing device and drop collection

Double emulsion drops produced using microfluidic flow focusing device (see Section 1.3.5) are injected into the squeezing device with a flow rate q using volume-controlled syringe pumps. We collect a mixture of double emulsion drops with thinner shells and single emulsion oil drops. The two types of drops can be separated by exploiting the density difference between the oil and the aqueous phase: The density of HFE-7500 is 1.6 times higher than that of water, and hence, the single emulsion drops sediment to the bottom of the collection. To make double emulsions float, they can be collected in an aqueous solution containing an appropriate amount of glycerol. In this case, the density of the collecting solution is significantly higher than that of the aqueous core of double emulsions. If the double emulsion shell, which is denser than the water/glycerol mixture, is sufficiently thin such that its volume fraction is small, the average density of the double emulsions is lower than that of the water/glycerol mixture. As a result, double emulsions

float, while single emulsions sink such that the two different types of drops can conveniently be separated.

3.3.3 Energy required to separate a double emulsion drop into two drops

Splitting a drop costs interfacial energy. We estimate the interfacial energy required to form a drop which has originally a shell thickness t_{s0}, into a drop which has a shell t_s by measuring the added surfaces between the two systems. The initial interfacial energy of the drop at rest, E_i is the sum of the interfacial energy of the inner aqueous drop and the oil shell and that of the oil shell with the outer aqueous phase

$$E_i = 4\pi\gamma R_i^2 + 4\pi\gamma(R + t_{s0})^2; \tag{3.1}$$

here R_i is the inner radius of the double emulsion drop. The sum of the interfacial energies of the resulting single emulsion drop and the double emulsion drop with a much thinner shell, E_a, is

$$E_a = 4\pi\gamma R_i^2 + 4\pi\gamma(R_i + t_s)^2 + 4\pi\gamma r^2; \tag{3.2}$$

here r is the radius of the remaining oil drop, t_{s0}, the shell thickness before the oil is pinched off, and t_s, the shell thickness after the oil drop has been pinched off. By volume conservation we obtain :

$$r^3 = (R_i + t_s)^3 - (R_i + t_{s0})^3 \tag{3.3}$$

and therefore by combining equation (3.2) and (3.3)

$$E_a = 4\pi\gamma R_i^2 + 4\pi\gamma(R_i + t_s)^2 + 4\pi\gamma((R_i + t_s)^3 - (R_i + t_{s0})^3)^{2/3} \tag{3.4}$$

Hence, the energy required to split a double emulsion drop with a shell thickness, t_{s0} into one with a shell thickness, t_s and a single emulsion oil drop; E_s is obtained by subtracting equation (3.4) from (3.1):

$$E_s = E_a - E_i = 4\pi\gamma((R_i + t_s)^2 - (R_i + t_{s0})^2 + [(R_i + t_s)^3 - (R_i + t_{s0})^3]^{2/3}) \tag{3.5}$$

3.4 Results and discussion

3.4.1 Device operation

We inject a solution containing double emulsion drops with an outer diameter of 84.1 ± 0.8 μm and a shell thickness of 5.21 ± 0.23 μm into the squeezing device, as shown in the optical micrographs in Figures 3.1A and B. These double emulsions are pushed through a microfluidic squeezer, schematically shown in Figure 3.1C. The collected solution contains equal numbers of single and double emulsion drops. The size distributions of the single and double emulsion drops is very narrow, yet their diameters are distinctly different, as examplified in the optical micrograph in Figure 3.1D. Because the density of the double emulsion drops is different from that of single emulsion drops, they can be separated in the collection vial if it contains a liquid with an intermediate density, as detailed in the experimental section 3.3.2.

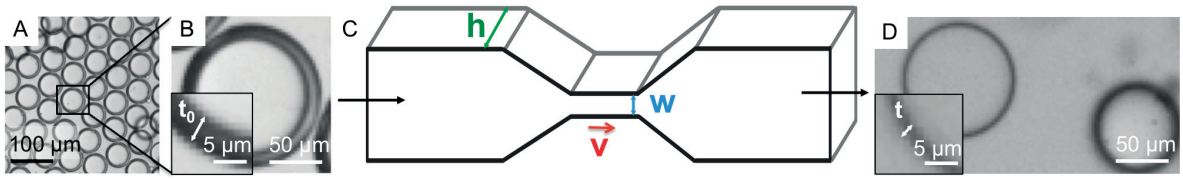

Figure 3.1: (**A**) Overview and (**B**) close view of double emulsion drops with an initial shell thickness t_{s0} (**C**) Schematic illustration of the squeezing device of height h containing a constriction of width w. The continuous phase flows at a speed v through the constriction. (**D**) Optical micrograph of a squeezed double emulsion drop with a shell thickness t_s *(inset)* and the oil drop that has been pinched off during the squeezing process *(right)*

The shells of collected double emulsions are much thinner than those of injected drops. To investigate the mechanism by which single emulsion oil drops form at the expense of the shell thickness of the double emulsion drops, we visualize their flow through constrictions using a high speed camera operated at 3000 frames per second. Because the drop diameter is larger than the channel height, they are deformed as soon as they enter the main channel. Remarkably, the deformed double emulsion drop is not symmetric. Instead, the center of the aqueous drop is located further upstream compared to that of the oil drop, resulting in an offset of the two drop centers, O, as shown in the inset of the optical micrograph in Figure 3.2A. Once the drop is pushed into the constriction, it deforms even more, as shown in time-lapse optical microscopy images in Figure 3.2A. At some point, it deforms so strongly that the leading end of the drop that is exclusively composed of oil is pinched off. The resulting single emulsion oil drop is completely detached from the double emulsion drop, whose shell thickness is significantly reduced, as shown in Figure 3.2A.

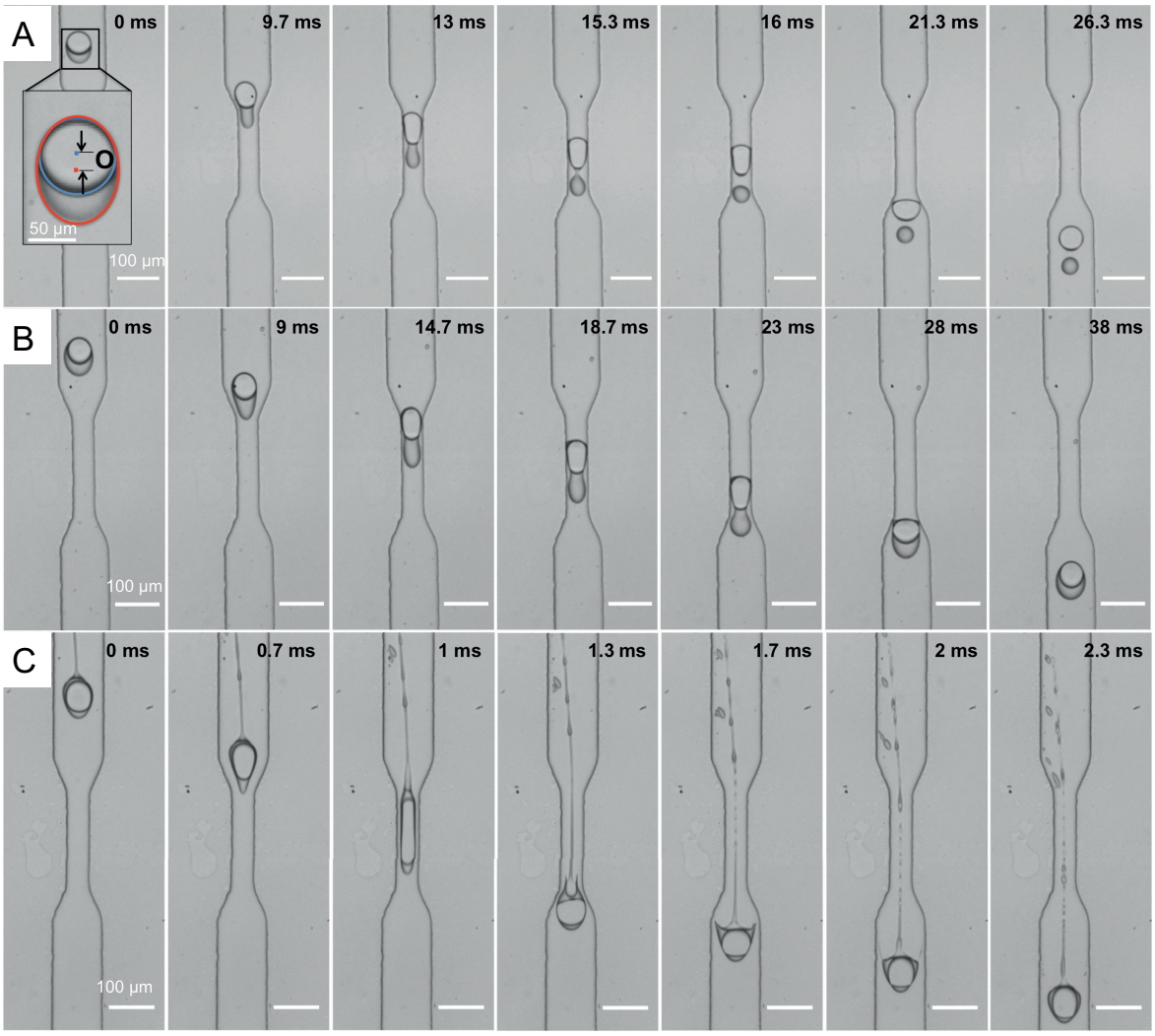

Figure 3.2: Optical time-lapse micrographs of double emulsion drops flowing through a 40-μm-wide and 60-μm-tall constriction at a flow rate of (**A**) 260 μL/h, (**B**) 150 μL/h, and **C**) 3750 μL/h. The inset in (**A**) defines the offset O of the center of the outer oil drop (red) and the inner aqueous drop (blue)

3.4.2 Interfacial energy associated with drop splitting

To investigate the reason for the offset of the two drop centers of the deformed double emulsions, we consider the pressure distribution within these drops. For drops contained in a microfluidic channel under laminar flow conditions, the pressure at their leading end is lower than that at their tailing end [109]. This pressure difference drives fluid flow inside the double emulsion drop. The resulting fluxes of the inner aqueous phase and the middle oil phase, $q_w = \Delta p / R_{H,w}$ and $q_o = \Delta p / R_{H,o}$, are inversely proportional to their hydrodynamic resistance, which we approximate to be that in a rectangular channel:

$$R_{H,n} = \frac{12\mu_n L}{1 - 0.63(h/w)} \frac{1}{wh^3} \tag{3.6}$$

here μ_n is the dynamic viscosity of the fluid, L the length of the channel, w its width, and h its height, as described in Section 1.3.2. The viscosity of the oil is eight times lower than that of the PEG-containing aqueous phase such that the hydrodynamic resistance for the oil to flow is eight times lower than that for the aqueous phase. Hence, the oil flows much faster toward the leading end of the double emulsion than the aqueous phase does, resulting in an offset, of the two drop centers, as shown in the inset of Figure 3.2A. In the constriction, this offset reach its maximum value, O_m, as shown in Figure 3.3B. The offset is directly correlated to the viscosity of each phase, therefore if the oil is more viscous that the inner phase, the core should flow faster than the shell. This offset is required to pinch a single oil drop off the leading end of the double emulsion drop.

However, this offset is not a sufficient condition for the drop pinch-off to actually occur. The injected double emulsion drops only split into a double emulsion with a thinner shell and a single emulsion oil drop if they are strongly deformed inside the constriction. We expect this deformation to be caused by the shear stress that acts on the drop while it passes this constriction. To investigate the influence of the shear stress on the drop deformation, we vary the shear stress:

$$\tau = \mu_c v(\frac{1}{w} + \frac{1}{h}) \tag{3.7}$$

by changing fluid flow velocity in the constriction, v, while we keep the other parameters constant; here μ_c is the dynamic viscosity of the continuous phase.

To quantify the drop deformation, we estimate the drop external surface area; because the diameter of the drop is much larger than the channel height such that it is strongly deformed in this direction, we approximate its cross-section as a rectangle. We measure the projected perimeter, C_l, of the drop from optical micrographs and multiply this value with the device height; C_l corresponds to the contour length of the drop when its deformation is maximal, as shown in the optical micrograph in Figure 3.3A. Therefore, this deformation corresponds to that just before the oil drop pinches off. Because the diameter of the drop is much larger than the channel height, the drop is strongly deformed and we approximate its cross-section to be rectangular. With this approximation, we estimate the drop external surface area, $A_d = C_l.h$, with h the height of the channel. Using this surface area, we calculate the deformation energy as $E_d = \gamma C_l h$; here γ is the interfacial tension between the oil and the water. To determine the relative deformation we compute the difference in surface area of the undeformed drop, $A_0 = 4\pi R^2$, with R the external radius of the drop, and that of the maximally deformed one, A_d, and normalise this difference with A_0:

$$\frac{\Delta A}{A_0} = \frac{A_d - A_0}{A_0} \tag{3.8}$$

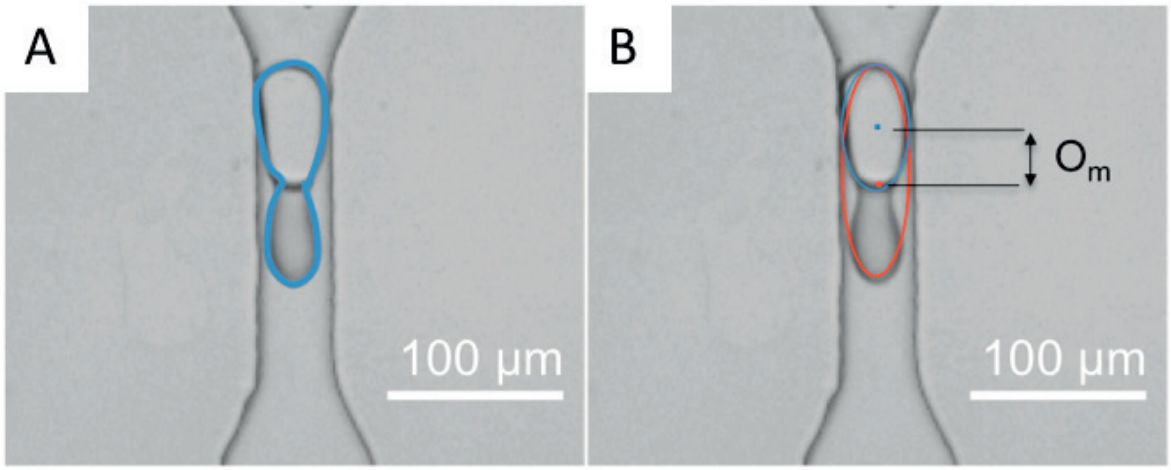

Figure 3.3: (**A**) Optical micrograph of a double emulsion before an oil drop pinches off. The line represents the contour length, C_l, used for calculating the deformation energy. (**B**) The distance between the center of the two ellipsoid is used to characterize the offset at maximum deformation, O_m.

For velocities above 4 cm/s, $\frac{\Delta A}{A_0}$ only weakly depends on v: it decreases by 10% if v is increased by a factor of 2.5, as shown in Figure 3.4A. This result indicates that there is a characteristic deformation above which double emulsion drops split into two drops. This deformation is reached if $v > 4$ cm/s. By contrast, if $v < 4$ cm/s, the shear stress is too low to deform the double emulsion drop sufficiently to cause pinch-off of a single emulsion oil drop. For example, if $v = 3.6$ cm/s, the normalized drop surface only increases by 40 %. This increase in surface area is insufficient to cause detachment of an oil drop such that the shell thickness of the double emulsion drop remains unchanged upon squeezing, as shown in the time-lapse optical micrographs in Figure 3.2B.

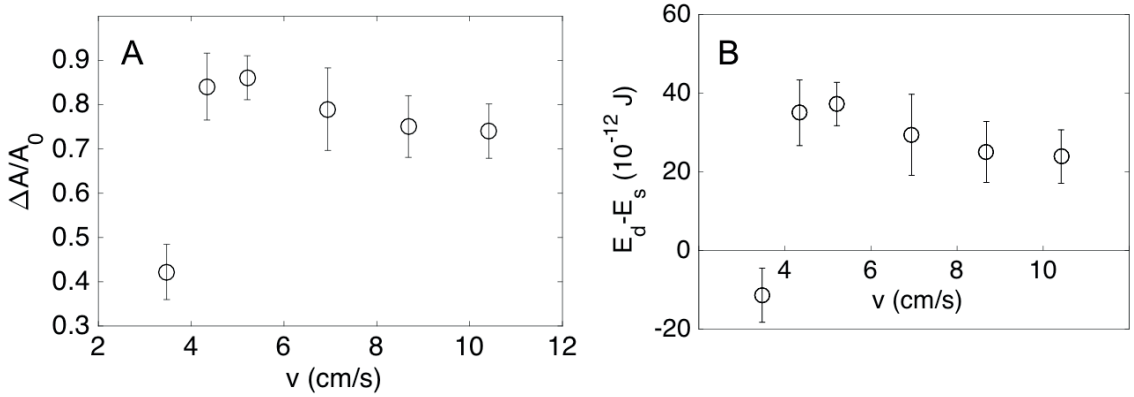

Figure 3.4: (**A**) Relative change in surface area normalized by the initial surface area, $\frac{\Delta A}{A_0}$, as a function of the velocity of the continuous phase in the constriction, v. (**B**) Difference in the interfacial energy of the maximally deformed injected double emulsion drop, E_d, and the sum of the interfacial energies of the double emulsion drop with a thinner shell and the single emulsion drop, E_s, as a function of v, for injected double emulsions with a diameter of 84.1 μm that are pushed through 20 μm wide and 60 μm tall constriction.

An increase in the deformation of a drop increases its interfacial area and therefore its interfacial energy. If the deformation is sufficiently high, we expect the system to be able to minimize the interfacial area by splitting the drop into two as this lowers the total interfacial energy [110]. To test this expectation, we estimate the changes in interfacial energies involved in the deformation by multiplying the total surface area with the interfacial tension of the fluorinated oil and water, $\gamma = 5$ mN/m. To test whether we can assume the interfacial tension to be in equilibrium while drops pass the constriction, we calculate the time for a surfactant to diffuse 20 nm, which is the length of a stretched surfactant molecule, using the diffusion coefficient for the perfluorinated surfactant in HFE-7500 [111]. This diffusion time is 100 times lower than the time it takes to deform the drop. Hence, we assume the interfacial tension to always be in equilibrium. While the drop passes the constriction, its interfacial area increases by up to 90% compared to that of a drop at rest. This corresponds to an increase in the interfacial energy of $8.5.10^{-11}$ J. In this case, the interfacial energy of the highly deformed double emulsion drop, $E_d = \gamma A_d$, is higher than interfacial energy the sum of the double emulsion drop with a thinner shell and a single emulsion drop, E_s, as shown in Figure 3.4B. The calculation of E_s is detailed in preamble in Section 3.3.3. Hence, it is energetically favorable to detach a single emulsion drop from the shell of a highly deformed double emulsion drop. By contrast, if $E_d < E_s$, no oil drop detaches, as observed in Figure 3.2B, which corresponds to the first data point in Figure 3.4B.

3.4.3 Minimal velocity required to split a drop

Drops deform because they are subjected to shear stresses. If the deformation of the double emulsion drop scales with the shear stress and therefore the fluid velocity in the constriction, we should be able to predict the minimal velocity, v_t, below which no drop detaches. Drops start to detach if the interfacial energy of the deformed drop is equal to the sum of the separated single and double emulsion drops. We expect the energy required to split an injected drop, E_s, to scale with the product of the shear stress and the constriction volume. To determine the minimum velocity at which drops must be pushed through constrictions to pinch off one single emulsion oil drop, we balance the additional interfacial energy, that must be created to pinch off the single emulsion oil drop, E_s, with the energy that results from the shear stress, E_τ. To estimate E_τ, we approximate the stress force F_τ in the constriction from the shear stress in the middle of the constriction caused by the four channel walls:

$$F_\tau = 4\mu l v\left(\frac{h}{w} + \frac{w}{h}\right) \tag{3.9}$$

here μ is the dynamic viscosity of the oil, l, the length of the constriction channel, v, the velocity in the channel, h its height and w its width. We convert F_τ into E_τ by multiplying it with the channel length, l:

$$E_\tau = 4\mu l^2 v\left(\frac{h}{w} + \frac{w}{h}\right) \tag{3.10}$$

By equating this expression with E_s, we obtain the minimum velocity at which drops must flow through constriction to allow an oil drop to pinch off:

$$v_t = \frac{\pi h w}{\mu l^2 (w^2 + h^2)} [(R_i + t_s)^2 - (R_i + t_{s0})^2 + ((R_i + t_{s0})^3 - (R_i + t_s)^3)^{2/3}] \tag{3.11}$$

Using this formula, we can calculate v_t to be 5.8 cm/s, which is in fair agreement with the experimentally observed threshold value of 4 cm/s.

3.4.4 Efficiency of the removal as a function of the velocity in the constriction

The shell thickness of double emulsion drops can usually be controlled with the fluid flow rates. To test whether this is also the case for double emulsions that have been squeezed through a constriction, we quantify the shell thickness, t_s, as a function of the fluid velocity in the constriction v. Because this thickness is below the resolution limit of an optical microscope, we measure the outer diameter of the double emulsion drop. We subsequently rupture this drop with isopropanol and measure the diameter of the resulting oil drop from optical micrographs. Using these two diameters and volume conservation, we can calculate the shell thickness, as detailed in Section 1.3.6.

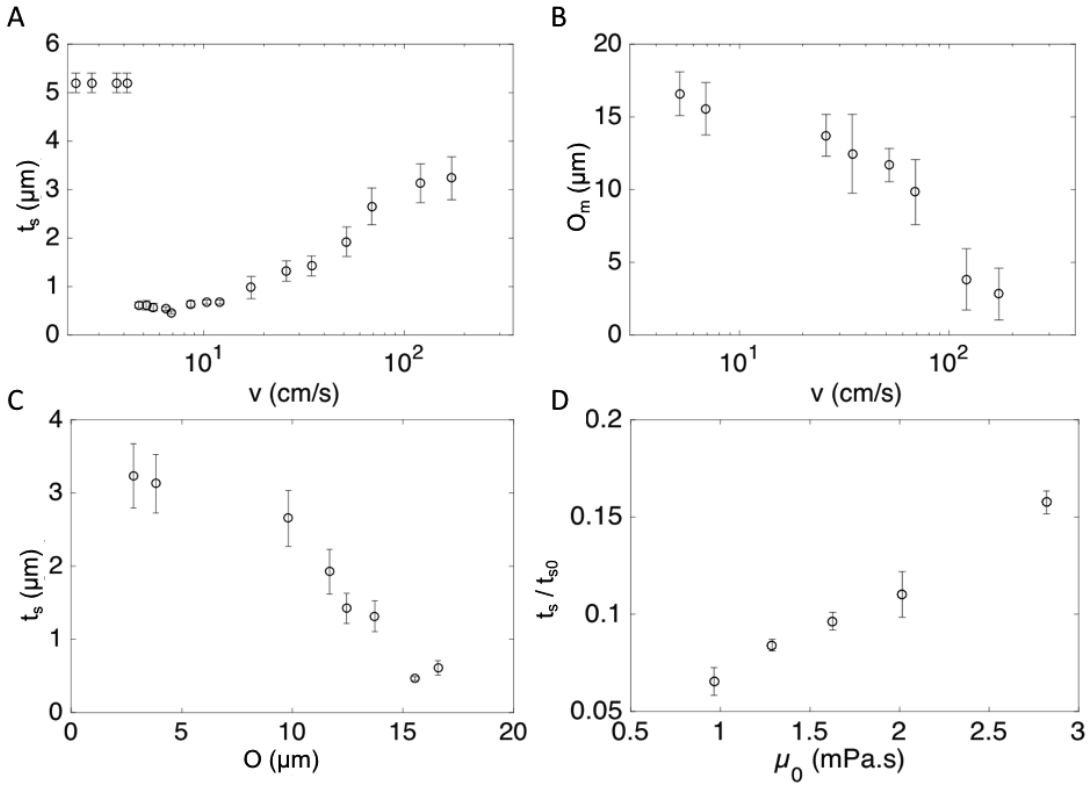

Figure 3.5: (**A**) Influence of the speed of the continuous phase in the constriction, v, on the shell thickness of double emulsion drops after they have been squeezed, t_s. (**B**) Offset of the centers of the inner and outer drops before they enter the constriction, O, as a function of v. (**C**) Influence of O on the shell thicknesses of the resulting double emulsion drops. (**D**) Relative shell thickness, t_s/t_{s0}, as a function of the viscosity of the oil phase, μ_0. For all these measurements, we employ a 20-μm-wide, 60-μm-tall constriction

The shell thickness of the collected double emulsion drops depends on the fluid velocity in the constriction. If double emulsions are pushed across the constrictions at v below 4 cm/s, no oil is removed and the shell thicknesses of the squeezed double emulsions are equal to those of the injected ones. By contrast, if double emulsions are pushed across the constriction at v > 4 cm/s, oil is removed such that their shell thicknesses decrease while they are squeezed. Remarkably, the amount of oil that is removed during the squeezing process decreases with increasing v for $v > 6$ cm/s. As a result, the shells of squeezed double emulsions are thinnest if they are pushed across at 4 cm/s $< v <$ 6 cm/s, as shown in Figure 3.5A. To investigate the reason for the increase in shell thickness with increasing v for $v > 6$ cm/s, we increase q even more to 3750 μL/h, corresponding to $v = 112$ cm/s and visualize the squeezing of drops with a high-speed camera. In this case, the positions of the centers of the inner aqueous and the outer oil drops are nearly identical and no large oil drop can detach. Instead, many much smaller oil drops are sheared off the surface of the double emulsion drop, as shown in the time-lapse optical micrographs in Figure 3.2C. To determine the reason for this change in the formation of oil drops, we quantify O as shown in Figure 3.2 and plot it as a function of v. The offset

decreases with increasing v, as shown in Figure 3.5B. This decrease in O is related to a change in the complex fluid flow inside the drop, which depends on parameters such as the drop size relative to the channel geometry, the capillary number, the viscosity ratios, and the interfacial tension [112,113]. Another contributing reason for the decrease in O with increasing v is a change in the driving force for fluids contained in the drop to flow toward its leading end: The pressure gradient Δp around the double emulsion drop decreases with increasing v. This decrease in Δp is caused by the decrease in the hydrodynamic resistance experienced by the continuous phase that is locally induced by the presence of a drop in the microfluidic channel, with increasing v [109]. Hence, the difference in the induced resistance of the aqueous phase $R_{h,w}$ and the oil phase $R_{H,o}$ inside the double emulsion drops decreases with increasing v, such that the offset of the drop centers decreases with increasing v. As the drop center offset becomes smaller, less oil can detach and the thickness of the resulting double emulsion increases, as shown in Figure 3.5C. Hence, there is an optimum flow rate where drops are sufficiently deformed for an oil drop to detach, yet where the offset of the two centers is still large enough such that a high fraction of the oil is pinched off.

The final shell thickness of the squeezed double emulsion depends on the volume of oil contained in the injected double emulsion drop upstream its neck that eventually results in the pinch-off of a single emulsion oil drop. This oil will remain in the shell of the squeezed double emulsion, and hence, it will determine its final shell thickness. Because the neck is always located at some distance apart from the interface of the innermost aqueous phase, there will always be some oil that remains in the shell of squeezed double emulsions. We expect the fraction of oil contained upstream the neck of the deformed double emulsion to increase with decreasing offset of the two drop centers. This offset depends on the difference in the hydrodynamic resistance experienced by the inner aqueous phase and the oil phase, and hence, it should scale with the ratio of their viscosities. Because in our case, the viscosity of the oil phase is lower than that of the aqueous phase, we expect the offset to become smaller with increasing oil viscosity, resulting in increased shell thicknesses of squeezed double emulsions. To test this expectation, we increase the viscosity of the oil by adding different amounts of Krytox^{TM} GPL, a more viscous fluorinated oil, to HFE-7500, as detailed in Section 2.8. Indeed, the shell thickness of squeezed double emulsions increases with the viscosity of the oil, as shown in Figure 3.5D.

3.4.5 Influence of the constriction geometry

The amount of oil that is removed from the shell of double emulsions while they are squeezed depends on the extent of their deformation. This deformation can be tuned with the operation parameters, such as the velocity with which double emulsions pass the constriction. Moreover, it can be tuned with the composition of the double emulsion, such as the viscosity ratios of the oil and the continuous phase. However, maybe the easiest way to control the drop deformation is by controlling the constriction geometry. To test whether we can indeed control the shell thickness

of squeezed double emulsions with the constriction geometry, we fabricate devices with heights between 40 and 100 μm, keeping their width constant at 20 μm. We inject double emulsion drops with 5.21 $\pm$ 0.23 μm thick shells and measure their minimal thickness, t_{min}, after their passage through the constriction as a function of its height. Their shell thickness decreases from 1.34 μm for $h = 100$ to 0.330 μm for $h = 40$ μm, as shown by the squares in Figure 3.6A. Similarly, if we increase w to 40 μm, the shell thickness increases with increasing height, albeit these shells remain thicker, as shown by the circles in Figure 3.6A. To relate the drop deformation to the oil removal, we plot the final shell thickness, t_{min}, normalised by the initial shell thickness, t_{s0}, as a function of the deformation index:

$$D.I. = \frac{(L_d - w_d)}{(L_d + w_d)} \tag{3.12}$$

here L_d is the length and w_d the width of the drop at its maximum deformation, as shown in the inset in Figure 3.6B. When $D.I. = 0$, the drop is at rest; otherwise, $D.I. > 0$ [109]. As expected, the relative shell thickness decreases with increasing drop deformation, as shown in Figure 3.6B. This result indicates that the volume of oil located upstream the neck that results in the pinch-off of the oil drop decreases with increasing deformation. Our result could indicate that the distance between the neck and the interface of the innermost aqueous drop decreases with increasing drop deformation. However, our result could also indicate that the offset of the two drop centers increases with increasing drop deformation such that more oil is located at the leading end of the injected double emulsion. To investigate the reason for the decrease in shell thickness with increasing drop deformation, we quantify the offset of the drop centers at the point of maximum deformation of the outer drop, O_m, immediately before the oil drop is pinched off, as a function L_d, as detailed in Figure 3.3B. The offset increases with L_d, as shown in Figure 3.6C, indicating that a stronger deformation results in an increased offset of the two drop centers, which enables pinching off a larger oil drop from the leading end of the double emulsion drop.

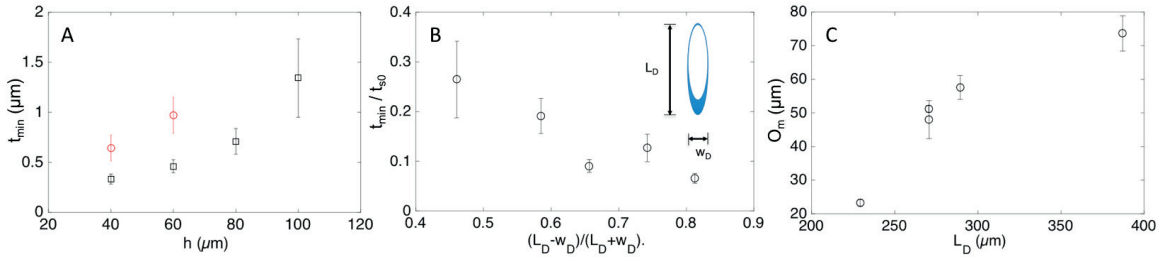

Figure 3.6: (**A**) Variation of the shell thickness, t_s, as a function of device height, h for (open square) 20-μm and (open circle) 40-μm-wide constrictions. (**B**) Influence of the maximum deformation of the drop, defined as the deformation index $D.I. = (L_d - w_d)/(L_d + w_d)$ on the relative shell thickness, t_{min}/t_{s0}. (**C**) Influence of the length of the outer drop at its maximum deformation, L_d, on the offset of the two drop centers when the drop is maximally deformed, O_m.

3.4.6 Influence of the shell of primary double emulsions

Our results indicate that the amount of removed oil scales with drop deformation. This deformation depends on the ratio of the double emulsion diameter to the constriction dimensions. However, we expect it to be independent of the initial shell thickness. To test this expectation, we produce 92-μm-diameter double emulsion drops with shell thicknesses varying between 5 and 9 μm. Indeed, in all cases, the shell thickness after squeezing is proportional to the initial shell thickness, as seen in Figure 3.8A, such that the relative change in the shell thickness is independent of the initial shell thickness, as shown in Figure 3.8B. In all cases, approximately 93 vol% of the oil is removed. Importantly, this procedure is not limited to the removal of fluorinated oils, but it can also be applied to remove hydrocarbon based oils, such as toluene, as shown in the timelapse in Figure 3.7.

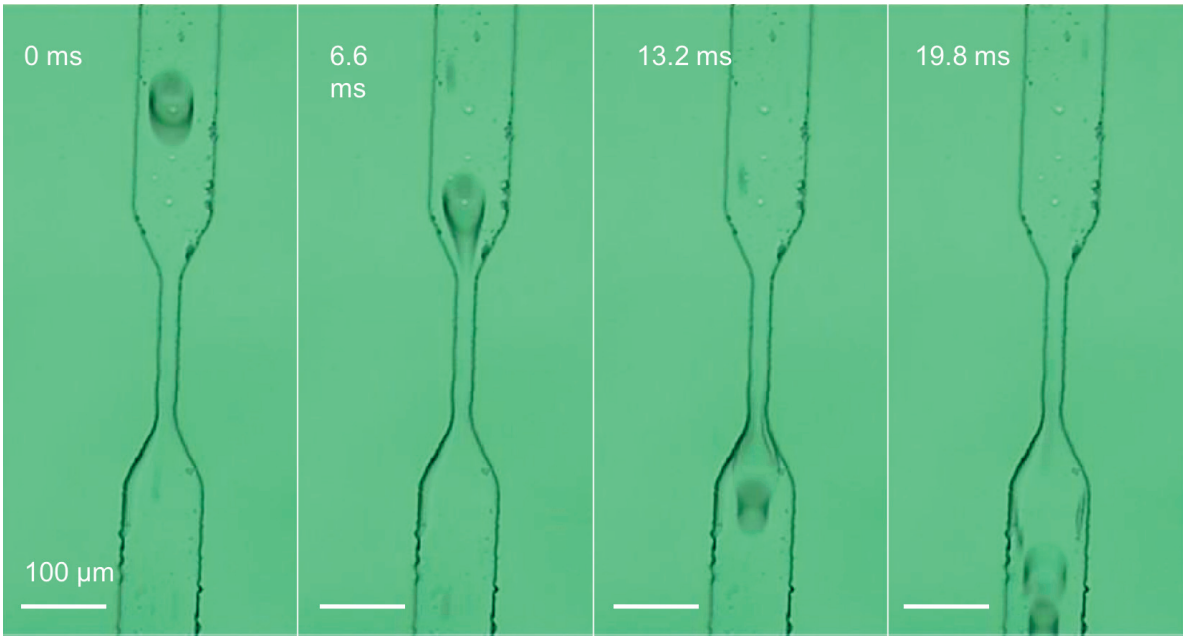

Figure 3.7: Optical time-lapse of the squeezing process for a double emulsion composed of a toluene middle phase

Hence, this device constitutes an efficient tool to remove the vast majority of oil from the shell of double emulsion drops, thereby enabling the production of drops with shell thicknesses well below 500 nm in an experimentally easy, reproducible process.

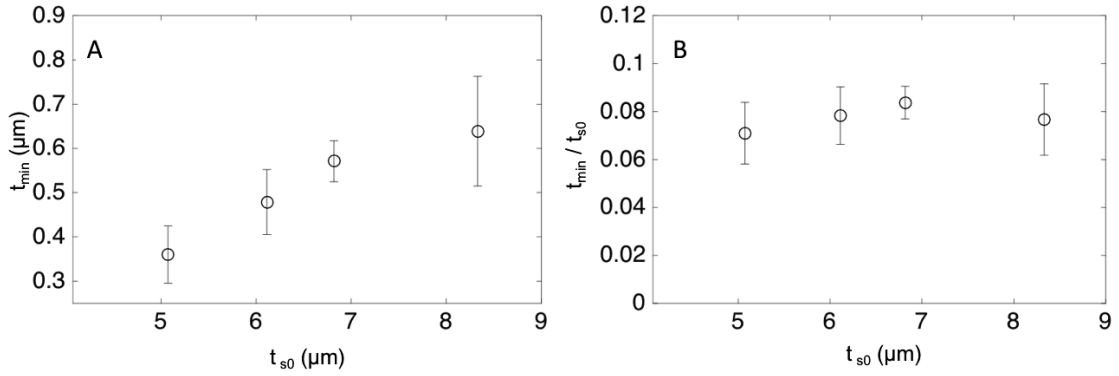

Figure 3.8: (**A**) Influence of the initial shell thickness, t_{s0} on the shell thickness of drops after they have been pushed through a 20-μm-wide, 60-μm-tall constriction, t_s. For each constriction, drops are injected at the optimum flow rate where most oil is removed. (**B**) Percentage of oil removed from double emulsion drops for different initial shell thicknesses, t_{s0}, if pushed through a 20-μm-wide, 60-μm-tall constriction. Drops are pushed through the constriction at the optimum flow rates where most oil is removed.

3.5 Conclusions

In this chapter,we present a microfluidic squeezing device that splits double emulsion drops into equal numbers of double emulsion drops with much thinner shells and single emulsion oil drops. Therefore, this device enables removal of up to 93 vol% of the oil, resulting in double emulsions with shell thicknesses down to 330 nm. As this oil removal relies on a pinch-off of a single emulsion drop from the double emulsion shell, any oil, including those that are non-volatile or have no solubility in water whatsoever, can be removed. Hence, this method constitutes an experimentally easy, versatile way to controllably and efficiently reduce the shell thickness of a wide range of double emulsions including those composed of biocompatible oils such as fluorinated oils. These double emulsions can be used as templates to make capsules with very thin shells whose composition is determined by that of the oil. Thus, this device has the potential to produce mechanically stable capsules with thin shells made from a much broader range of materials than is currently possible.

Chapter 4

Scalable production of double emulsion drops with thin shells

Antoine Vian, Baptiste Reuse and Esther Amstad

In previous chapter we present a device that reduce the shell of primary double emulsions drops to submicron values. In this chapter, we introduce a new microfluidic device that achieve this at high throughput, the aspiration device.

This chapter is adapted from the paper entitled **"Scalable production of double emulsion drops with thin shells"**, authored by Antoine Vian, Baptiste Reuse and Esther Amstad, published in *Lab on a Chip*, in 2018, volume 18, pages 1936–1942 [2].

Contents

4.1 Abstract 49
4.2 Introduction 49
4.3 Material and methods 51
4.3.1 Device fabrication 51
4.3.2 Quantification of drop velocity in the main channel 51
4.3.3 Modelling 52
4.4 Results and discussions 55
4.4.1 Operation of the aspiration device 55
4.4.2 Influence of fluids flow rate on device operation 57
4.4.3 Influence of the number of microchannels on removal efficiency 63
4.4.4 Influence of primary double emulsions shell thicknesses 64
4.4.5 Influence of the oil phase 65
4.5 Conclusion 67

4.1 Abstract

Double emulsions are often used as containers to perform high throughput screening assays and as templates for capsules. These applications require double emulsions to be mechanically stable such that they do not coalesce during processing and storage. A possibility to increase their stability is to reduce the thickness of their shells to sufficiently low values that lubrication effects hinder coalescence. However, the controlled fabrication of double emulsions with such thin shells is difficult. Here, we introduce a new microfluidic device, the aspiration device, that reduces the shell thickness of double emulsions down to 240 nm at a high throughput; thereby, the shell volume is reduced by up to 95%. The shell thickness of the resulting double emulsions depends on the pressure profile in the device and hence on the fluid flow rates in the channels and is independent of the shell thickness of the injected double emulsions. Therefore, this device enables converting double emulsions with polydisperse shell thicknesses into double emulsions with well-defined, uniform thin shells.

4.2 Introduction

Double emulsion drops are often used as picoliter-sized vessels to conduct chemical [114, 115], biochemical reactions [116, 117] and for high throughput screening assays [118–120]. These drops

can be produced at high frequencies allowing compartmentalization of large quantities of reagents in a short amount of time [83, 121, 122]. To take advantage of the possibility to produce large quantities of samples in a minimum amount of time, they must be analyzed at high rates. A fast read-out technique that is routinely used in biology is fluorescence activated cell sorting (FACS) [25,28,29,123]. However, this technique has thus far only been applied for characterizing analytes that are dispersed in aqueous solutions, such as cells [120]. This requirement is not limiting if colonies of cells are analyzed because they are typically dispersed in aqueous solutions. By contrast, many drops encompassing analytes, such as reagents, proteins, or individual cells, are aqueous such that they are dispersed in an oil that has a low solubility in water. To sort aqueous drops containing reagents using FACS, they have been loaded into W/O/W double emulsion drops, which are aqueous drops contained in larger oil-based drops that are dispersed in an aqueous surrounding [28, 29, 118–120, 124]. For these assays to be truly useful, double emulsions must be stable against coalescence. The mechanical stability of double emulsions increases with decreasing shell thickness: the hydrodynamic resistance increases with decreasing shell thickness, thereby hampering the oil flow inside the shell and introducing lubrication effects [125]. The impeded oil flow in the shell retards the motion of the innermost aqueous drop relative to the outer oil drop, thereby delaying or even preventing the innermost aqueous drop from merging with the continuous aqueous phase [126,127]. As a result of this lubrication effect, local variations in thickness of the double emulsion shells decrease with decreasing shell thickness, as detailed in Section 1.3.6 [39].

Double emulsions with controlled shell thicknesses can be assembled using microfluidics [39, 80, 128]. These drops usually have shells with thicknesses ranging from a few μm up to several tens of μm. Double emulsions with much thinner shells, below 1 μm, can be produced from microfluidic glass capillary devices [95, 106, 129–133]. However, the fabrication of these devices is tedious. Moreover, they often produce mixtures of single and double emulsion drops that must be separated after they have been produced, as detailed in Section 1.3.7. To facilitate the production of double emulsions with thin shells, microfluidic devices made of PDMS have been developed [105]. These devices produce double emulsions with shell thicknesses down to 4 μm. Their shell thickness can be reduced if double emulsions are pushed through constrictions, as detailed in Chapter 3 [1,105]. However, this reduction in the shell thickness is only controlled and reproducible if one double emulsion passes the constriction at a time; this requirement limits the throughput of these devices. Devices that reduce the shell thickness of double emulsions below 1 μm at a rate similar or even exceeding their production rate remain to be established. These devices would facilitate the use of double emulsions for high throughput screening assays and open up new possibilities to employ them as templates to produce capsules with welldefined thin shells.

In this chapter, we report a microfluidic device, the aspiration device, that reduces the thickness of W/O/W double emulsion shells down to 240 nm at a rate similar to the typical production rate of double emulsions in flow focusing devices. This is achieved by injecting primary W/O/W double emulsions with thick shells into the main microfluidic channel. The main channel is intersected by many much smaller shunt channels that remove up to 95 vol% of the oil contained in the double emulsion shells. This new microfluidic aspiration device allows processing hundreds of double emulsions at the time. Thereby, it offers possibilities to produce double emulsions with thin shells at throughputs that are at least an order of magnitude higher than what could previously been achieved.

4.3 Material and methods

4.3.1 Device fabrication

We fabricate the microfluidic aspiration device from PDMS using soft lithography as described in Chapter 1 [85,86]. It consists of a main channel that is 80 μm tall and 60 μm wide and guides the drops through the aspiration section. Within the aspiration section, each of two oppositely positioned sides of the main channels is intersected by $n = 30$ parallel shunt channels with cross sections of 10 μm x 20 μm. Each of these shunt channels leads into one of two large aspiration reservoirs that are connected to a single outlet. The surfaces of the shunt channels are treated to be wetting to the middle phase. To reduce the shell thickness of W/O/W double emulsions, where the oil is perfluorinated, we treat the channels with a HFE 7500-based solution containing 1 vol% perfluorinated trichlorosilane. To reduce the shell thickness of W/O/W double emulsions where the oil is hydrocarbon-based, we refrain from any surface modification because the PDMS surface is already hydrophobic. If the surface treatment between the oil and the channel is not made properly, the oil can wet the surface of the channels. This spreading prevents a good function of the device and an efficient removal of the oil.

4.3.2 Quantification of drop velocity in the main channel

We measure the velocity of the drops in the main channel at each junctions between the main channel and a microchannel, k, using time-lapse optical microscopy images acquired with a high speed camera operated at 3000 frames per second, as examplified in Figure 4.1.

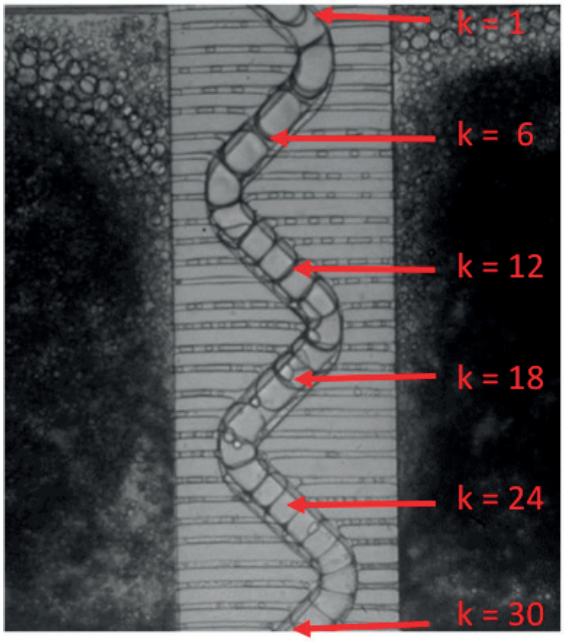

Figure 4.1: Optical micrograph of the aspiration section in operation with the location, k, where the average velocity of drops is quantified.

4.3.3 Modelling

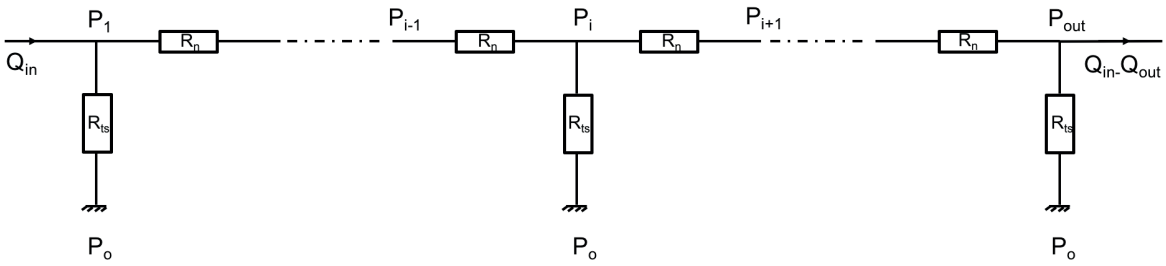

Figure 4.2: Schematic illustration of the electric circuit analogue used to estimate the pressure profile within the channels. R_n corresponds to the hydrodynamic resistance in the main channel between each shunt channel and R_{ts} is the resistance associated with each pair of shunt channel.

To estimate the pressure profile within the main channel, we employ an electric circuit analogue, as schematically shown in Figure 4.2. Because all the shunt channels lead into one of the two large reservoirs and the two reservoirs are connected to each other, we approximate the pressure at the end of each shunt channel to be the same, P_0. Moreover, we approximate the resistance of the main channel in each section between adjacent junctions to be R_n. The length of the shunt channels varies from 80 to 200 μm. Nevertheless, to simplify the model, we approximate hydrodynamic resistances of all shunt channels to be equal to R_s corresponding to a length of 100 μm. Within the aspiration section, pairs of shunt channels intersect the main channel at opposite sites, as shown in Figures 4.5B and 4.5C. We describe this pair of shunt

channels with parallel resistances: $\frac{1}{R_{ts}} = \frac{1}{R_s} + \frac{1}{R_s} = \frac{2}{R_{ts}}$, where R_s is the total resistance of the shunt channels at any given junction. At each junction, we apply the node law to relate the different pressures in the channels that lead into this junction. For example, at junction k we obtain:

$$P_k\Big(\frac{2}{R_n} + \frac{1}{R_{ts}}\Big) - \frac{P_{k-1} + P_{k+1}}{R_n} = \frac{P_0}{R_{ts}} \tag{4.1}$$

where P_k is the pressure in junction k, P_{k+1}; the pressure in junction $k+1$, P_{k-1}; the pressure in junction $k-1$. We quantify the pressure differences between the different channel sections and therefore set $P_0 = 0$ as a base point. We write this node equation for each node and obtain n equations with n unknown variables. The boundary conditions are determined by the injection and withdraw rates. Therefore, we can relate the injection rate, Q_i and the flow rate at the output of the main channel $Q_i - Q_w$ to the pressure profile in the main channel using:

$$A.P = Q \tag{4.2}$$

$$\begin{bmatrix} \frac{1}{R_n} + \frac{1}{R_{ts}} & \frac{-1}{R_n} & 0 & \dots & 0 \\ \frac{-1}{R_n} & \frac{2}{R_n} + \frac{1}{R_{ts}} & \ddots & \ddots & \vdots \\ 0 & \ddots & \ddots & \ddots & 0 \\ \vdots & \ddots & \ddots & \frac{2}{R_n} + \frac{1}{R_{ts}} & \frac{-1}{R_n} \\ 0 & \dots & 0 & \frac{-1}{R_n} & \frac{1}{R_n} + \frac{1}{R_{ts}} \end{bmatrix} . \begin{bmatrix} P_1 \\ P_2 \\ \vdots \\ \vdots \\ \vdots \\ P_{n-1} \\ P_n \end{bmatrix} = \begin{bmatrix} Q_i \\ 0 \\ \vdots \\ \vdots \\ \vdots \\ 0 \\ Q_i - Q_w \end{bmatrix}$$

In this case, the matrix is invertible because its determinant is not equal to zero. Hence, we can calculate the pressure profile in the channel by inverting matrix A:

$$P = A^{-1}.Q \tag{4.3}$$

Using this equation, we obtain the pressure profile throughout the channel at each junction k. The pressure obtained is always relative to the pressure in the reservoir at the output of the shunt channel that is arbitrarily set to 0. We convert the pressure profile into a flow rate profile inside the main channel using:

$$Q_k = \frac{P_{k+1} - P_k}{R_n} \tag{4.4}$$

The pressure drops rapidly in the initial parts of the aspiration section and levels off thereafter, as shown in Figure 4.3A. As a result, the flow rate in the aspiration section also decreases rapidly upstream the junction where the 15^{th} shunt channel intersects the main channel and decreases more slowly thereafter, as shown in Figure 4.3B. Note that this profile is obtained for a continuous flow that does not encompass any drops. When drops are present in the main

channel, they strongly increase the resistance of the main channel [109] such that we expect the actual pressure decrease in the main channel to be much higher than what is estimated in Figure 4.3A. However, we do not expect the drops to strongly influence the shape of the pressure profile.

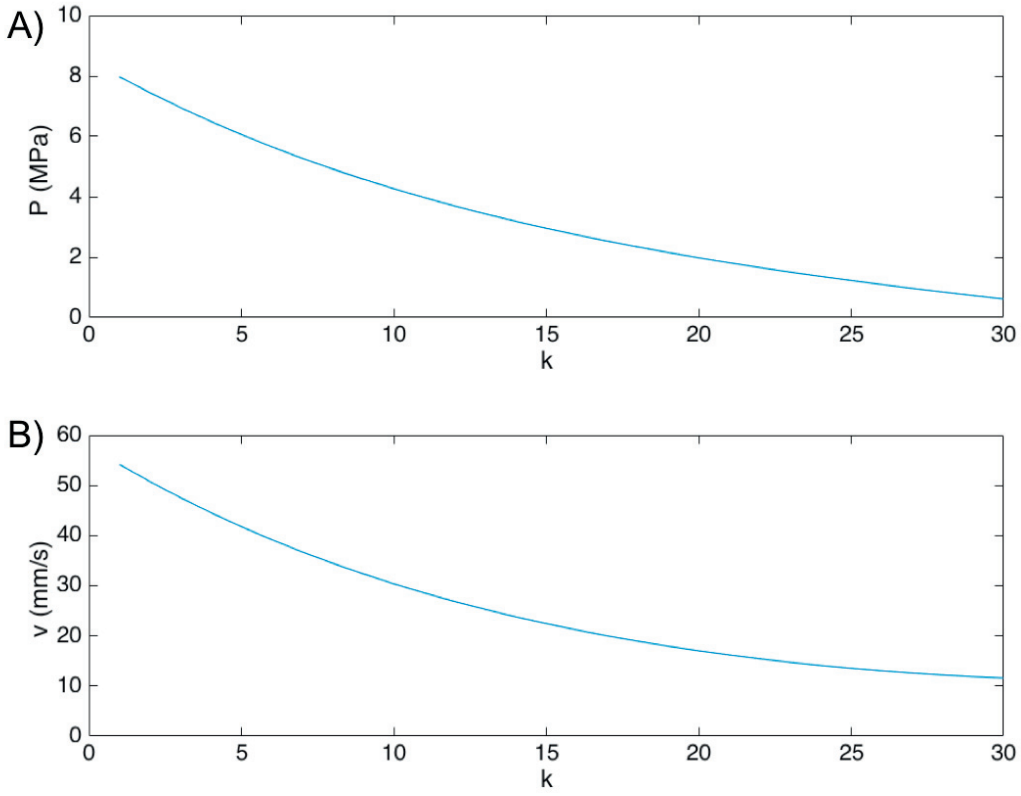

Figure 4.3: (**A**) Pressure profile along the main channel, P, as a function of the location in the main channel, represented by the junction number, k between a microchannel and the main channel of the device. (**B**) Velocity profile for a continuous fluid, v, derived from the calculated pressure profile as a function of the number of shunts channels located upstream the location of interest, k. For these calculations, we fixed Q_i at 1000 μL/h and Q_w at 800 μL/h.

From our model, we can deduce the pressure profile in the channel as a function of Q_i and Q_w. If $\Delta Q = Q_i$ - $Q_w = 300$ μL/h is kept constant and Q_i is varied between 1000 μL/h and 2000 μL/h, the pressure at the beginning of the channel depends on Q_i. By contrast, the pressure at the end of the aspiration section is nearly independent of Q_i, as seen in Figure 4.4A. If Q_i = 1000 μL/h but ΔQ is varied between 100 μL/h and 400 μL/h, the pressure in the initial parts of the aspiration section is very similar whereas the pressure in the final parts of the aspiration section increases with decreasing ΔQ, as seen in 4.4B.

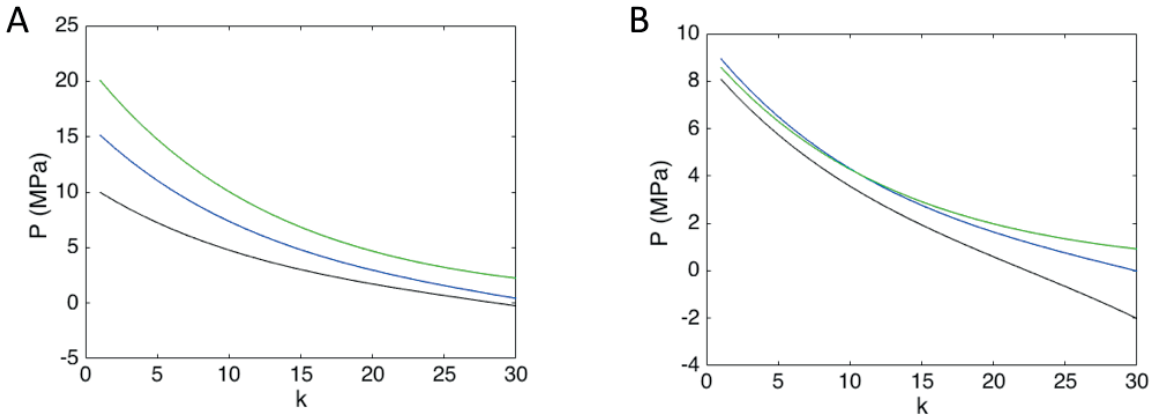

Figure 4.4: Variation of the pressure profile in the main channel as a function of flow rates. (**A**) Pressure in the main channel, P, as a function of the junction location in the channel, k, if ΔQ = 300 μL/h and Q_i = 1000 μL/h (black), 1500 μL/h (blue) and 2000 μL/h (green). (**B**) Pressure in the main channel, P, as a function of the location, k, for Q_i= 1000 μL/h and ΔQ = 400 μL/h (black), 200 μL/h (blue) and 100 μL/h (green)

4.4 Results and discussions

4.4.1 Operation of the aspiration device

The device contains an inlet for as-produced primary double emulsions, inlet a, that leads into a main channel, as shown schematically in Figure 4.5A. The double emulsions flow through the aspiration section where two opposite sides of the main channel are intersected by shunt channels; unless stated otherwise, each of these sides is intersected by n = 30 shunt channels, as schematically illustrated in Figure 4.5B and shown on the optical micrograph in Figure 4.5C. The main channel has a sinusoidal shape to increase its contact area with the shunt channels. These shunt channels lead into one of two aspiration reservoirs that are both connected to outlet b, as shown in Figure 4.5A. To control the spacing of the processed double emulsions with thin shells, we introduce a flow focusing junction downstream the aspiration unit, as indicated by the black arrows in Figure 4.5C.

The aspiration device removes oil contained in W/O/W double emulsions most efficiently, if they are injected at a high density such that they jam inside the main channel. To increase the density of double emulsions, we up-concentrate them by letting them sediment or cream for at least 10 min before a fraction of the surrounding aqueous phase is removed. The up-concentrated double emulsions are introduced into the aspiration device using syringe pumps at an injection rate Q_i. To tune the amount of oil that is removed through the shunt channels we withdraw fluid through two aspiration reservoirs that are connected to an outlet at a withdraw rate Q_w. The vast majority of the surrounding aqueous phase that initially separates adjacent double emulsions is removed through the shunt channels such that the double emulsions are jammed

within the main channel. At the concentration used here, we did not observe any coalescence of drops in the channel. To increase the spacing between adjacent drops after they passed all the shunt channels, we introduce a flow-focusing junction downstream the aspiration section and inject the outermost phase at a rate Q_o. The resulting double emulsion drops with thin shells are collected through a second outlet. To quantify the shell thicknesses of double emulsions, we measure the outer radius of the intact double emulsions from optical micrographs. The double emulsions are subsequently broken using isopropanol and the size of the resulting single emulsion oil drop is measured from optical microscopy images. Using volume conservation, we calculate the shell thickness from the radius of the intact double emulsion drop and the volume of the oil drop that forms after the double emulsion is broken, as previously reported in Chapter 1 [1, 95, 104, 126].

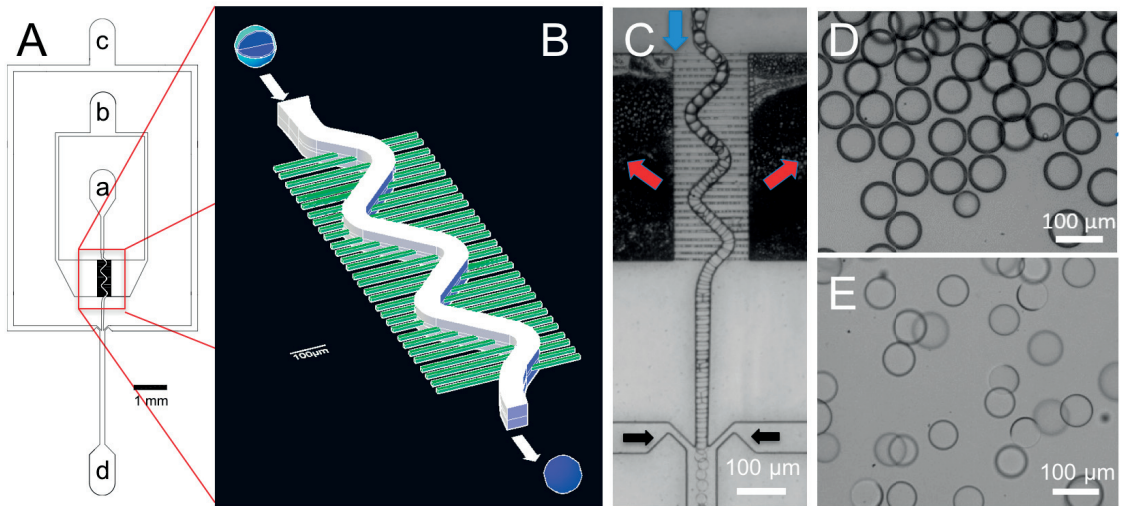

Figure 4.5: The microfluidic aspiration device. (**A**) Schematic illustration of the microfluidic aspiration device that contains an inlet for double emulsions drops (a), an outlet that enables withdrawing oil from the double emulsions (b), and an inlet for the outermost aqueous solution (c). Processed double emulsions are collected through outlet (d). (**B**) 3D schematic illustration of the aspiration section where the shell thickness of double emulsions is reduced, as schematically illustrated with double emulsions containing an aqueous core (blue) and an oil shell (light blue). The aspiration section contains a main channel (white) that is intersected by many much smaller shunt channels (green). (**C**) Optical microscopy image of the aspiration device in operation. The double emulsion drops flow through a sinoidal shaped main channel, as indicated by the blue arrow, and oil is removed through shunt channels as indicated by the red arrows. To increase the spacing between processed double emulsions, an outermost aqueous phase is injected downstream the aspiration section, as shown by the black arrows. ((**D**) and (**E**)) Optical micrographs of double emulsions drops (**D**) before and (**E**) after being processed with the aspiration device. Double emulsions have an external radius of (**D**) $R = 42.9 \pm 0.5$ μm and (**E**) $R = 36.0 \pm 0.6$ μm and a shell thickness of (D) $t_s = 5.92 \pm 0.64$ μm and (**E**) $t_s = 0.24 \pm 0.05$ μm.

W/O/W emulsions with an external radius of $R = 42.9 \pm 0.5$ μm and a shell thickness of $t_s = 5.92 \pm 0.64$ μm are produced using PDMS-based flow focusing devices described in Section 2.2 [91]. To reduce the thickness of their oil shells, we inject them into the aspiration device at

a rate $Q_i = 1000$ μL/h, as shown by the blue arrow in Figure 4.5C. Oil is removed through the shunt channels at a withdraw rate, $Q_w = 900$ μL/h, as indicated by the red arrows in Figure 4.5C. While the drops pass the initial parts of the aspiration section, a large fraction of the surrounding aqueous phase flows through the shunt channel into outlet b such that the distance between adjacent drops gradually decreases until they start to jam. To spatially separate the processed double emulsions with thin shells, we introduce a flow focusing junction downstream the aspiration section through which we inject an aqueous outer solution at a rate $Q_o = 800$ μL/h, as indicated by the black arrows in Figure 4.5C. The resulting double emulsions have much thinner shells, as a comparison of the optical micrographs of double emulsions before and after they have been processed with the aspiration device in Figure 4.5D and E reveals. Indeed, the shell thickness of double emulsions that have been processed with the aspiration device is reduced from $t_s = 5.92 \pm 0.64$ μm to 0.24 ± 0.05 μm. As a result of the reduction in shell thickness, the radius of the processed double emulsion is slightly reduced to $R = 36.0 \pm 0.6$ μm.

4.4.2 Influence of fluids flow rate on device operation

The operation mode of microfluidic devices typically depends on the fluid flow rates. To explore the different operation modes of the aspiration device, we vary the withdraw and injection rates from 50 μL/h to 2000 μL/h. If the withdraw rate is higher than the injection rate, $Q_w > Q_i$, the vast majority of fluids, including the double emulsion drops, are aspirated through the shunt channels such that very few double emulsions exit the main channel, as indicated by the grey area in Figure 4.8A and the optical micrograph in Figure 4.8B. Instead, much smaller double emulsions, whose diameter is of order of the width of the shunt channels are formed at their exits, as shown in Figure 4.6.

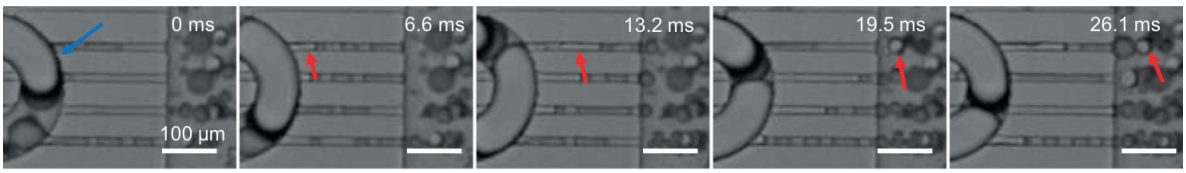

Figure 4.6: Optical time-lapse illustrating the production of double emulsion with 20 μm diameter. The blue arrow indicates a deformed primary double emulsion drop flowing in the main channel. The red arrow follows the formation of secondary much smaller emulsions in the microchannels.

This operation resembles the extrusion used, for example, to process vesicles [134] and can be employed to reduce the size of double emulsions. However, this operation mode does not offer a good control over the shell thickness of double emulsions such that we do not further investigate it here. By contrast, if the injection rate is higher than the withdraw rate, $Q_i > Q_w$, double emulsions remain intact. Hence, if $Q_i > Q_w$, we can reduce the shell thickness of double emulsions without significantly altering their diameter.

To control the spacing of the processed double emulsions, we introduce a flow focusing junction downstream the aspiration section and inject an aqueous phase containing a surfactant, PVA, through it. We assume this additional fluid not to impact the operation of the device and the final shell thickness of double emulsions because the width of the main channel increases three-fold at the flow focusing junction. To verify this assumption, we compare the hydrodynamic resistance of the main channel downstream the flow focusing junction on that of the main channel in the aspiration section (See Section 1.3.2):

$$R_H = \frac{12\eta L}{1 - 0.63(h/w)} \frac{1}{h^3 w} \tag{4.5}$$

here μ is the dynamic viscosity of the fluid, L the length of the channel, w its width, and h its height. Hence for two equally long channels that are filled with an identical fluid but have different heights, $h_1 = h_2 = 80$ μm and widths, $w_1 = 60$ and $w_2 = 180$ μm, and therefore different hydrodynamic resistances R_1 and R_2 we obtain:

$$\frac{R_1}{R_2} = \left[\frac{1 - 0.63(h_2/w_2}{1 - 0.63(h_1/w_1)} \right] \frac{w_2 h_2^3}{w_1 h_1^3} = 5.6 \tag{4.6}$$

Hence, the hydrodynamic resistance of the channel downstream the aspiration section is more than five-fold lower than that of the aspiration section,

To verify this assumption, we vary Q_o from 300 to 6000 μL/h, keeping Q_i and Q_w constant. Within the tested flow rate range, Q_o does not significantly influence the double emulsion shell thickness: varying Q_o by a factor of 20 results in shell thickness variations of less than 10%, as shown in Figure 4.7.

To spatially separate the double emulsions that are jammed in the aspiration section in the final parts of the aspiration device, we introduce an aqueous phase downstream the aspiration section. This outer phase is injected at a rate, Q_o. To test the influence of Q_o on the shell thickness of processed double emulsions, we vary Q_o from 300 μL/h to 6000 μL/h and keep the injection and withdraw flow rates constant at $Q_i = 1000$ μL/h and $Q_w = 800$ μL/h. Our results demonstrate that the shell thickness of processed double emulsions is independent of the flow rate of the outer fluid, Q_o, as shown in Figure 4.7.

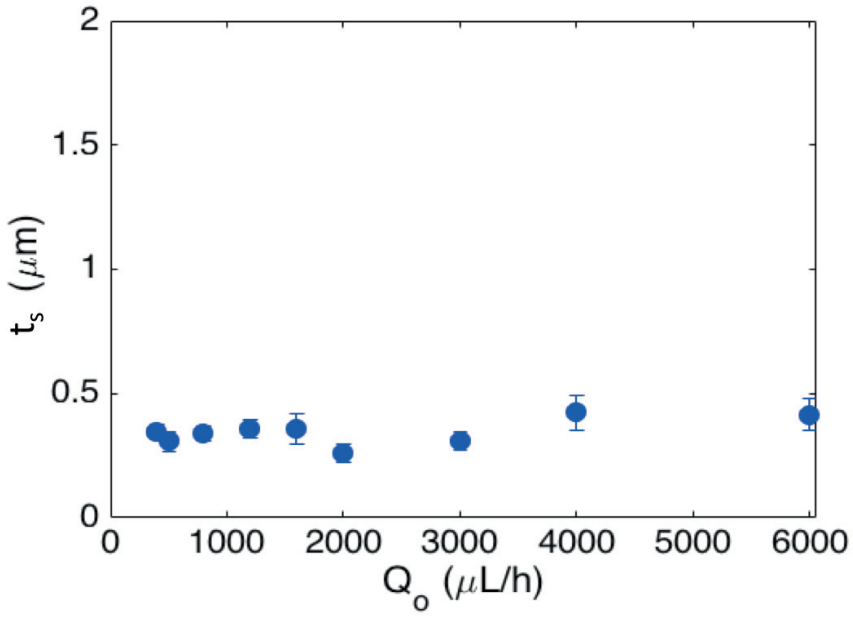

Figure 4.7: Influence of the flow rate of the outer channel Q_0 on the final shell thickness, t_s, of processed double emulsion drops; Q_i = 1000 μL/h and Q_w = 800 μL/h

Therefore, we keep Q_o constant at 800 μL/h for all the remaining experiments and do not further investigate this parameter.

The dimensions of double emulsion drops generated in microfluidic flow focusing devices depend on the fluid flow rates. To test if this is also the case for the aspiration device, we vary the injection and withdraw rates for $Q_i > Q_w$. We consider the aspiration device to function properly, if the standard deviation of the shell thickness, σ, is below 0.1 μm. This is the case if double emulsions are injected at rates not exceeding the withdraw rates by more than 50% and if $Q_i > 250$ μL/h, as summarized by the green shaded area in Figure 4.8A and shown in the optical micrograph in Figure 4.8C. By contrast, if $Q_i < 250$ μL/h or if $Q_i > 0.5$ Q_w, the shell thicknesses of the processed double emulsions are polydisperse, as summarized by the red shaded area in Figure 4.8A and in the optical micrograph in Figure 4.8D. We assign this behavior to the pressure profile in the device: the pressure in the main channel within the aspiration section decreases because a significant fraction of the liquid is removed through the shunt channels [117]. As a result, the pressure difference between the main channel and the aspiration reservoir, and therefore the pressure gradient across the shunt channels, gradually decreases within the aspiration section, as detailed in Section 4.3.3. With decreasing pressure gradient across the shunt channels, the driving force for oil to be removed from the double emulsion shells is reduced. At some point, the pressure gradient is so small that no oil is removed anymore. In fact, if the ratio of the withdraw to the injection rate is too low, the pressure gradient in the shunt channels located towards the end of the aspiration section becomes negative such that some of the oil contained in the reservoir is re-injected into the main channel, as shown in the optical micrograph in Figure 4.8D. This re-injected oil broadens the distribution of the shell thicknesses of the

processed double emulsions. Based on these results, the remaining experiments are conducted in the green shaded area.

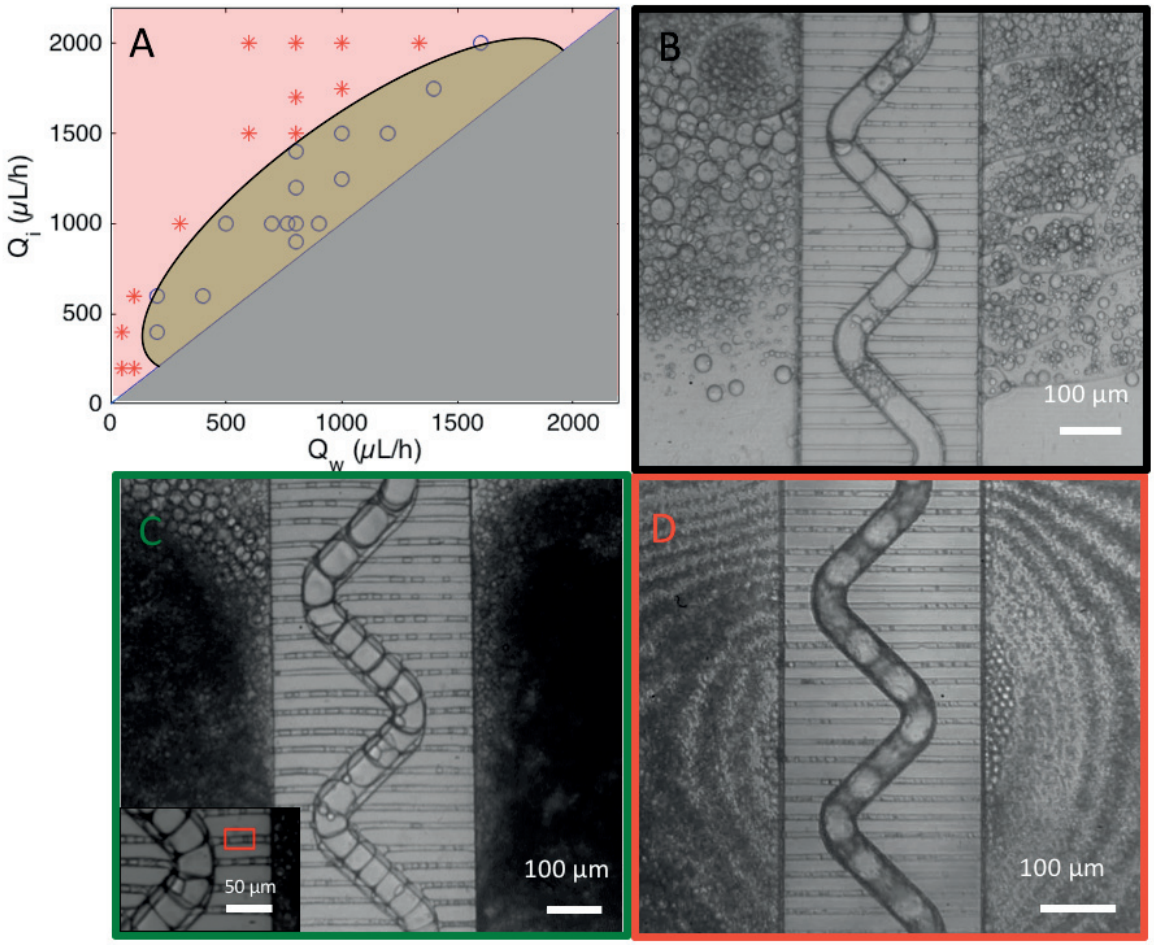

Figure 4.8: Operation of the aspiration device. (**A**) Influence of the injection rate, Q_i and the withdraw rate, Q_w, on the operation of the device. Operation conditions that result in double emulsions with a standard deviation of the shell thickness $\sigma \geq 0.1$ μm ($\star$), and $\sigma \leq 0.1$ μm ($\circ$). If $Q_w > Q_i$, the vast majority of double emulsions exit the device through the shunt channel such that we cannot control their shell thickness; this regime is indicated in grey. Based on the results, we indicate the optimum operation conditions in green and conditions where the device fails to consistently remove oil in red. **(B-D)** Optical micrographs of the aspiration device operating (**B**) in the grey area where the majority of double emulsions exit the device through the shunt channels, (**C**) under optimal conditions, and (**D**) when it fails.

The dimensions of emulsions produced in microfluidic devices can often be tuned with the fluid flow rates. To test if this is also the case for the aspiration device, we vary Q_i from 1600 μL/h to 900 μL/h and keep Q_w constant at 800 μL/h. The shell thickness linearly decreases with decreasing Q_i, as shown by the red diamonds in Figure 4.9A. Similarly, if we decrease Q_w from 800 μL/h to 200 μL/h and keep Q_i constant at 900 μL/h, the shell thickness linearly increases, as shown by the blue circles in Figure 4.9A. The excellent agreement of the shell thicknesses obtained by varying either Q_i or Q_w and keeping the other flow rate constant suggests that the

shell thickness depends on the difference in Q_i and Q_w, $\Delta Q = Q_i$ - Q_w only and does not depend their absolute values. To test this suggestion, we vary the absolute values of Q_i and Q_w, keeping ΔQ constant at 200 μL/h. Indeed, the shell thickness of double emulsions is independent of the absolute values of Q_i and Q_w, as shown in Figure 4.9B.

Our results suggest that the shell thickness of processed double emulsions is determined by the pressure gradient across the shunt channels and hence, by the pressure profile in the aspiration section. To better understand this result, we estimate the pressure profile across the main channel using an electric circuit analogue, as shown in Figure 4.2 and detailed in Section 4.3.3. For constant ΔQ, the model predicts the pressure to drop quickly in the first part of the aspiration section and level off thereafter as seen in Figure 4.3A. Interestingly, while the pressure in the initial parts of the aspiration section depends on Q_i, it varies very little with the absolute value of Q_i at the end of the aspiration section, as shown in Figure 4.3A. To test the validity and accuracy of the model, we convert the pressure profile into a velocity profile of the drops in the main channel, as detailed in Figure 4.3B, and compare it to experimental results. To experimentally quantify the velocity profile, we monitor the flow of the drops in the aspiration section using a high-speed camera and measure the drop speed as a function of the location within the channel, as examplified in Figure 4.1 and detailed in Section 4.3.3. Because liquid is continuously removed through the shunt channels, the speed of the drops in the main channel successively decreases, well in agreement with our model, as a comparison of the symbols and the solid line in Figure 4.9C reveals. As expected, the initial speed of injected drops increases with increasing Q_i. Our model predicts the speed of the drops in the final parts of the aspiration section to only depend on ΔQ. To test this prediction, we keep ΔQ constant at 300 μL/h and vary Q_i between 1000 μL/h and 2000 μL/h. Indeed, the velocity of the drops at the end of the aspiration section is the same, 18 mm/s, as shown in Figure 4.9C, well in agreement with our model. To further experimentally test our model prediction, we inject the drops at a constant rate Q_i and vary ΔQ. While the speed of the double emulsions in the initial part of the aspiration section is the same, their velocity in the final section decreases with decreasing ΔQ, as shown in Figure 4.9D. For example, the speed of double emulsions injected with Q_i = 900 μL/h decreases from 53 mm/s to 5 mm/s if ΔQ = 100 μL/h, but decreases only to 12 mm/s if ΔQ = 200 μL/h. These results demonstrate that even though we employ a very simple model that, for example, neglects any contribution of the drops contained in the main channel to its induced hydrodynamic resistance [109], it correctly captures influences of fluid flow rates on the pressure and velocity profile in the main channel. These parameters are directly related to the shell thickness of processed double emulsions such that we can use this model to optimize the device design and operation conditions.

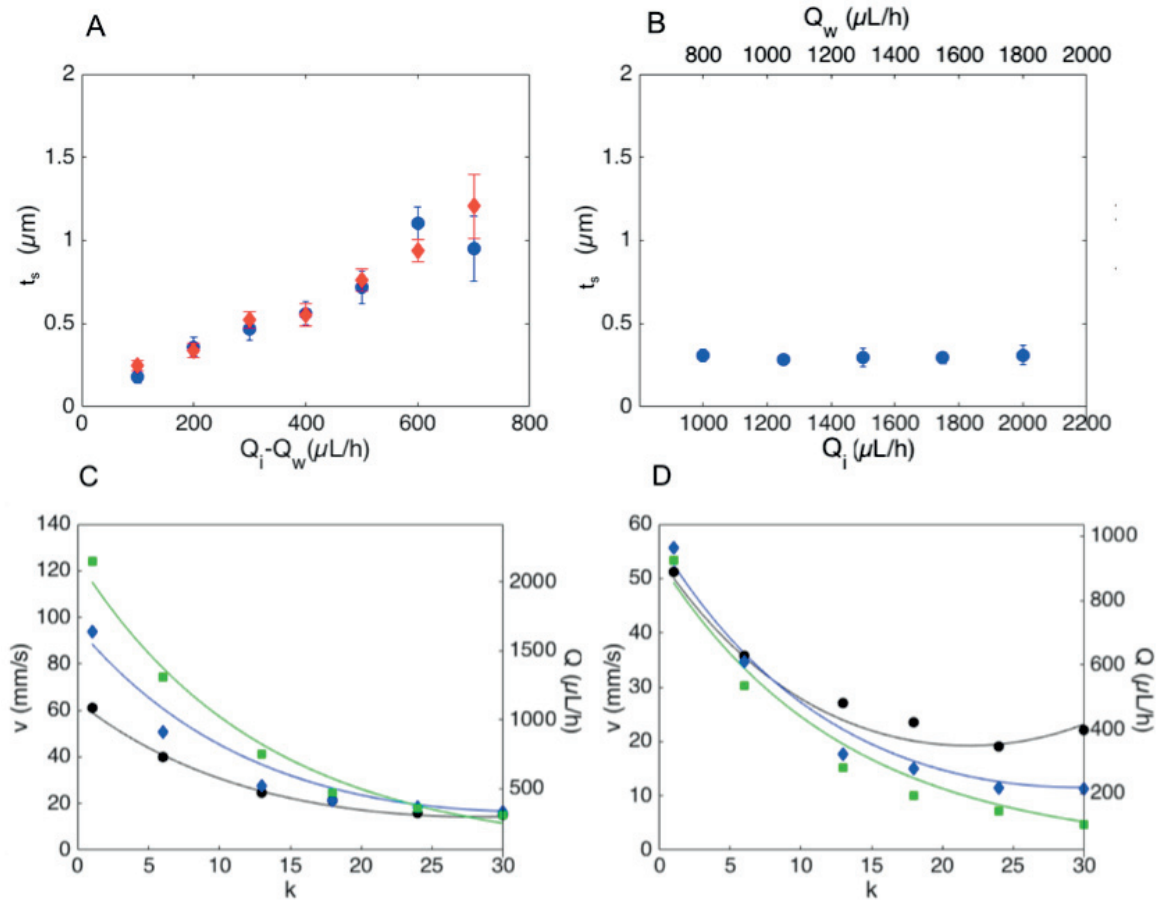

Figure 4.9: Influence of fluid flow rates on the shell thickness,t_s of processed double emulsions. (**A**) Influence of the injection rate, Q_i, and withdraw rate, Q_w, on the thickness of processed double emulsions, t_s, if Q_i is varied and Q_w is kept constant at 800 μL/h (♦) or if Q_w is varied and Q_i is kept constant at 1000 μL/h (•). (**B**) Influence of Q_i and Q_w on t_s if ΔQ is kept constant at 200 μL/h. (**C**) Velocity of drops, v, and corresponding flow rate, Q, as a function of their location in the main channel measured as the number of shunt channels located upstream the location of interest, k, for ΔQ = 300 μL/h and Q_i = 1000 μL/h (•), 1500 μL/h (♦) and 2000 μL/h (■). The velocity profile of fluids is estimated using an electric circuit analogue using Q_i = 1000 μL/h (black solid line), 1500 μL/h (blue solid line) and 1000 μL/h (green solid line). (**D**) Speed profile, v, and corresponding fluid flow rate, Q, in the main channel as a function of the location in main channel, k, for Q_i = 1000 μL/h and ΔQ = 100 μL/h (■), 200 μL/h (♦) and 400 μL/h (•). The corresponding calculated values are shown by the solid lines.

The velocity of the drops strongly decreases as they pass the first 15 shunt channels and levels off thereafter as seen in Figure 4.9C and D. The non-linear deceleration of drops in the aspiration section suggests that the amount of removed fluid quickly decreases as drops pass the aspiration device. However, it is unclear whether the total amount of removed fluid directly correlates with the amount of oil removed from the double emulsion shells.

4.4.3 Influence of the number of microchannels on removal efficiency

To decouple the removal of the continuous phase from that of the oil, we fabricate aspiration devices with n = 10, 20, 43 and 57 shunt channels and measure the thickness of double emulsions processed with these devices. Thereby, we keep the injection and withdraw rates constant at Q_i = 1000 μL/h and Q_w = 800 μL/h. Devices with no more than 20 shunt channels fail to efficiently and consistently remove the oil from double emulsion shells: these devices remove a considerable amount of the continuous phase but only a limited amount of the oil. For example, devices with n = 10 shunt channels reduce the shell by only 39 vol% whereas devices with n = 20 shunt channels reduce the shell volume by 54 vol%. This oil removal is much lower than achieved in devices with n = 30 shunt channels where it amounts to 95 vol%, as summarized in Figure 4.10. We assign the much lower oil removal efficiency obtained in devices with n = 20 to the density of the drops in the main channel: while these devices remove a considerable amount of the continuous phase, adjacent drops are still spatially separated from each other by the continuous phase such that they do not jam. By contrast, for devices with n = 20, a sufficient amount of continuous phase is removed such that drops jam. This observation suggests that jamming is crucial for an efficient removal of the oil. In line with this observation, the shell thickness distribution of double emulsions processed in devices with n = 20 is much broader than if processed in devices with more shunt channels, as shown by the large error bars in Figure 4.10.

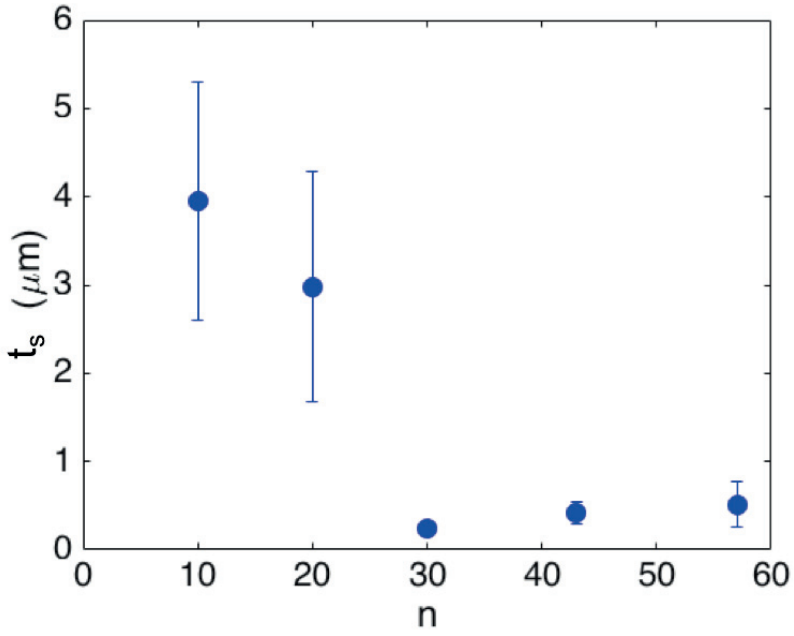

Figure 4.10: Influence of the number of shunt channels, n, on the shell thickness of processed double emulsions, t_s, that were injected with Q_i = 1000 μL/h, whereas Q_w = 800 μL/h and Qo = 800 μL/h.

Our results suggest that oil is most efficiently removed if drops are jammed. To test if we can reduce the shell thickness of double emulsions even more, we prolong the time jammed drops are in the aspiration section by increasing the number of shunt channels. If we process double emulsions in devices with $n = 43$ shunt channels, they have slightly thicker shells than if processed in device with $n = 30$. Their shell thickness increases even more if n is increased to 57, as shown in Figure 4.10. These results indicate that there is an optimum number of shunt channels. If this optimum is exceeded, the pressure gradient across the shunt channels located furthest downstream becomes negative such that some of the oil, that initially has been removed from double emulsion shells, is re-injected into them further downstream. For W/O/W double emulsions composed of a shell with a viscosity of order of that of water, and for $\Delta Q = 200$ μL/h, this optimum is around $n = 30$.

4.4.4 Influence of primary double emulsions shell thicknesses

Our results indicate that the shell thickness of double emulsions processed with the aspiration device depend on the velocity at the end of the channel only. Therefore, we expect it to be independent of the shell thickness of the primary double emulsions. To test this expectation, we produce primary double emulsions with shell thickness varying between $t_s = 2.31 \pm 0.22$ μm and $t_s = 7.01 \pm 0.73$ μm. These double emulsions are injected into the aspiration device at $Q_i = 1000$ μL/h and we withdraw fluids at $Q_w = 800$ μL/h. Independent of the shell thickness of primary emulsion drops, that of the processed double emulsion drops is $t_s = 0.37 \pm 0.11$ μm, as shown in Figure 4.11A. These results suggest that the aspiration device can reduce the distribution of shell thicknesses in double emulsions. To demonstrate this feature, we fabricate a mixture of double emulsions with an external radius of 53.1 ± 1.8 μm, whose shell thicknesses vary from 5 to 20 μm, as shown in the optical micrograph in Figure 4.11B. After this mixture has been processed with the aspiration device, we obtain double emulsions whose shell thicknesses vary by as little as 80 nm, as indicated by the narrow distribution of the shell thicknesses of double emulsions shown in Figure 4.11C. These results demonstrate the potential of the aspiration device to process polydisperse single-core double emulsions into double emulsions with well-defined shell thicknesses and thereby to facilitate the control over their mechanical stability and permeability.

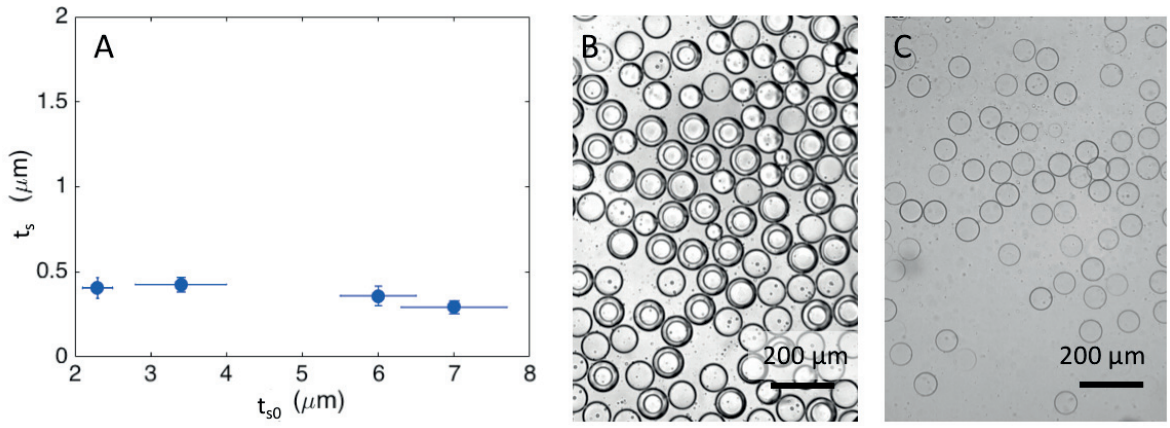

Figure 4.11: Influence of the shell thickness of primary double emulsions. (**A**) Influence of the shell thickness of primary double emulsions, t_{s0}, on that of processed counterparts, d, for initial double emulsions with t_{s0}, = 2.3 ± 0.2 μm, 3.4 ± 0.6 μm, 6 ± 0.5 μm and 7 ± 0.7 μm. (**B-C**) Optical micrographs of (**B**) primary double emulsions that have polydisperse shell thicknesses with t_{s0} = 10.3 ± 6.2 μm and (**C**) double emulsions after they have been processed with the aspiration device, whose shell thickness is t_s = 0.272 ± 0.081 μm.

4.4.5 Influence of the oil phase

The aspiration device removes up to 95 vol% of the oil from the shell of double emulsions. We expect the fraction of removed oil to depend on the fluid viscosity because this parameter influences the hydrodynamic resistance of the shunt channels and hence the pressure gradient across them. To test this expectation, we vary the viscosity of the oil, η, from 0.9 to 2.7 mPa.s by adding different amounts of Krytox^{TM} GPL, a more viscous perfluorinated oil, to HFE 7500 ^{TM}, as detailed in Chapter 2 [1]. Indeed, the amount of oil that is removed decreases with increasing oil viscosity such that the velocity of the double emulsions at the end of the aspiration section increases, as shown in Figure 4.11A. As a result, the shell thickness of the processed double emulsion increases with increasing oil viscosity, as shown in Figure 4.11B.

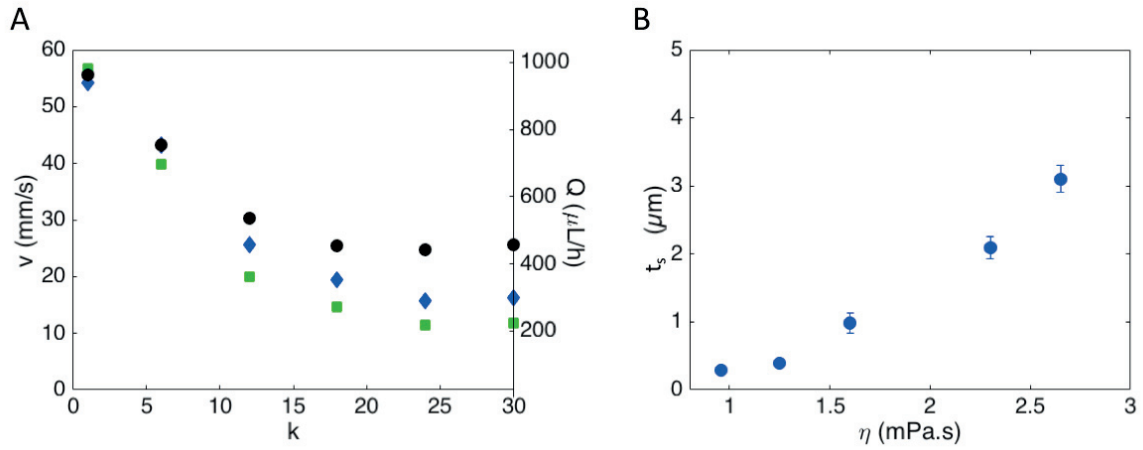

Figure 4.12: Influence of the oil viscosity. (**A**) Velocity of drops, v, as a function of the number of shunt channels located further upstream, k, of double emulsions with oil shells whose viscosity is η = 0.96 mPa.s (■), 1.25 mPa.s (♦) and 1.6 mPa.s (●). The flow rates are kept constant at Q_i = 1000 μL/h, Q_w = 800 μL/h, and Q_o = 800 μL/h. (**B**) Influence of the viscosity of the oil, η, contained in the double emulsion shells on their shell thickness, t_s. Double emulsions have been processed with Q_i = 1000 μL/h, Q_w = 800 μL/h and Q_o = 800 μL/h.

To demonstrate the versatility of the device, we produce primary W/O/W double emulsions with different oils. In particular, we employ a hydrocarbon-based oil, oleic acid, and a liquid crystal (4-cyano-4-n-pentylbiphenyl, Sigma). The aspiration device reduces the volume of double emulsion shells composed of oleic acid by 83% from 4.67 ± 0.29 μm to 0.88 ± 0.21 μm. Similarly, the volume of shells composed of a liquid crystal is reduced by 81% from 5.70 ± 0.49 μm to 1.20 ± 0.21 μm, as shown in Figure 4.13. These results demonstrate that the aspiration device is not limited to the removal of perfluorinated oils but can be employed to remove many other fluids from shells of double emulsions.

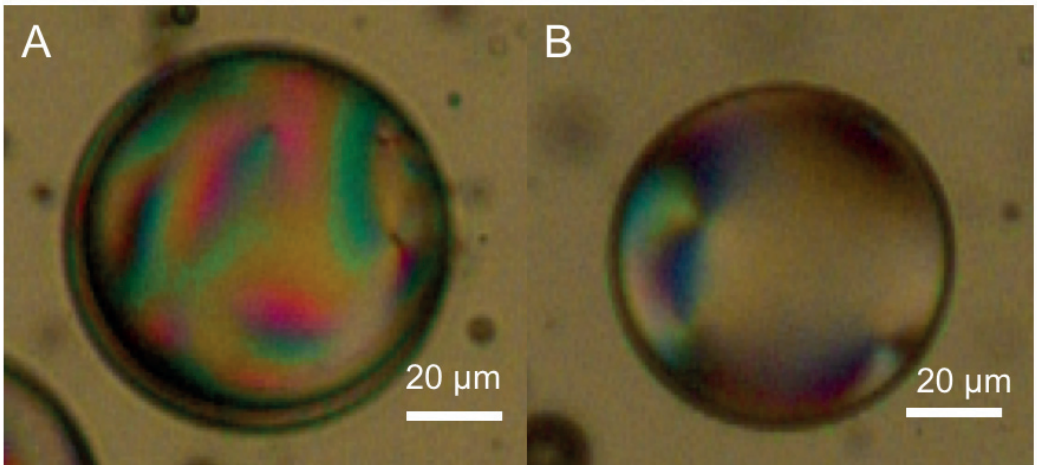

Figure 4.13: Optical micrographs acquired with polarized light of W/O/W double emulsions where the oil is a liquid crystal (**A**) before they are processed where t_s = 5.70 ± 0.49 μm and (**B**) after having been processed where t_s = 1.20 ± 0.21 μm.

4.5 Conclusion

We introduce a microfluidic aspiration device that enables reducing the shell volume of up to 1000 double emulsions per second by up to 95 vol%. The resulting double emulsions have shell thicknesses down to 240 nm. Importantly, the oil removal does not rely on a partitioning of the solvent into the continuous phase nor does it involve solvent evaporation. Hence, this device allows reducing the shell thickness of double emulsions made of a wide range of different fluids including non-volatile fluids or fluids that have a very low solubility in the outermost phase. Moreover, this device has the potential to reduce the shell thickness distribution of double emulsions produced through high throughput bulk emulsification methods because the shell thickness of the processed double emulsions is independent of that of injected double emulsions. The shell thickness of processed double emulsions only depends on the pressure profile in the device which can be controlled with the fluid flow rates and the viscosity of the oil. Therefore, this device offers new possibilities to fabricate capsules with thin shells whose thickness is well defined such that their stability and permeability can be closely controlled at high throughputs; this is of particular importance if capsules are used as delivery vehicles.

Chapter 5

Submicron shell double emulsion drops for screening assays

Antoine Vian, Gianluca Etienne and Esther Amstad

In this chapter, we study the influence of the shell thickness of double emulsions on their permeability. We demonstrate that double emulsions passively release hydrophilic components that are for practical purposes immiscible in the oil shell. We demonstrate that this transport of reagents across the shell can be limited if the shell is sufficiently thin.

This chapter is adapted from the paper entitled **"Cross-talk between emulsion drops: How are hydrophilic reagents transported across oil phases?"**, authored by Gianluca Etienne, Antoine Vian, Marjan Biocanin, Bart Deplancke and Esther Amstad, currently in refereed proceedings [3].

For the results presented in this chapter, G.E. synthetized the surfactant and performed the experiment to show the formation of spontaneous droplets in the cuvette and drew the schematic of a possible transport mechanisms. In addition he participated in writing the introduction. I performed the leakage experiments and developed the Matlab code for the analysis of the leakiness of double emulsions. I participated in writing the introduction and wrote the result and discussion part.

Contents

5.1 Abstract 69
5.2 Introduction 69
5.3 Material and methods 70
5.3.1 Production of double emulsions 70
5.3.2 Production of submicron shell double emulsions 70
5.3.3 Leakage measurements 71
5.3.4 Custom made MATLAB image analysis 71
5.4 Results 72
5.5 Discussion 75
5.6 Conclusion 76

5.1 Abstract

In this chapter, we investigate the passive transport of reagents across the shell of double emulsion drops that leads to cross-contaminations and hence limits the accuracy of droplet-based screening assays. To be truly efficient, those assays must be used with drops acting as closed containers to avoid that encapsulants are exchanged between different double emulsion drops. We demonstrate that this uncontrolled reagent transport can be decreased by at least an order of magnitude if the shell thickness of double emulsions is decreased down to submicrometer values. Based on our results, we suggest that fluorophores are transported across the oil shell by nanometer-sized droplets that spontaneously form in the shell of the double emulsions. This formation of small droplets is reduced if the shell becomes sufficiently small.

5.2 Introduction

Double emulsion drops produced with microfluidic devices can be used for biological screening assays at high throughputs [69, 119, 135–139]. However, for these assays to be truly useful, each drop should be impermeable to encapsulants to avoid cross-contaminations between drops. Drop-based screening assays are most often performed using single emulsion drops dispersed in perfluorinated oils. These oils are selected because they are biocompatible [140–142], have a high gas solubility, [96, 143, 144] and are compatible with PDMS devices [87]. Most frequently, the surfactant used for drop stabilization is composed of two perfluorinated polyether blocks that are interspaced by a hydrophilic PEG-based block, as shown in Section 2.1 [96, 97]. However the use of surfactants comes with an important disadvantage: Surfactants contribute to

spontaneous exchanges of reagents between different drops that are dispersed in perfluorinated oils [58, 145–151]. This cross-contaminations reduces the accuracy of drop-based screening assays [151] and therefore limits their performance and usefulness. The degree to which reagents are exchanged depends on their composition [147, 152–154]. It can be reduced if the viscosity of the oil is increased [146], if sugar [155], or bovine serum albumin (BSA) [145] is added to the aqueous phase, by lowering the surfactant concentration [145, 150], or by replacing surfactants with nanoparticles [9]. However the exact mechanism by which reagents are exchanged remains to be determined. Reagents might be transported across the oil by aggregates or inverse micelles that spontaneously form if surfactants self-assemble [145, 150, 151]. Additionally they could also be transported across the oil by aqueous drops that spontaneously form at liquid-liquid interfaces [156–159].

In this chapter, we establish the suitability of double emulsions with submicron shells for screening assays. To explain how reagents can permeate across the shell of W/O/W double emulsions stabilized with amphiphilic block copolymers, we propose a simple mechanism by which reagents are exchanged between two phases. Our results suggest that small aqueous drops with diameters of the order of hundreds of nanometers spontaneously form at the water oil interface and transport hydrophilic reagents across the oil shell. We demonstrate that the spontaneous formation of drops at the liquid-liquid interface and therefore the cross-contaminations can be reduced by at least an order of magnitude if the thickness of double emulsion shells is reduced to dimensions that are of the same order as the diameter of the small aqueous drops.

5.3 Material and methods

5.3.1 Production of double emulsions

Water-oil-water double emulsions were produced by injecting the liquids with syringe pumps (Cronus Sigma 1000, Labhut, UK). The outer phase was injected at 3000 μL/h, the middle phase at 700 μL/h, and the inner phase at 900 μL/h. The inner phase is composed of water containing 15 wt% PEG with a molecular weight of 6000 Da (Carl Roth, Germany) and 0.1 wt% fluorescein disodium salt (Carl Roth, Germany). The middle phase is composed of HFE-7500 containing 1mM of fluorinated surfactant. The outer aqueous phase is composed of water containing 10 wt% PVA (Mw = 13-18 kDa, Sigma-Aldrich, USA). The osmolarity of the two aqueous phases were measured using an Osmometer (Advanced Instruments, Fiske 210) and matched by adding D(+)-Saccharose (Carl Roth, Germany).

5.3.2 Production of submicron shell double emulsions

Double emulsions with shells thickness below 1 μm were produced using the microfluidic aspiration device presented in Chapter 4. Double emulsions with an outer diameter of 92.1 $\pm$

0.9 μm and a shell thicknesses, $t_s = 8.40 \pm 0.62$ μm were injected in the microfluidic aspiration device at $Q_i = 900$ μL/h. Oil was withdrawn through the shunt channels at a rate of $Q_w = 800$ μL/h. To spatially separated double emulsions with thin shells, an additional aqueous phase containing PVA was injected downstream the aspiration section at $Q_o = 800$ μL/h.

5.3.3 Leakage measurements

To minimize the influence of PVA on the transport of encapsulants, double emulsions were washed with an osmotically balanced aqueous solution containing sucrose. To wash the sample, 10 μL double emulsions was added to 1 mL water, double emulsions sedimented and the supernatant was removed. This procedure was repeated three times. Double emulsions were added into plastic wells that have previously been filled with the aqueous washing solution. Wells were sealed with mineral oil (Sigma-Aldrich, USA) to prevent evaporation of the water. Fluorescent microscopy images were recorded every 10 min with 15 ms exposure and analyzed using a custom-made MATLAB code that detects the double emulsions and quantifies the intensity inside each double emulsion over time.

5.3.4 Custom made MATLAB image analysis

A Matlab code was developed to monitor the leakage of double emulsion. The first command consists of importing the timelapse fluorescence images of double emulsions and converting them into an image sequence. Consequently, all the images are converted into 8-bits as seen in Figure 5.1B. Hence if a pixel is dark its value is 0 px, if it is at its maximum brightness its value is at 256 px. We then calculate the average pixel value of all the pixels in the image: A. If a pixel is above this value, A, used as threshold, it is selected to be labeled as fluorescent, if a pixel value is below, it is selected to be labeled as background, as exemplified by respectively the white selected pixels and the black background, seen in Figure 5.1C. We then calculate the mean intensity within the fluorescent pixels: A_F. Similarly we calculate the mean intensity within the background pixels: A_B. The mean fluorescent intensity of the drops for a given image is then determined as: I = A_F - A_B.

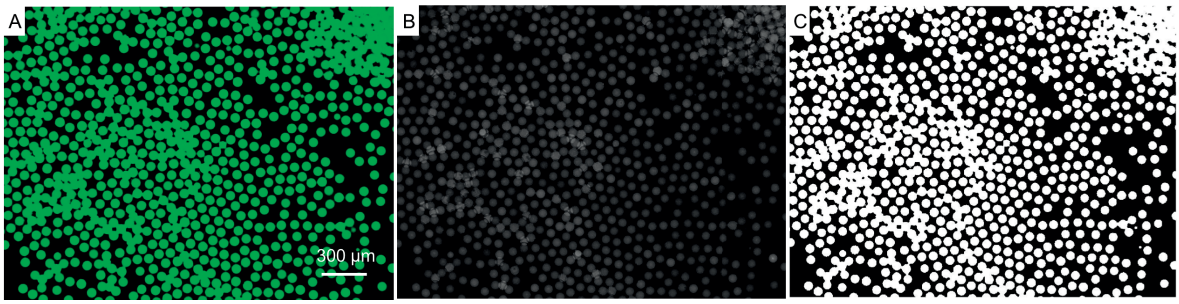

Figure 5.1: Analysis of the leakage of double emulsions using a custom-made MATLAB code (**A**) Fluorescent image of double emulsions with 0.1 % fluorescein in their core. Each green circle corresponds to a double emulsion. (**B**) Image converted in 8-bits. (**C**) In white: Selected pixels whose intensity is above the mean treshold A and hence that are labeled as fluorescent. In black: Selected pixels whose intensity is below the threshold A that are labeled as background

5.4 Results

W/O/W double emulsion drops with a shell thickness, $t_s = 9.91 \pm 0.52$ μm, and a diameter of 90.4 ± 0.7 μm containing 0.1 % fluorescein in their core are produced with a microfluidic double emulsion device (as described in Section 1.3.5). They are thoroughly washed with an aqueous solution to remove PVA initially contained in the continuous phase. To prevent osmotic pressure gradients that would change the dimensions of double emulsions during collection and storage, we balance the osmolarities of the two aqueous phases using D-saccharose. Drops are then placed in closed wells and observed with fluorescence microscopy. The vast majority of fluorophores are released in less than 5 hours, as seen in Figure 5.2. This is surprising because the solubility of fluorescein in the oil phase is very low, suggesting that this transport cannot solely be caused by diffusion.

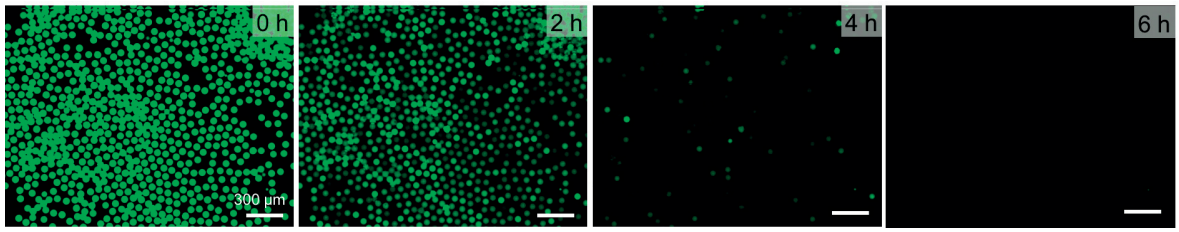

Figure 5.2: Optical fluorescent microscopy timelapse of double emulsion with $t_s = 9.91 \pm 0.52$ μm.

To determine the mechanisms of the transport through the membrane, we first develop a very simple model of an oil-water interface. A solution of HFE-7500 containing 1 mM of surfactant is covered with a water layer. Immediately after the sample is prepared the solution is transparent. However after 10 hours, the sample becomes turbid even though it is not mechanically agitated, as shown in Figure 5.3A. By contrast, when pure oil without surfactant is put in contact with water, the oil remains transparent, as shown in Figure 5.3B. These results indicate that objects

that are within the size of the wavelength of visible light are created. Inverse micelles usually have sizes well below the wavelength of visible light [144]. Our results suggest that small aqueous drops form at the liquid-liquid interface by analogy to what has been reported for osmotically stressed double emulsions [156–158]. Hence our this that small droplets that are within the range of hundreds of nanometers can form in the absence of osmotic pressure gradients and if block copolymers are used as surfactants. Therefore small aqueous droplets that spontaneously form might act as transport vehicles for fluorescein within the oil phase.

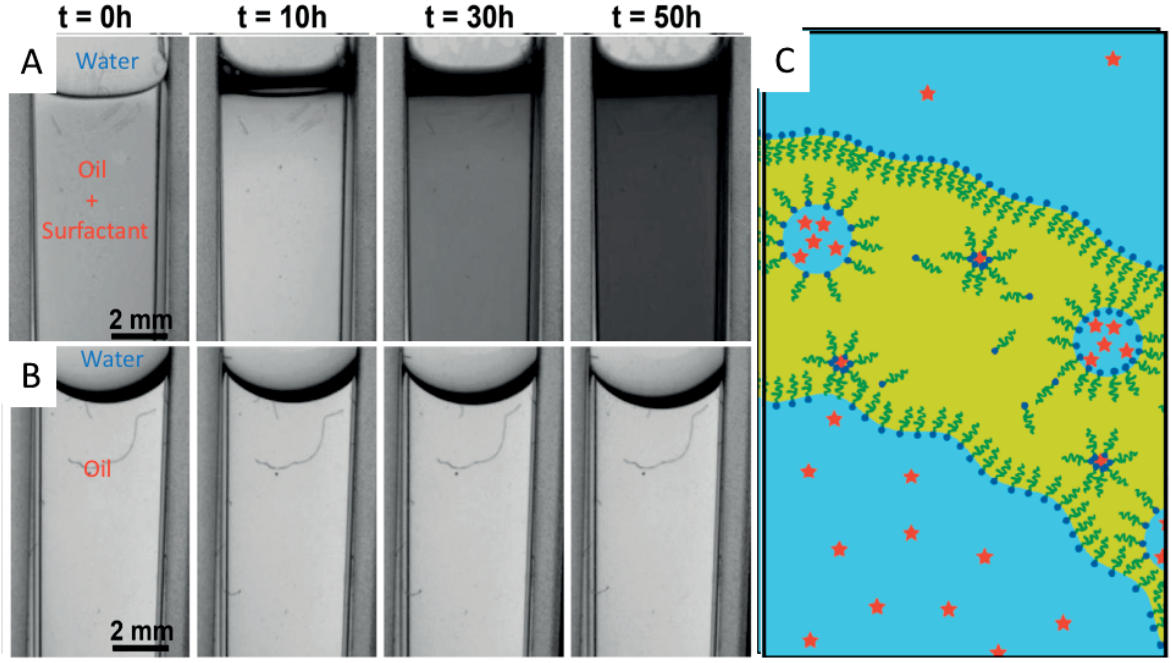

Figure 5.3: Spontaneous formation of small aqueous drops in perfluorinated oils. (**A,B**) Time-lapse photographs of fluorinated oil (HFE7500) (**A**) with 1 mM of fluorinated surfactant (**B**) without surfactant. (**C**) Schematic illustration of the proposed mechanism responsible for leakage of reagents across the membrane. Image is not to scale

If the transport of reagents is caused by hundred nanometer diameter droplets, we expect it to be slowed down if we reduce the shell thickness to values that are similar to those of the diameter of the small spontaneously formed drops. To produce double emulsions with submicron shell thicknesses, we employ the microfluidic aspiration device and produce double emulsions with shell thicknesses down to $t_s = 330$ nm [2]. The amount of fluorescein that is released from double emulsion drops with shell thicknesses that vary from $t_s = 8.40 \pm 0.62$ μm to $t_s = 0.330 \pm 0.060$ μm is measured every 10 min for 15 h. Remarkably the vast majority of fluorescein is released after 6 h for double emulsions with $t_s = 8.40 \pm 0.62$ μm, as shown in Figure 5.4A. By contrast, if t_s is reduced to 330 nm, only 15 % of the initial intensity is lost after 15h, as shown in Figure 5.4B .

Our results suggest that the leakage rate scales with the shell thickness of the drop. To test this hypothesis, we produce double emulsions with five different shell thicknesses, $t_s = 13.46$

$\pm$ 1.23 μm, 9.91 $\pm$ 0.52 μm, 6.75 $\pm$ 0.48 μm, 4.68 $\pm$ 0.48 μm and t_s = 0.33 $\pm$ 0.06 μm, all the double emulsions contain 0.1 % fluorescein in their core. We then measure the fluorescent intensity of the drops every 10 min for 15 h. The mean fluorescence intensity for each image of the timelapse is calculated as the average pixel intensity for all droplets using a custom made Matlab program. For double emulsions with t_s =13.4, 9.8, 6.3 and 4.1 μm; the vast majority of fluorescein is released after respectively, 200, 300, 460 and 600 min. By contrast, double emulsions with submicron shells only release 15 % of the initial intensity is lost after 15 h, as shown in Figure 5.4C. Hence there is a clear correlation between the shell thickness and the leakage time of these drops.

The rate of leakage can be characterized by the slope by which the intensity decreases over time. To characterize this slope, we define τ as the time necessary for the fluorescent intensity to decrease by 50 % from its original value. We repeat this observation in five independent experiments and retrieve the values for τ. For double emulsions with t_s = 13.4 μm, τ = 80 min. As the shell thickness is decreased down to t_s = 4 μm, τ increases up to 200 minutes. By contrast, for shells as thin as 330 nm, τ = 1600 min. Hence τ of double emulsions with submicron shells is an order of magnitude higher than that of drops whose shell thickness is above a micrometer. Our results suggest that double emulsion drops with extremely thin shells are candidates for producing non-leaky capsules that reduce cross-contaminations without negatively impacting the stability of drops, as shown on Figure 5.4C.

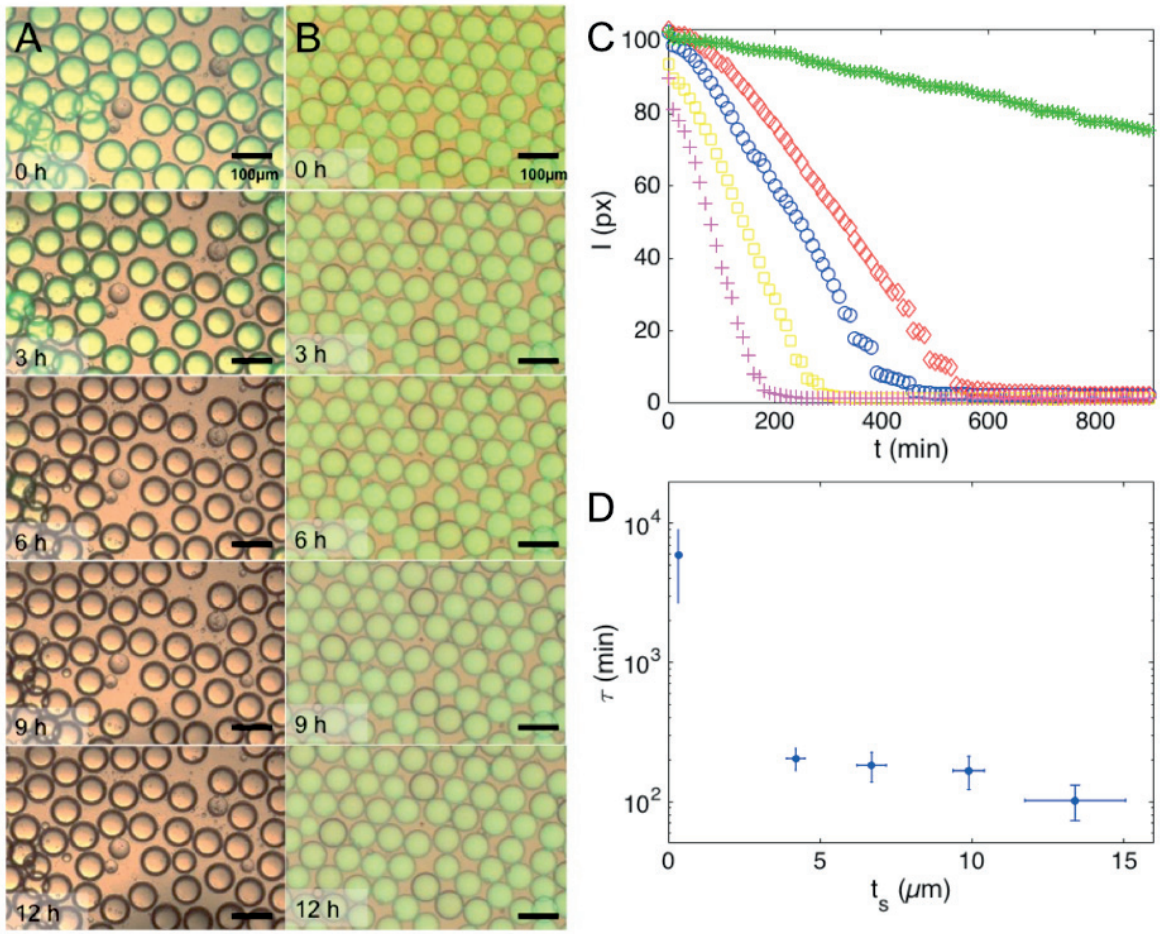

Figure 5.4: (**A**) Timelapse of superimposed optical and fluoresence migrographs of double emulsion drops with shell thickness $t_s = 8.40 \pm 0.62$ μm containing 0.1 % fluorescein in their cores. (**B**) Timelapse images of double emulsion drops with thin shells , $t_s = 0.33 \pm 0.06$ μm, containing fluorescein in their cores. (**C**) Decrease of intensity, I, as a function of time , t, in in double emulsions with shell thicknesses; $t_s = 13.46 \pm 1.23$ μm , (+); $t_s = 9.91 \pm 0.52$ μm, (□); $t_s = 6.75 \pm 0.48$ μm, (○); $t_s = 4.68 \pm 0.48$ μm , (◇), $t_s = 0.33 \pm 0.06$ μm , (∗). (**D**) Influence of the shell thickness, t_s, on the leakage time, τ. The error bars in x and y directions correspond to the standard deviations measured from five independent leakage experiments.

5.5 Discussion

We assign the decrease in permeability to the steric hindrance that prevents the formation of aqueous droplets in the oil shell. The thinner shells have a higher hydrodynamic resistance that slows down the convective flow of oil within the membrane, thereby reducing the propensity for small aqueous drops to form at the liquid-liquid interface. Therefore, transport of components across the double emulsion shell is reduced when the shell thickness of double emulsion drops is reduced. These results demonstrate that the permeability of double emulsions can be reduced by more than an order of magnitude without changing the composition of the surfactants by simply reducing the thickness of the oil shell. This reduction in shell thickness constitutes an

elegant way to minimize the transport of reagents across the shell of double emulsion drops, and thereby offering new ways to improve the accuracy of screening assays.

5.6 Conclusion

Emulsion drops are frequently employed as reaction vessels to conduct high throughput screening assays. The accuracy of these assays is often compromised by the exchange of reagents contained in different drops that causes cross-contaminations. Here, we demonstrate that the transport of reagents across the oil phase is caused by aqueous drops with diameters of the order of hundreds nanometers that spontaneously form in the oil phase. The propensity of these small drops to form and hence, the leakiness of large double emulsion drops can be strongly decreased if their shell thickness is reduced to values similar to the diameter of the small drops that spontaneously form in the oil. In this case, the formation of these drops is likely sterically hindered such that almost no encapsulants are transported across thin shells. From these mechanistic insights, design rules for emulsion processes can be derived that offer a tighter control over the permeability of emulsion drops. Hence, this understanding might open up new possibilities to use drop-based screening assays also for applications that require a high accuracy, including applications in pharmacy and food industries.

Chapter 6

Mechano-responsive microcapsules with thin, homogeneous shells

Antoine Vian and Esther Amstad

In this chapter, we use the microfluidic aspiration device presented in Chapter 4 to produce double emulsion with shell thickness below one micrometer that are used as templates to form capsules. We assess the homogeneity and the mechanical properties of those capsules and compare them to capsules possessing inhomogeneous shell thicknesses.

This chapter is adapted from the paper entitled **"Mechano-responsive microcapsules with thin, homogeneous shells"**, authored by Antoine Vian and Esther Amstad, currently in refereed proceedings [4].

Contents

6.1 Abstract 79
6.2 Introduction 80
6.3 Materials and methods 81
6.3.1 Double emulsion composition 81
6.3.2 Microcapsule fabrication 82
6.3.3 Imaging 82
6.3.4 Quantification of capsule footprint 82
6.3.5 Quantification of the permeability of capsules 82
6.3.6 Calculation of cumulative leakage 83
6.4 Results and discussions 83
6.4.1 Production of capsules with thin shells 83
6.4.2 Mechanical stability of capsules 87
6.4.3 Permeability of capsules 90
6.5 Conclusions 92

6.1 Abstract

Capsules often prolong the shelf-life of active ingredients, such as many drugs, food additives, or cosmetic substances, because they delay oxidation of these substances or prevent their reactions with molecules contained in the surrounding. If appropriately designed, these capsules can offer an additional benefit: they allow close control over the timing and location of the release of active ingredients. To take advantage of these features, capsules must possess shells whose thickness and composition is well-defined. However, the shell thickness of capsules often varies considerably even within a single capsule, thereby hampering good control over the release kinetics of encapsulants. These variations in shell thickness can be reduced, and hence the degree of control over the release kinetics increased, if shells are made thin. Unfortunately, the controlled fabrication of mechanically stable microcapsules with well-defined sub-μm thick shells is difficult. Here, we introduce a method to fabricate capsules with uniform, semi-permeable shells whose thickness is as low as 400 nm. This is achieved using water-oil-water double emulsions with 800 nm thick shells. The shell of the resulting capsules occupy less than 2 % of their volume, thereby minimizing their footprint. Despite their thin shells, these capsules are mechanically very robust: They withstand pressures up to 1.3 MPa without deformation and they remain intact if exposed to pressures up to 2.75 MPa. Moreover, while they are permeable towards water, they retain

encapsulants with molecular weights as low as 562 Da, even if dried and re-dispersed. The thin shells of the capsules open up new possibilities to use them to functionalize materials with at least one dimension that is small, such as coatings, where thick shells introduce defects, or as building blocks of new types of functional materials.

6.2 Introduction

Ideally, capsules are impermeable to encapsulants during storage and when applied, release their content on demand [129]. Capsules are often produced through spray-drying [160] or from single emulsion drops where the surface of drops is solidified for example through interfacial polymerization [161, 162], or phase separations [163]. These methods typically offer a limited control over the thickness of capsule shells, thereby compromising the control over the timing of the release of encapsulants as detailed in Section 1.2.4 [164–167]. Capsules can also be produced from double emulsion drops by solidifying their shell [39, 168]. The thickness of the so-formed capsule shells depends on the composition and dimensions of the double emulsion shell. Double emulsions with well-defined dimensions can be produced with microfluidic devices; these drops have diameters ranging from 60 to 700 μm and shell thickness varying between 2 and 140 μm; the shells of these capsules occupy between 20 to 85 % of the total capsule volume, thereby limiting the relative concentration of encapsulants contained in them [54, 56, 84, 168, 169]. The fabrication of capsules with thick shells from double emulsion drops comes at an additional cost: While the average thickness of these capsule shells is well-defined, the local shell thickness varies considerably within each capsule. This difference can be assigned to variations in the shell thickness of double emulsion drops that are caused by the density difference between the liquid that forms the innermost drop and the liquid that constitutes the outermost drop. This density difference causes an offset of the two drop centers, such that the shells are very thin on one side of the double emulsion drops whereas they are very thick on the opposite side [54]. This heterogeneity in shell thickness compromises the control over the diffusion time of encapsulants across the shell and hence, the control over the kinetics of the diffusion-limited release, as detailed in Section 1.3.6 [24, 93, 170].

This potential limitation can be alleviated if capsules are composed of a material that has a low affinity to the encapsulants. In most cases, encapsulants are either hydrophilic or hydrophobic and hence have a low affinity towards fluorinated materials. As a result of the low affinity, capsules with shells composed of perfluoropolyether retain more than 98 % of low molecular weight encapsulants, such as Allura Red and $CaCl_2$, over a period of four weeks, even though the thinnest part of their shell is below 20 μm [169]. This feature, combined with their thermal stability and chemical and biological inertness, [171] renders them attractive for applications that do not involve oral or intravenous administration of reagents. However, the shells occupy

approximately 70 % of the capsule volume, [169] thereby limiting the amount of reagents contained in them. Moreover, because perfluorinated polymers are chemically inert, they cannot easily be degraded such that residues of empty capsules might introduce defects into the materials encompassing them or they cause negative side-effects if used as dispersed delivery vehicles. The volume occupied by the shell can be reduced if they are produced from double emulsions with thin shells. These thin shells offer an additional benefit: the thickness of their shells is much more uniform because the fluid flow in thin shells is limited by lubrication effects such that the centers of the innermost and the outer drops are not offset [39, 126, 127]. Double emulsions with thin shells can be assembled using dedicated microfluidic glass capillary devices, as detailed in Section 1.3.7 [95, 106, 129, 131–133]. However, the fabrication and operation of these devices is tedious. Double emulsions with thin shells can also be produced from standard double emulsions by reducing their shell thickness, for example if pushed through constrictions, as detailed in Chapter 3 [1], or processed with the microfluidic aspiration device that removes the vas majority of the fluid contained in the shells through shunt channels, as detailed in Chapter 4 [2]. However, these double emulsions have never been employed as templates to produce polymeric capsules with thin, solid shells that display a low permeability towards encapsulants.

In this chapter, we combine the benefit of the chemical inertness of perfluorinated polymers and the low footprint of capsules made from double emulsions with thin shells: We fabricate 63 μm diameter capsules with homogeneous fluorinated shells that are as thin as 0.4 μm, such that the shell occupies as little as 2 % of the capsule volume. We investigate their mechanical properties and the permeability of these capsules towards low molecular weight encapsulants and compare these parameters to those of capsules whose shell has an identical composition but is 25 times thicker. Despite of their thin shells, these capsules are mechanically robust: they can withstand pressures up to 1.3 MPa without buckling. When exposed to higher pressures or when dried, they buckle but remain intact such that the permeability towards low molecular weight encapsulants remains unchanged. Because perfluorinated shells have a low affinity towards hydrophilic additives, they retain more than 98 % of the encapsulants with a molecular weight as low as 562 Da, such as Patent Blue V, for at least 4 weeks. However, when subjected to mechanical stress, they break, thereby releasing the encapsulants.

6.3 Materials and methods

6.3.1 Double emulsion composition

The core of double emulsions is composed of 7.5 wt% PEG (Mw = 6 kDa) and 5 wt% partially hydrolyzed PVA (Mw = 13 - 18 kDa) as an inner phase; PVA is added to increase the stability of the double emulsion drops. The fluorophilic shell is made of 75 wt% monoacrylate, 1H,1H,7H-Dodecafluoroheptyl acrylate, 15 wt% of diacrylate, 1H,1H,6H,6H-Perfluoro-1,6-hexyl

diacrylate, and 10 wt% fluorinated oil, HFE 7500, that contains 2 % of a photoiniator, 2-Hydroxy-2-methylpropiophenone; the fluorinated oil is added to increase the contrast of the double emulsions in the optical microscope. As an outer phase, we employ an aqueous phase containing 10 wt% partially hydrolysed PVA (Mw = 13 - 18 kDa).

6.3.2 Microcapsule fabrication

To convert double emulsions into capsules, they are exposed to UV illumination for 5 min (Omnicure Series 1000 UV). The resulting microcapsules are washed with deionized water to remove residual PVA.

6.3.3 Imaging

Optical images are acquired with a Nikon Eclipse Ti-S Inverted Microscope and Scanning electron microscope images are acquired with a Zeiss FESEM Supra55VP, operated using secondary electron detection at an acceleration voltage of 1 kV. Samples are deposited onto a one-side polished Si-wafer and coated with 10 nm of Platinium-Palladium coating to render it electronically conductive. UV-vis spectra are acquired with a PerkinElmer UV/Vis Spectrometer Lambda 40.

6.3.4 Quantification of capsule footprint

The footprint of capsules is defined as the volume fraction of the shell compared to the total volume of the drops. Because perfluorinated polymers have a low affinity to water, we assume the perfluorinated polymers to be collapsed if dispersed in aqueous solutions such that we approximate the shell thickness of capsules, d, in aqueous solutions to be similar to that measured in the dry state. Using this approximation, we estimate the volume fraction of the capsule occupied by the shell, the footprint F, as

$$F = \frac{(R^3 - (R-d)^3)}{R^3} \tag{6.1}$$

where R is the external radius of the capsule.

6.3.5 Quantification of the permeability of capsules

To measure the permeability of the capsules, we disperse 60 μL of polymerized capsules with thin shells, whose core is labelled with 2 % patent V into an Eppendorf tube containing 1 mL of deionized water. To acquire statistics, each data point is measured on four independent samples. The amount of dye contained in the supernatent is quantified as a function of the incubation time using UV-Vis spectroscopy (Perkin Elmer Lambda 365).The maximum intensity absorbance for the blue dye, A, is obtained at $\lambda = 637.5$ nm. This wavelength is used to quantify the amount of blue dye contained in the supernatent.

6.3.6 Calculation of cumulative leakage

To estimate the maximum amount of dye that can leak form the double emulsion, we disperse 0.06 mL of an aqueous solution containing 2 % blue dye in 1 mL of deionized water; this volume corresponds to the estimated cumulative volume of all the capsule cores contained in a sample. We measure the absorbance at $\lambda = 637.5$ nm, A_{max}. The absorbance measured for the supernatent of a sample, A, is normalized to A_{max} giving us the cumulative leakage intensity, I:

$$I = \frac{A}{A_{max}} \tag{6.2}$$

6.4 Results and discussions

6.4.1 Production of capsules with thin shells

We employ water-oil-water double emulsions as templates to produce capsules; these double emulsions are fabricated using PDMS based microfluidic flow focusing devices, as detailed in Section 2.2 and shown in Figure 6.1A [91]. To facilitate the fabrication of these double emulsions and to increase their stability, we add 7.5 wt% PEG and 5 wt% PVA to their cores. The oil shell is composed of a fluorinated oil, HFE7500, that contains 75 wt% of a fluorinated monoacrylate, 15 wt% diacrylate, and a photoinitiator. These double emulsions are dispersed in an aqueous phase containing 10 wt% PVA. Double emulsions are formed in microfluidic flow focusing devices by injecting the inner and middle phases are a rate of $Q_i = Q_m = 500$ μL/h into the device [91]. The outer phase is injected at $Q_o = 4000$ μL/h. The resulting double emulsions have a diameter of $R = 40 \pm 0.8$ μm and a shell thickness of $t_s = 9.21 \pm 0.91$ μm such that the shell occupies 30 % of the volume of the double emulsion

To reduce the volume occupied by the shell and therefore to minimize the footprint of the capsule, the shell of the double emulsion templates must be made thinner. To reduce the shell thickness of double emulsions, we process them with the microfluidic aspiration device. The aspiration device consists of a main channel whose cross-section is 60 μm x 70 μm. However, the diameters of double emulsions that can be processed with the aspiration devices is by no means limited to this narrow range. If the dimensions of the main channel are adjusted, double emulsions with diameters ranging from 10 μm up to a few 100 μm can be processed with this technique. The main channel is intersected by many much smaller fluorophilic shunt channels that lead into two reservoirs, as shown in Figure 6.1C and detailed in Chapter 4. Primary double emulsions are injected into the aspiration device at $Q_{in} = 900$ μL/h. To maximize the volume of oil that shunt channels remove from the shells of double emulsions, we reduce the pressure in the reservoirs by retracting fluids at $Q_w = 800$ μL/h [2]. Due to the reduced pressure in the reservoir, some of the continuous phase is also removed through the shunt channels such that primary double emulsions are up-concentrated while they flow through the aspiration

section. To increase the spacing between adjacent processed double emulsions after they exited the aspiration section, and thereby to facilitate their handling further downstream, we space them apart by injecting an aqueous solution through a flow focussing junction at $Q_{out} = 1500$ μL/h, as shown in the optical micrograph in Figure 6.1C [2]. The resulting double emulsions have an external diameter of $R = 32.5 \pm 1.0$ μm and a shell thickness as low as $t_s = 0.79 \pm 0.19$ μm, as examplified on the optical micrograph in Figure 6.1D. To convert double emulsions into capsules, their shells must be solidified. This can be achieved by exposing the double emulsions to UV light to initiate the polymerization reaction of the acrylates. The polymerized capsules are washed with deionized water before they are further characterized.

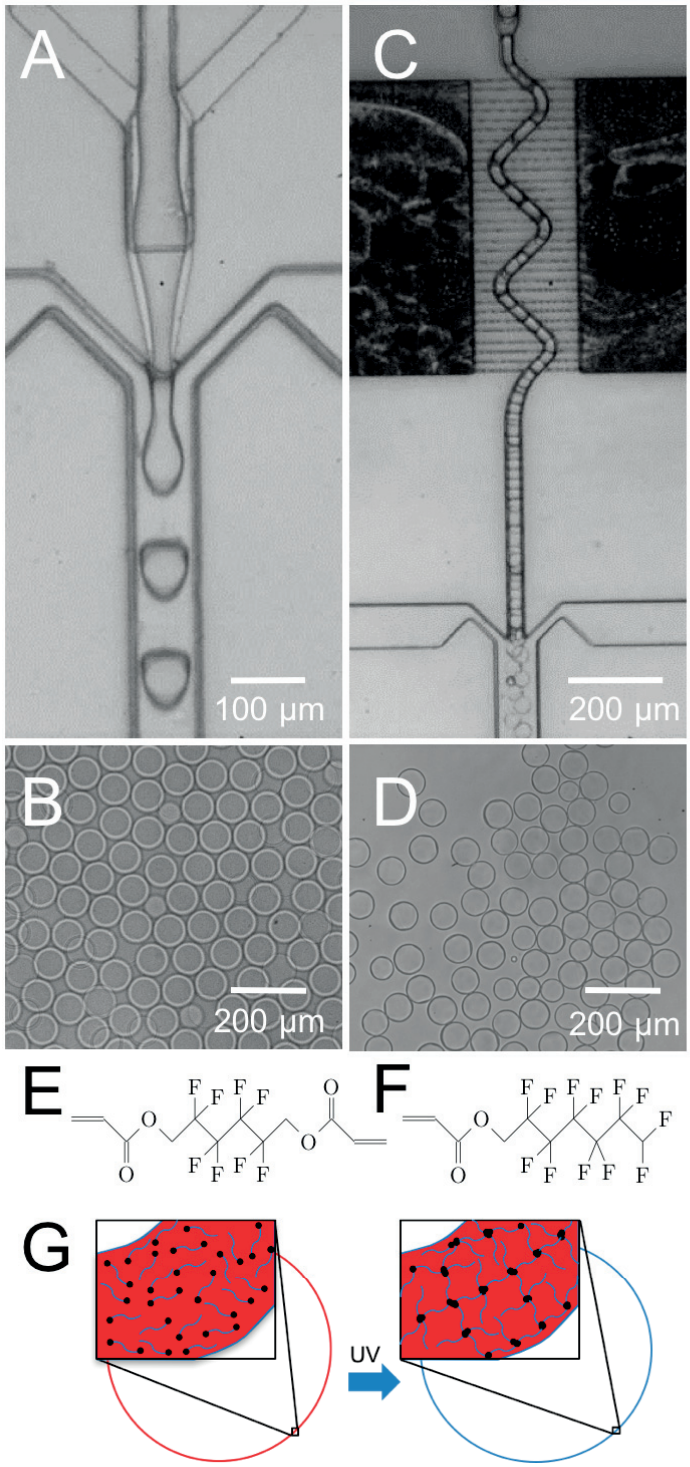

Figure 6.1: Optical micrographs of (**A**) a microfluidic double emulsion drop maker in operation and (**B**) the resulting double emulsions with shell thicknesses of 9.21 ± 0.91 μm. (**C**) Optical micrograph of the microfluidic aspiration device in operation and (**D**) the resulting double emulsions with shell thicknesses of 0.79 ± 0.19 μm. (**E ,F**) Schematic illustration of fluorinated (**E**) 1H,1H,6H,6H-Perfluoro-1,6-hexyl diacrylate and (**F**) 1H,1H,7H-Dodecafluoroheptyl acrylate. (**G**) Schematic illustration of water-oil-water double emulsions before they have been exposed to UV light, where their shells contain monomers (left) and thereafter, where monomers were crosslinked to form polymeric shells (right).

The degree of control over the mechanical properties of capsules and the release of active ingredients contained in them depends on the composition and dimensions of the capsule shells. To closely control these parameters, the thickness of the capsule shells must be uniform and well-defined. Optical micrographs of capsules made from as-produced double emulsion templates reveal large heterogeneities in the shell thickness, as shown in Figure 6.2A. By contrast, no significant differences in the shell thickness can be measured if capsules are produced from processed double emulsions whose shell thickness is below 1 μm, as shown in Figure 6.2B. However, potential heterogeneities in the dimensions of capsules with thin shells are difficult to quantify using optical microscopy because the average thickness of these shells is close to or even below the resolution limit of standard optical microscopes. To visualize the capsules with a higher resolution, we image dried capsules with scanning electron microscopy (SEM). Because of gravity, intact capsules will preferentially align with the thickest part of their shell facing the substrate such that the homogeneity of the capsule thickness is difficult to assess from SEM images of intact capsules, as shown in Figures 6.2C and D. To determine the homogeneity of the capsule thickness, we cut dried capsules with a razor blade and image them using SEM. Capsules produced from as-fabricated double emulsions have a shell thickness that varies over a wide range with the thickest part being at least 14 μm and the thinnest part being smaller than 3 μm, as seen in Figure 6.2E. By contrast, capsules made from processed double emulsions have uniform shells that are as thin as 400 nm, as shown in Figure 6.2F. These results indicate that in processed double emulsions, gravitational forces are outweighed by lubrication forces such that the center of the innermost aqueous core of the double emulsion templates is close to that of the outer, perfluorinated core [93, 95, 126].

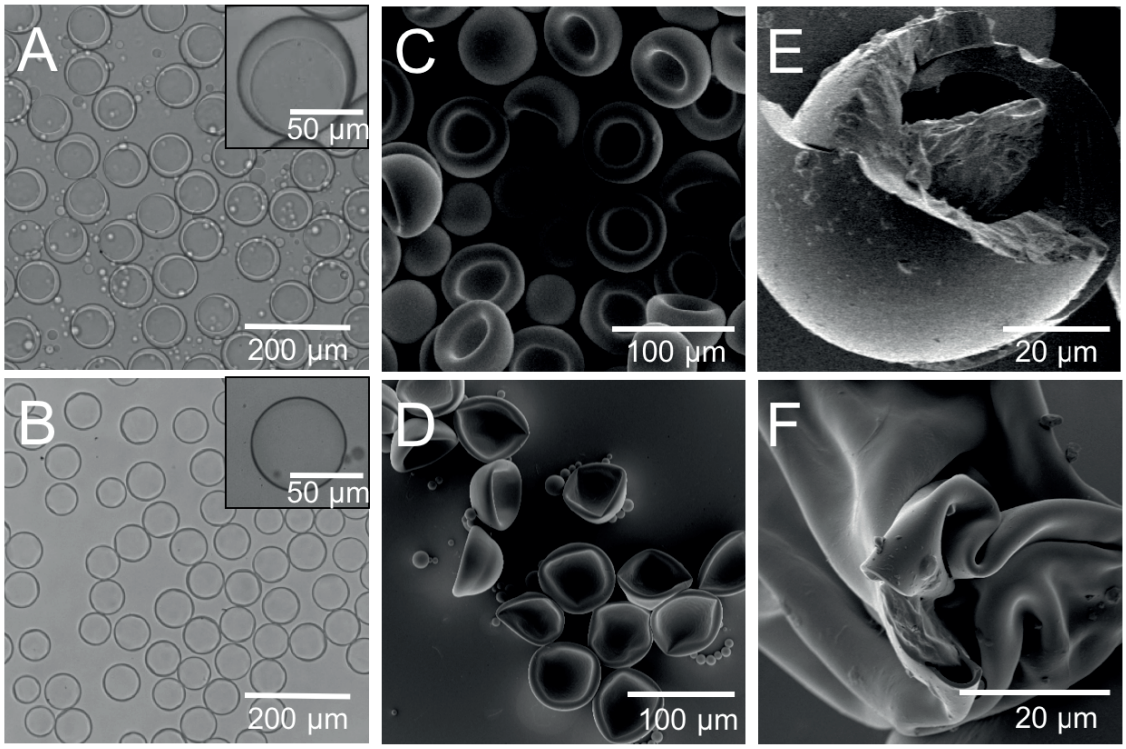

Figure 6.2: (**A , B**) Optical microscopy images of capsules made from (**A**) as-produced double emulsion templates; their shell is 9.8 μm thick and (**B**) processed double emulsions; their shells is 0.8 μm thick. (**C - F**) SEM images of (**C ,D**) intact and (**E ,F**) cut capsules produced from (**C ,E**) primary double emulsions with thick shells and (**D ,F**) processed double emulsions with shin shells.

6.4.2 Mechanical stability of capsules

The rigidity and mechanical stability of capsules typically increases with increasing shell thickness [172]. Hence, we expect the rigidity of capsules produced from double emulsions with thick shells to be significantly higher than that of capsules produced from double emulsions with 14 times thinner shells. To test this expectation, we mechanically deform capsules by placing them between two glass slides and applying weight on the top glass slide. To qualitatively assess the rupture strength of capsules, 20 μL of capsules are deposited on a glass slide. Those capsules are compressed by a 1 x 1 cm^2 glass slide that is loaded with different weights. Optical images are taken after samples have been compressed with different weights and used to determine the fraction of intact capsules, as shown in Figure 6.3. The capsules remain intact if they are loaded with 700 g and gradually start breaking if the load is increased until all capsules break if subjected to a load of 4 kg. Remarkably, the fraction of capsules with thick heterogeneous shells that ruptures at a defined load is very similar to that of capsules with thin homogeneous shells, as seen in Figure 6.3. These results suggest that the thinnest parts of capsules with heterogeneous shell thicknesses have similar dimensions to those of capsules with thin homogeneous shells and that these thin parts determine the rupture strength of capsules with heterogeneous

shell thicknesses.

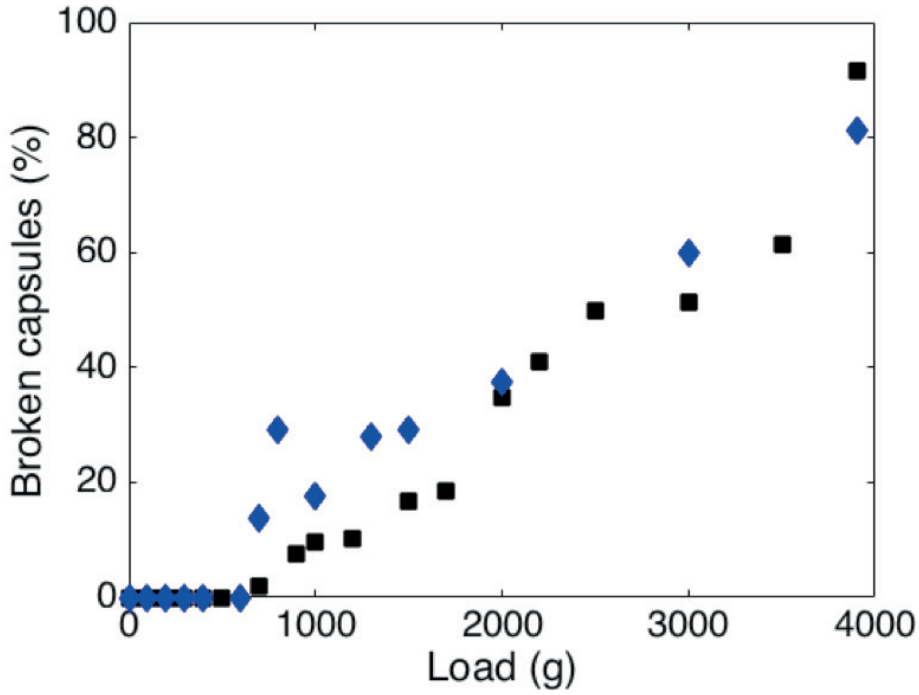

Figure 6.3: (**A**) Percentage of broken capsules whose shell is (■) thin and homogeneous and (⧫) thick and heterogeneous as a function of the load applied on the top glass slide.

To determine the mechanical properties of the capsules more quantitatively, we subject them to osmotic pressure differences. The osmolarity of the capsule core is kept constant at 0.2 Osmol/L. We vary the osmolarity of the outermost aqueous phase by changing the concentration of NaCl contained in it between 0.1 and 0.66 M, corresponding to osmolarities ranging from 0.2 to 1.22 Osmol/L. To convert the osmotic pressure difference into the pressure acting on the capsule shell, we use the Van't Hoff law: $\pi = 2.\Delta c.R.T$; here π is the pressure applied to the capsule, Δc is the difference of osmolarity between the core and the outer phase of the capsule, R the gas constant, and T the temperature of the surrounding. Hence, as a result of the difference in the osmolarities of the two aqueous solutions, the capsules are subjected to osmotic pressures ranging from 0 to 2.75 MPa. To assess the mechanical stability of the capsules, we incubate them under these conditions for 3 h at room temperature and quantify the percentage of intact capsules using optical microscopy. Capsules with heterogeneous, thick shells start to buckle if subjected to a pressure of 1.36 MPa. Interestingly, capsules with homogeneous thin shells start buckling at the same pressure, as shown in Figures 6.4C and D. The fact that these capsules buckle if subjected to an osmotic pressure indicates that they are permeable towards water but impermeable towards NaCl. However, the pressure required to induce buckling is significantly higher than that reported for capsules composed of hydrocarbon-based shells with similar dimensions [93]. Both types of perfluorinated capsules remain intact even if osmotically stressed with pressures up to 2.75 MPa. These results indicate that the thinnest parts the

heterogeneous shells must be almost as thin as shells of capsules produced from processed double emulsions, whose shell is 400 nm, supporting our qualitative loading results. There is one important difference in the buckling behavior between capsules with thick heterogeneous shells and those with thin homogeneous shells: Capsules with heterogeneous shell thickness buckle at one single location only because they have one location that is very thin, as shown in Figure 6.4A. By contrast, capsules with homogeneous shells buckle at multiple locations such that their projected area becomes significantly smaller than that of capsules with thicker shells, as shown in Figure 6.4B. These results indicate that a reduction in the shell thickness of the capsules does not negatively impact their mechanical properties.

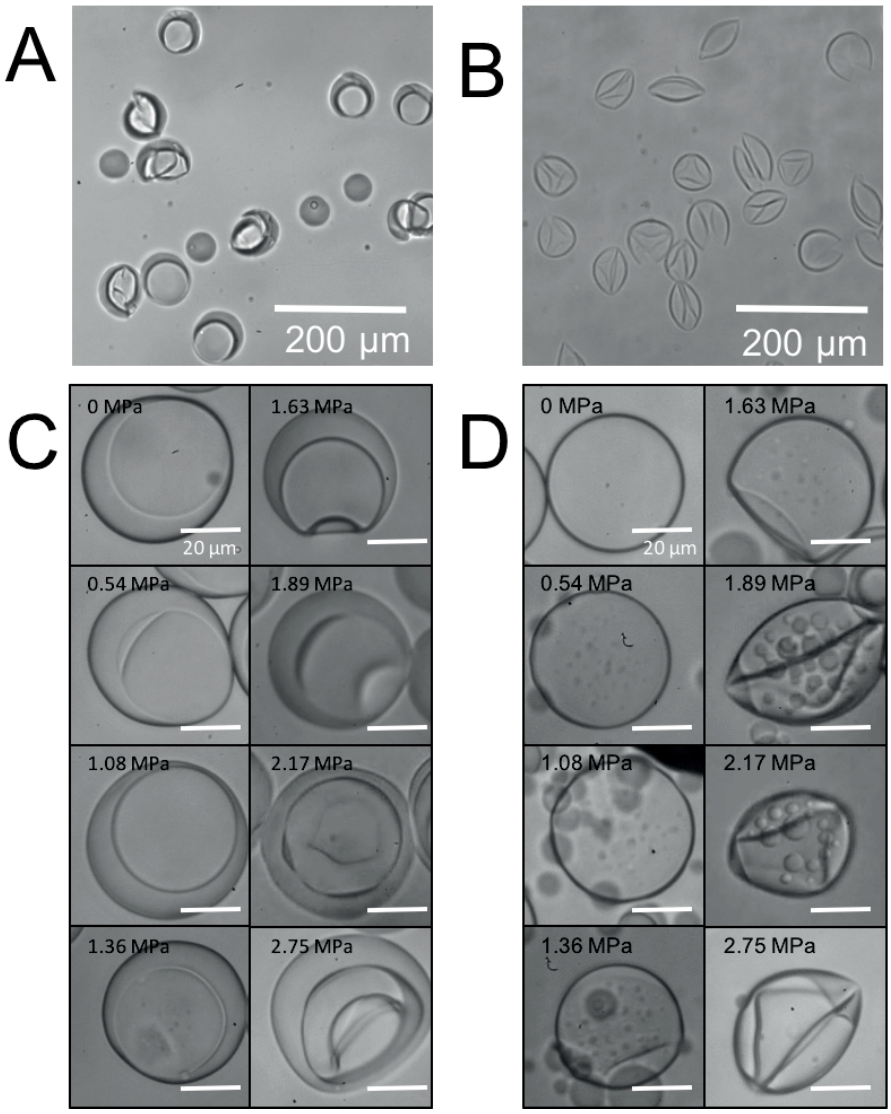

Figure 6.4: (**A**,**B**) Optical images of capsules with (**A**) thick and (**B**) thin shells after having been compressed with 4 kg load. (**C**,**D**) Time-lapse optical microscopy images of capsules with (**C**) thick and (**D**) thin shells if subjected to osmotic pressure differences ranging from 0 to 2.75 MPa

6.4.3 Permeability of capsules

The permeability of capsules often scales with their shell thickness because this parameter determines the distance encapsulants must diffuse to cross the shell [164, 165]. To test the permeability of our capsules, we load them with 2 % of Patent Blue V, a dye with a molecular weight of 562 Da, and disperse them at 6 vol % in a dye-free aqueous solution. To quantify the release of encapsulants, we monitor the absorbance of the supernatant as a function of the incubation time, as detailed in Section 6.3.5. Even though the shells of capsules are as thin as 400 nm, more than 98 % of the encapsulants are retained over the course of four weeks, as demonstrated by the small increase in absorbance in the supernatant, shown in Figure 6.5. This permeability is much smaller than that measured for hydrocarbon-based capsules where the vast majority of encapsulants with similar molecular weights are released within 7 days [170]. These results show the potential of our capsules to store reactive agents for a prolonged time even if their shell is thin and release them on demand if exposed to appropriate mechanical stimuli.

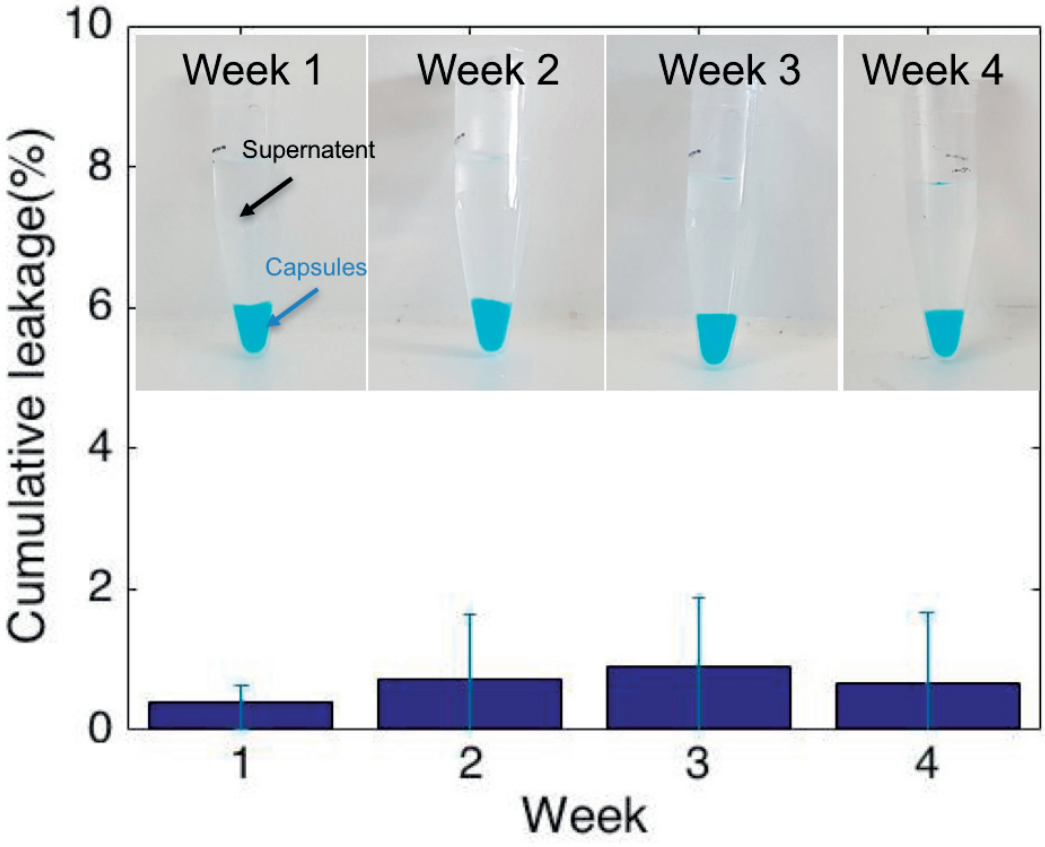

Figure 6.5: Cumulative leakage of capsules with thin shells as a function of time. Photographs of the capsules sedimented in the Eppendorf tube as a function of time is presented as insets.

It is often advantageous to store and transport capsules in a dried state because they can be stored at higher densities and the samples are lighter. These advantages can only be leveraged if capsules remain intact during drying and re-hydration cycles such that their permeability does

not change. To test if our capsules fulfill these requirements, we dry capsules containing 2 wt% Patent Blue V at 70 °C overnight to ensure all the water is removed. When capsules are re-dispersed in deionized water, they retain the spherical shape within 1 hour, indicating that water diffuses through the membrane into the cores, as shown in Figures 6.6A and B. This drying and re-hydration cycle can be repeated at least three times without compromising the integrity of capsules. Importantly, their permeability towards the dye does not measurably increase upon drying and re-hydration: the fluorescence intensity of the cores of capsules before and after they have been dried and re-hydrated is within experimental error the same, even if their shells are as thin as 400 nm as exemplified in Figure 6.6. These results demonstrate that despite their thin shells and hence, their low footprint, our capsules display a similar mechanical stability and permeability as capsules with much thicker shells. This opens up new possibilities to store capsules containing high concentrations of reagents in a dried state and at high densities and re-hydrate them before usage.

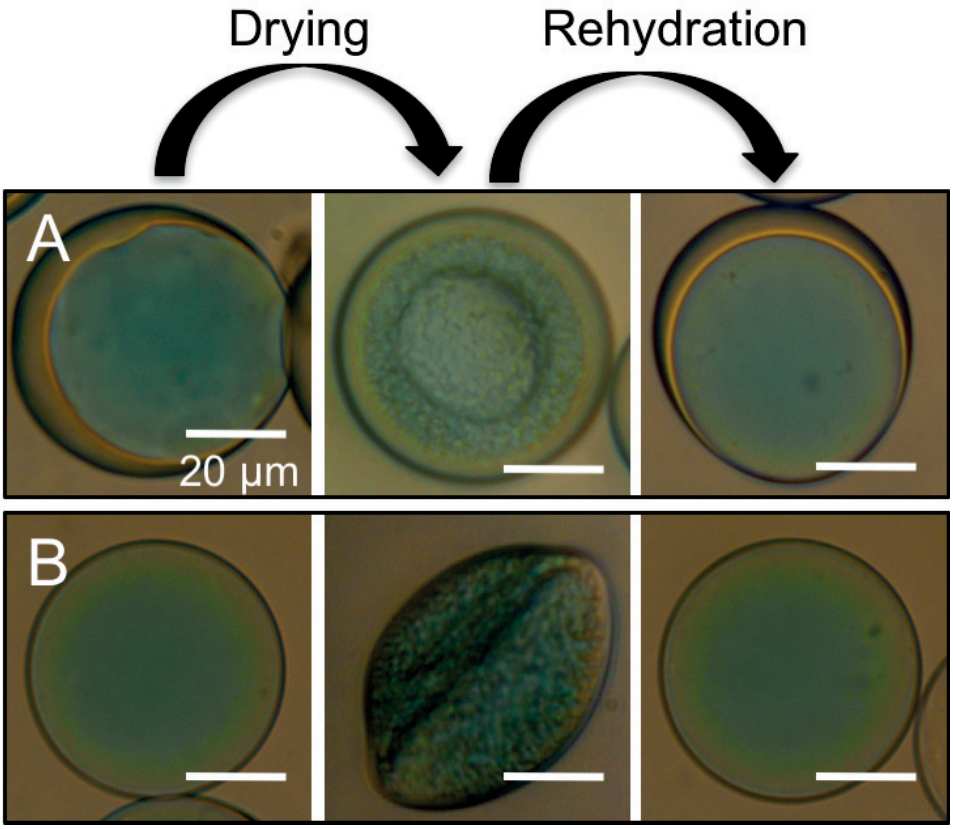

Figure 6.6: Optical microscopy images of capsules with (**A**) heterogeneous and (**B**) homogeneous shell thicknesses containing a blue dye in their core. Capsules are imaged before they are dried (left), in a dry state (middle), and after being re-hydrated (right).

6.5 Conclusions

We report the production of microcapsules with well-defined sizes and uniform shells using water-oil-water double emulsions with sub-μm thick shells as templates. The shells of these capsules are as thin as 400 nm such that the dry shell occupies only 2 % of the total capsule volume. Despite of their thin shells, the capsules are mechanically robust such that they withstand pressures of at least 1.08 MPa without being deformed and pressures up to 2.75 MPa without losing their integrity. Moreover, these semi-permeable capsules can be dried and re-dispersed at will. Because the shell is composed of a perfluorinated polymer, the capsules display a low permeability also towards small encapsulants such as Patent Blue V even though their shells are very thin; they retain more than 98 % of the encapsulants over the course of 30 days. These capsules open up new possibilities to prolong the lifetime of encapsulants because they can be stored in a dried state under an inert atmosphere. Moreover, the small footprint of these capsules combined with the high flexibility of their shells enables their use in materials with at least one dimension that is small, such as coatings. This might enable the conversion of two component coatings into a single component or a much more efficient functionalization of materials with appropriate reagents to impart self-healing properties to them.

Chapter 7

Conclusion and Outlook

In this work, we introduce microfluidic tools to controllably form double emulsion drops with submicron shells. These double emulsions can be used as reaction vessels for example to conduct high throughput screening assays. They can also be used as templates for the formation of capsules with thin shells that have extremely low footprints and an excellent retention of encapsulants.

A simple method to reduce the shell thickness of double emulsions is to squeeze them through a constriction. The squeezing device splits primary double emulsion drops into double emulsions with shells as thin as 330 nm and a single emulsion drop. This squeezing device constitutes an experimentally simple, versatile tool to controllably and efficiently reduce the shell thickness of a wide range of double emulsion drops. However this device can only process one double emulsion at a time, thus limiting the throughput.

To increase the throughput, we developed the aspiration device that enables processing of primary W/O/W double emulsions into secondary double emulsions with shell thickness as thin as 240 nm at a rate of up to 1000 double emulsions per second. Moreover, this device enables processing of primary double emulsions produced through high throughput bulk emulsification methods because the shell thickness of the processed double emulsions does not depends on that of the primary double emulsions. The shell thickness of processed double emulsions only depends on the pressure profile in the device which can be controlled with the fluid flow rates and the viscosity of the oil. Therefore, this device offers new possibilities to form capsules whose shell thickness is well defined such that their permeability and stability is well controlled at high throughput.

Both microfluidic devices mechanically remove parts of the middle oil phase of double emulsion drops to reduce the shell thickness of double emulsions. Hence double emulsions whose shell is made of a wide range of different oils including non-volatile oils or fluids that have a low solubility in the outermost phase can be processed. Thus those devices have the potential to controllably

produce mechanically stable double emulsions with thin shells that can serve as templates to produce capsules made from a much broader range of material than currently possible.

Additionnally we show that double emulsion drops with thin shells produced with the aspiration device have a significantly lower permeability than double emulsions with thicker shells. Indeed we demonstrate that the permeability of double emulsions produced through these devices can be decreased by at least an order of magnitude if the shell is reduced to submicrometer values. Hence these drops might be well-suited vessels for conducting drop-based screening assays also for applications that require a high accuracy, including applications in pharmacy and food industries.

Finally we show that double emulsions with thin shell produced with the aspiration device can be used as templates to form uniform solid capsules with a homogeneous shell. The shell of this capsules only occupies 2% of the total capsule volume such that the footprint is very low. Despite their very thin shells they can withstand pressure of up to 1.08 MPa without deformation. Additionally these capsules can be dried and redispersed in aqueous media at will. Because their shell is composed of a fluorinated polymer, they display a very low permeability for molecules with molecular weights as low as 562 Da: they retain more than 98% of encapsulants over the course of four weeks. Multiple applications can benefit from these capsules since they can prolong the lifetime of encapsulants because they can be stored in a dry state in an inert atmosphere. Moreover, those capsules have a really low footprint and a high flexibility that allow their use in materials with at least one dimension that is small, such as coatings. This might enable the much more efficient functionalization of materials with appropriate reagents to impart self-healing properties to them.

The homogeneity of the thin shell capsules is an advantage for controlling timing of the release of encapsulant. For inhomogeneous capsules, when the trigger is activated encapsulants are released faster at locations where the shell is thinner, whereas it is slower at locations were the shell is thicker, as shown in Chapter 1. Hence the total time for release of encapsulants from a capsule upon activation by a trigger is less well defined compared to that of homogeneous thin shells. Moreoever, in thin shell double emulsion drops, activated release can be switched on or off rapidly, thereby enabling pulsed release. One route that seems promising is controlled release triggered by nanoparticles. For example upon activation with an external non invasive trigger some nanoparticles can heat. Plasmonic nanoparticles such as gold nanoparticles heat when subjected to light of a certain wavelength [173, 174], whereas superparamagnetic iron oxide nanoparticles (SPIONs) will heat if subjected to an alternating magnetic field [175–177]. Those nanoparticles can be coated and embedded in the membrane of capsules and locally heat the surrounding polymer matrix [178]. Therefore capsules with solid homogeneous thin shells capsules that possess a controllable permeability might open up new possibilities in their use as

delivery vehicles for repetitive control release of encapsulants or as building block of responsive macroscopic materials.

As preliminary studies we showed that we can coat iron oxide nanoparticles with a fluorinated polymer, Krytox^{TM} to render them fluorophilic. The iron oxide nanoparticles (SPION) are initially stabilized at pH 8 in an aqueous solution containing 0.1wt% of Krytox^{TM}. Upon vigorous mixing, they are transferred in the fluorinated phase, as shown in Figure 7.1A. Remarkably those nanoparticles still remain separated after phase transfer in the fluorinated phase as shown with transmission electronic microscopy (TEM) in image Figure 7.1B. We succeeded to incorporate them inside the membrane of capsules with a submicrometer shell that are responsive to magnetic fields, as shown in Figure 7.1C and D. A next step would be to study the release of encapsulants from these capsules upon exposure to an alternating magnetic field.

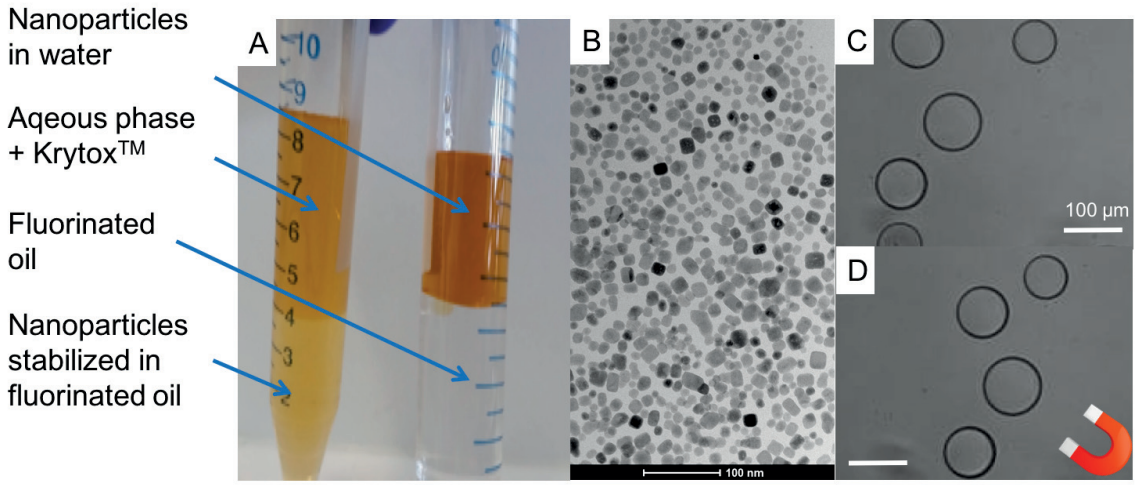

Figure 7.1: Magnetically responsive fluorinated double emulsions. (**A**) Phase transfer of SPIONs from the aqueous phase with 0.1 wt% Krytox^{TM} (*left*), and control experiment without Krytox^{TM}. (**B**) TEM image of coated SPIONs dispersed in the fluorinated phases. (**C**) Double emulsions with submicron shells containing fluorinated coated SPIONs in their shell. (**D**) Response of double emulsions with submicron shells to a static external magnet.

Hence this work paves the way to produce capsules with extremely thin shells that can be used for pulsed triggered release through AC magnetic fields. Since magnetic fields constitute a non-invasive trigger these grafted microcapsules could open up new applications in drug delivery for example.

Appendices

Appendix A

Force-responsive polymersomes inspired by the marine bioluminescence of dinoflagellates

Omar Rifaie-Graham, Nikolas F.B. Galensowske, Charlie Dean, Jonas Pollard, Sandor Balog, Mohamed Chami, Antoine Vian, Esther Amstad, Marco Lattuada and Nico Bruns

In this work we demonstrate the release mechanism of shear responsive polymersomes. These polymersomes are composed 5% of adenine-thymine base pairs in their membranes. When sheared, the membrane becomes porous and encapsulants are released. When a solution of shear responsive polymersomes is introduced in three successive constriction channels of cross sections 20∗100 μm^2 the fluorescent intensity after these constriction increases by 44% as seen in Figure A.1. By contrast, no surge was observed if the polymersomes are not shear responsive.

This work is currently under review and details are presented in reference [179].

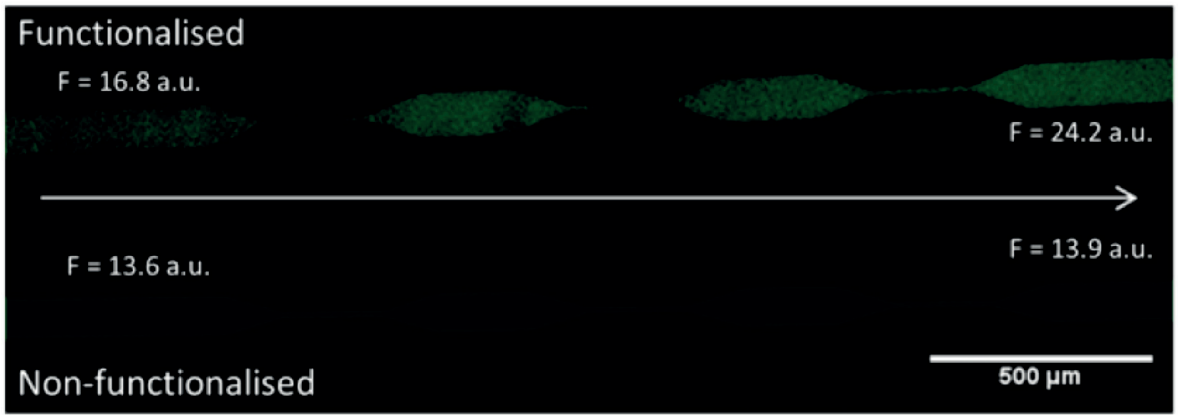

Figure A.1: A dispersion of sodium fluorescein-filled shear responsive polymersomes flowed from left to right through a microfluidic device featuring several constrictions (top). Sodium fluorescein-filled non shear-responsives polymersomes were stimulated in the same manner (bottom). The flowrate was set at 10 mL/h (F= fluorescence intensity).

Appendix B

Abbreviations

- **BSA**: Bovine Serum Albumine
- **ETPTA**: Ethoxylated trimethylolpropane triacrylate
- **FACS**: Fluorescence activated cell sorting
- **LCST**: Lower critical solution temperature
- **O/W**: Oil-in-water
- **O/W/O**: Oil-in-water-in-oil
- **PAA**: Poly(acrylic acid)
- **PDMS**: Poly(dimethylsiloxane)
- **PEG**: Poly(ethylenglycol)
- **PIP**: Poly(isoprene)
- **PLA**: Poly(lactic acid)
- **PLGA**: Poly(lacticglycoacid)
- **PMMA**: Poly(methylmetacrylate)
- **PNIPAM**: Poly(N-isopropylacrylamide)
- **PPHA**: Poly(phthaldehyde)
- **PS**: Poly(styrene)
- **PVA**: Poly(vynilalcohol)

- **SEM**: Scanning Electron Microscope
- **TEM**: Transmission Electron Microscope
- **TETA**: Triethylentetramine
- **UV**: Ultraviolet
- **W/O**: Water-in-oil
- **W/O/W**: Water-in-oil-in-water
- **UV**: Water-in-oil

Appendix C

Notations

- A_0: Interfacial area of a primary double emulsion drop
- C_l: Contour length of the drop when maximally deformed
- ΔA: Difference in interfacial area between separated state and emulsified state
- ΔG_γ: Interfacial energy between separated state and emulsified state
- ΔQ: Difference between injection flow rate and withdraw flow rate
- D_I: Deformation index
- E_D: Energy of deformation
- E_S: Splitting energy
- F: Capsule footprint
- γ: Interfacial tension
- h: Height of the constriction
- l: Length of the constriction
- L_D: Length of the drop at maximum deformation
- q_o: Flow rate of the middle oil phase
- q_w: Flow rate of the internal aqueous phase
- Q_i: Injected flow rate of the inner phase

- Q_k: Flow rate at each junction, k
- Q_m: Injected flow rate of the middle phase
- Q_o: Injected flow rate of outer phase
- Q_{out}: Injected flow rate of continuous phase for the aspiration device
- L: Length of the drop when maximally deformed
- O: Offset between inner and outer drop centers
- O_M: Offset inner and outer drop centers when drop is maximally deformed
- R: External radius of double emulsions
- R_h: Hydraulic resistance
- R_n: Hydraulic resistance between junctions
- R_{ts}: Hydraulic resistance of shunts microchannels
- r: Radius of the single droplet obtained after rupturing of a double emulsion
- t_{min}: Minimum shell thickness of processed double emulsions
- t_s: Shell thickness of double emulsions
- t_{s0}: Shell thickness of primary double emulsions
- v: Speed of the fluid in the channel
- w: Width of the constriction
- w_D: Width of the drop at maximum deformation

Appendix D

Curriculum Vitae

ANTOINE VIAN
ORCID : 0000-0001-8774-320X
11 avenue Tissot
1006 Lausanne, Switzerland
+41788312580
antoine.vian@epfl.ch

4th year PhD graduate at EPFL (Ecole Polytechnique Federale de Lausanne)

EDUCATION

2014 September — **EPFL, Soft Material Lab:** PhD Student on Encapsulation of materials through microfluidics**.** We developed a new tool to produce homogeneous microcapsules from double emulsion templates. Not only those capsule show low permeability and high resistance, but they also release few residuals when broken. They could prove useful in application such as fast screening assays.
PhD defense: 7 Nov 2018.

2013 September — **MBA College des ingénieurs:** Part time management courses and applied experience in Paris Transportation Company (RATP).

2009 September — **ESPCI Paris** - Student (Ecole Supérieure de Physique et de Chimie Industrielle de la ville de Paris), graduate engineering school of physics, chemistry and biology, belonging to the **top French graduate engineering schools, the ParisTech group** (www.paristech.fr).
ESPCI: 10 rue Vauquelin 75006 Paris (www.espci.fr)

2006 September — **LYCEE STANISLAS – Prep classes-** University level preparation in maths, physics, chemistry, and technology for the nationwide competitive entrance exam of the French "Grandes Ecoles", at lycée Stanislas

RESEARCH EXPERIENCE

May-August 2013 — **ASSEMBLY OF INORGANIC MICROCAPSULE WITH MICROFLUIDICS - Harvard School of Applied Science. Boston. Supervisor: Prof. Esther Amstad** .

Sept-Dec 2012 — **MODELIZATION OF SURFER ON WAVES-LadHyx (Hydrodynamic Lab of Ecole Polytechnique Paris) -** Physic of Sports Department, Research Internship . **Supervisor: Prof. Christophe Clanet**

March-July 2012 — **BACTERIA GROWTH TRACKING WITH MICROFLUIDIC DEVICE-LCMD ESPCI Paris -** Research Internship **Supervisor: Dr. Laurent Boitard**

January-April 2012 — **ACOUSTIC AND OPTIC INTERFERENCE FOR MEDICAL IMAGING-Institut Langevin ESPCI Paris -** Research Internship. **Supervisor: Dr. François Ramaz**

July-December 2011 — **SPATIAL INTERFEROMETRY – Thales Alenia Space Cannes -** Six month internship in optic interferometry. **Supervisor: Dr Stéphane Ménard**

TALK AND CONFERENCES

05/2018 — MEGA Seminar series, EPFL, Lausanne (Oral Presentation)
11/2017 — APS Physics Division of Fluid Dynamics, Denver, (Oral Presentation)
07/2017 — Microfluidics 2017, EMBL, Heidelberg (Poster)
02/2017 — Swiss Soft Days, University of Geneva, Geneva (Poster)
12/2016 — Fontiers2016, Swiss-Japanese NanoBio Engineering and Medicine, EPFL, Lausanne (Poster)
06/2016 — IGM Seminar, EPFL, Lausanne (Oral Presentation)
06/2016 — GDR MicroNanoFluidique, Institut Microfluidique Pierre Gille de Gennes, Paris (Poster)
10/2015 — Swiss Soft Days, Adolphe Merckle Institute, Fribourg (Poster)
06/2015 — 5th International Colloids Conference, Amsterdam (Poster)

TEACHING EXPERIENCES

2015-2018 **TEACHING ASSISTANT - EPFL – Lausanne.** EPFL BACHELOR COURSE: Heat and Mass Transfer

2015-2018 **MASTER THESIS AND MASTER PROJECT SUPERVISOR, EPFL – Lausanne.** In the course of my PhD I supervised one student (Baptiste Reuse) for his master thesis and seven students for their semester projects.

2012-2013 **TUTORIALS FOR UNDERGRADUATE , Prepa Stanislas – Paris.** Preparation for the national competitive oral exam for "Grande Ecoles"

LANGUAGE AND COMPUTER SCIENCE

Languages *French :* mother tongue; *English* : fluent; *Spanish* : intermediate level; *Russian* : Beginner level

Computer skills Matlab, C Programming, Microsoft Office, AutoCAD, LATEX.

SCIENTIFIC ACHIEVEMENTS

Paper in Reviewing Process

Mechano-responsive microcapsules with thin, homogeneous shells
A. Vian, E. Amstad
In this work, we demonstrate the formation of solid shell capsules from double emulsion drops with sub-micrometer shell thickness as template.

Nanometer-sized emulsion drops: transport vehicles for hydrophilic reagents in oil phases
G. Etienne, A. Vian, M. Biocanin, B. Deplancke, E. Amstad
In this work, we demonstrate the formation of a aqueous nanometer sized drops within the oil phase and demonstrate its effect on the core leakage from polymer capsules

Force-responsive polymersomes inspired by the marine bioluminescence of dinoflagellates
O. Rifaie-Graham, N. Galensowske, C. Dean, J. Pollard, S. Balog, M. Chami, A. Vian, E. Amstad, M. Lattuada and N. Bruns
We show the release of encapsulants from adenine-thymine grafted membrane polymersomes under the influence of shear

Paper Published

Scalable production of double emulsion drops with thin shells
A.Vian, B. Reuse, E. Amstad, Lab Chip, (2018) DOI: 10.1039/C8LC00282G
In this work, we describe a device that allows the formation of double emulsion, drops in drops, with a shell as seen as hundreds of nanometer in a high throughput and reliable fashion. This invention pave the way for production of capsules with very low footprint.

Reducing the shell thickness of double emulsions using microfluidics
A.Vian, V. Favrod, E. Amstad, Microfluid Nanofluidics, (2016) DOI: 10.1007/s10404-016-1827-x
We describe a phemomenon by which the oil of double emulsion drop detaches from the main core of the double emulsion drop

Patent

Device and methods for shell phase removal of core shell capsules
A.Vian, E. Amstad (2017) WO/2017/199123
This patent describes the functioning of the device presented on the Lab Chip paper

List of Figures

1.1 Different types of emulsion 4
1.2 Surfactant in drops 5
1.3 Formation of a capsule from a single emulsion water in oil drop 6
1.4 Temperature induced release 8
1.5 Triggered encapsulant release 10
1.6 Mechano-responsive capsules 11
1.7 Time delay before encapsulatant is released as a function of the shell thickness. . 12
1.8 Microfluidic co-flow devices 13
1.9 Example of electric circuit model describing the fluid flow in a simple microfluidic device with parallelized channel 14
1.10 Optical microscopy images of the drop production with microfluidic devices. . . . 15
1.11 Production of glass and PDMS device 17
1.12 Production of double emulsions with microfluidic devices 18
1.13 Techniques for measuring the shell thickness of double emulsions 20
1.14 Schematic representation of inhomogeneity in the shell thicknesses of double emulsions 20
1.15 Production of double emulsions with thin shells in glass capillary devices 22

2.1 Chemical structure of the fluorinated surfactant 25
2.2 Schematic illustration of the double emulsion device 26
2.3 Shell thickness of double emulsion drops mesured with three different techniques, as a function of the flow rate of the middle phase of the microfluidic double emulsion device 28
2.4 Viscosity of the middle phase as a function of the volume percentage of GPL added to the initial solution 31

3.1 Operation of the microfluidic squeezing device 37
3.2 Optical time-lapse micrographs of double emulsion drops flowing through a 40-μm-wide and 60-μm-tall constriction 38
3.3 Quantification of the deformation of a double emulsion drop 40
3.4 Interfacial energy of double emulsion drops through a constriction 40

3.5 Influence of the speed and the viscosity of the continuous phase in the constriction on the shell thickness of double emulsion drops after they have been squeezed . . 43
3.6 Influence of the constriction geometry 45
3.7 Optical time-lapse of the squeezing process for a double emulsion composed of a toluene middle phase 46
3.8 Influence of the shell of primary double emulsions 47

4.1 Locations for the measurement of drop velocity in the device 52
4.2 Schematic illustration of the electric circuit analogue of the aspiration device . . 52
4.3 Pressure and velocity profile in the main channel 54
4.4 Variation of the pressure profile in the main channel as a function of flow rates . 55
4.5 Operation of the aspiration device 56
4.6 Optical time-lapse illustrating the production of double emulsion with 20 μm diameter 57
4.7 Influence of the flow rate of the outer channel on the final shell thickness of processed double emulsion drops 59
4.8 Device operation zone 60
4.9 Comparison of theoretical model with experimental datas 62
4.10 Influence of the number of shunt channels on the shell thickness of processed double emulsions 63
4.11 Influence of the shell thickness of primary double emulsions 65
4.12 Influence of the oil viscosity 66
4.13 Optical micrographs acquired with polarized light of double emulsions with liquid cristal middle oil phase 66

5.1 Analysis of the leakage of double emulsion with custom-made Matlab code 72
5.2 Optical fluorescent microscopy timelapse of double emulsion release 72
5.3 Spontaneous formation of small aqueous drops at an O/W interface 73
5.4 Leakage efficiency as a function of the shell thickness of double emulsions 75

6.1 Production of capsules with thin shells 85
6.2 Characterization of capsules homogeneity with SEM 87
6.3 Percentage of broken capsules as a function of the load applied 88
6.4 Resistance of capsules to external stress 89
6.5 Cumulative leakage of thin shells capsules over four weeks 90
6.6 Optical microscopy images of capsules 91

7.1 Magnetically responsive fluorinated double emulsions 96

A.1 Shear responsive polymersomes 100

Bibliography

[1] Antoine Vian, Valentine Favrod, and Esther Amstad. Reducing the shell thickness of double emulsions using microfluidics. *Microfluidics and Nanofluidics*, 20(12):1–9, 2016.

[2] Antoine Vian, Baptiste Reuse, and Esther Amstad. Scalable production of double emulsion drops with thin shells. *Lab on a Chip*, 18(13):1936–1942, 2018.

[3] Gianluca Etienne, Antoine Vian, Marjan Biocanin, Bart Deplancke, and Esther Amstad. Cross-talk between emulsion drops: How are hydrophilic reagents transported across oil phases? *In reviewing process*, 2018.

[4] Antoine Vian and Esther Amstad. Mechano-responsive microcapsules with thin, homogeneous shells . *In reviewing process*, 2018.

[5] Nattapong Prichapan and Utai Klinkesorn. Factor affecting the properties of water-in-oil-in-water emulsions for encapsulation of minerals and vitamins. *Songklanakarin Journal of Science and Technology*, 36(6):651–661, 2014.

[6] David Julian McClements. Food Emulsions: Principles, Practice, and Techniques. *International Journal of Food Science & Technology*, 36(2):223–224, 2001.

[7] Kjersta Larson-Smith and Danilo C. Pozzo. Pickering emulsions stabilized by nanoparticle surfactants. *Langmuir*, 28(32):11725–11732, 2012.

[8] Bernard P. Binks. Particles as surfactants—similarities and differences. *Current Opinion in Colloid & Interface Science*, 7(1-2):21–41, 2002.

[9] Ming Pan, Liat Rosenfeld, Minkyu Kim, Manqi Xu, Edith Lin, Ratmir Derda, and Sindy K Y Tang. Fluorinated pickering emulsions impede interfacial transport and form rigid interface for the growth of anchorage-dependent cells. *ACS Applied Materials and Interfaces*, 6(23):21446–21453, 2014.

[10] Raphael Tomasi. *Multiscale cytometry of 3D cell cultures in microfluidic hydrogel arrays.* PhD thesis, Université Paris-Saclay, 2016.

[11] Gerald Muschiolik. Multiple emulsions for food use. *Current Opinion in Colloid & Interface Science*, 12(4-5):213–220, 2007.

[12] C. Lobato-Calleros, E. Rodriguez, O. Sandoval-Castilla, E. J. Vernon-Carter, and J. Alvarez-Ramirez. Reduced-fat white fresh cheese-like products obtained from W1/O/W2multiple emulsions: Viscoelastic and high-resolution image analyses. *Food Research International*, 39(6):678–685, 2006.

[13] Julia Weiss, Inta Scherze, and Gerald Muschiolik. Polysaccharide gel with multiple emulsion. *Food Hydrocolloids*, 19(3):605–615, 2005.

[14] Axel Benichou, Abraham Aserin, and Nissim Garti. Double emulsions stabilized by new molecular recognition hybrids of natural polymers. *Polymers for Advanced Technologies*, 13(10-12):1019–1031, 2002.

[15] A. Edris and B. Bergnståhl. Encapsulation of orange oil in a spray dried double emulsion. *Die Nahrung*, 45(2):133–137, 2001.

[16] Doo Hyun Lee, Yeong Mee Goh, Joong Soo Kim, Han Kon Kim, Hak Hee Kang, Kyung Do Suh, and Jin Woong Kim. Effective formation of silicone-in-fluorocarbon-in-water double emulsions: Studies on droplet morphology and stability. *Journal of Dispersion Science and Technology*, 23(4):491–497, 2002.

[17] V. Muguet, M. Seiller, G. Barratt, O. Ozer, J. P. Marty, and J. L. Grossiord. Formulation of shear rate sensitive multiple emulsions. *Journal of Controlled Release*, 70(1-2):37–49, 2001.

[18] Myung Han Lee, Seong Geun Oh, Sei Ki Moon, and Seong Youl Bae. Preparation of silica particles encapsulating retinol using o/w/o multiple emulsions. *Journal of Colloid and Interface Science*, 240(1):83–89, 2001.

[19] Katsunori Yoshida, Tomoko Sekine, Fumiaki Matsuzaki, Toshio Yanaki, and Michihiro Yamaguchi. Stability of vitamin A in oil-in-water-in-oil-type multiple emulsions. *Journal of the American Oil Chemists' Society*, 76(2):1–6, 1999.

[20] M. Gallarate, M. E. Carlotti, M. Trotta, and S. Bovo. On the stability of ascorbic acid in emulsified systems for topical and cosmetic use. *International Journal of Pharmaceutics*, 188(2):233–241, 1999.

[21] Masahiro Nakano. Places of emulsions in drug delivery. *Advanced Drug Delivery Reviews*, 45(1):1–4, 2000.

[22] D. Vasiljevic, G. Vuleta, and M. Primorac. The characterization of the semi-solid W/O/W emulsions with low concentrations of the primary polymeric emulsifier. *International Journal of Cosmetic Science*, 27(2):81–87, 2005.

[23] Tapan Kumar Giri, Chhatrapal Choudhary, Ajazuddin, Amit Alexander, Hemant Badwaik, and Dulal Krishna Tripathi. Prospects of pharmaceuticals and biopharmaceuticals

loaded microparticles prepared by double emulsion technique for controlled delivery. *Saudi Pharmaceutical Journal*, 21(2):125–141, 2013.

[24] Bing Jie Sun, Ho Cheung Shum, Christian Holtze, and David A. Weitz. Microfluidic melt emulsification for encapsulation and release of actives. *ACS Applied Materials and Interfaces*, 2(12):3411–3416, 2010.

[25] Todd P. Lagus and Jon F. Edd. High-throughput co-encapsulation of self-ordered cell trains: cell pair interactions in microdroplets. *RSC Advances*, 3(43):20512, 2013.

[26] Huifa Zhang, Gareth Jenkins, Yuan Zou, Zhi Zhu, and Chaoyong James Yang. Massively parallel single-molecule and single-cell emulsion reverse transcription polymerase chain reaction using agarose droplet microfluidics. *Analytical Chemistry*, 84(8):3599–3606, 2012.

[27] Wei Yun Zhang, Wenhua Zhang, Zhiyuan Liu, Cong Li, Zhi Zhu, and Chaoyong James Yang. Highly parallel single-molecule amplification approach based on agarose droplet polymerase chain reaction for efficient and cost-effective aptamer selection. *Analytical Chemistry*, 84(1):350–355, 2012.

[28] Enrico Mastrobattista, Valerie Taly, Estelle Chanudet, Patrick Treacy, Bernard T. Kelly, and Andrew D. Griffiths. High-throughput screening of enzyme libraries: In vitro evolution of a β-galactosidase by fluorescence-activated sorting of double emulsions. *Chemistry and Biology*, 12(12):1291–1300, 2005.

[29] Kalia Bernath, Mingtan Hai, Enrico Mastrobattista, Andrew D. Griffiths, Shlomo Magdassi, and Dan S. Tawfik. In vitro compartmentalization by double emulsions: Sorting and gene enrichment by fluorescence activated cell sorting. *Analytical Biochemistry*, 325(1):151–157, 2004.

[30] David C. Bibby, Nigel M. Davies, and Ian G. Tucker. Mechanisms by which cyclodextrins modify drug release from polymeric drug delivery systems. *International Journal of Pharmaceutics*, 197(1-2):1–11, 2000.

[31] C. E. Mora-Huertas, H. Fessi, and A. Elaissari. Polymer-based nanocapsules for drug delivery. *International Journal of Pharmaceutics*, 385(1-2):113–142, 2010.

[32] Alison Downham and Paul Collins. Colouring our foods in the last and next millennium. *International Journal of Food Science and Technology*, 35(1):5–22, 2000.

[33] H. Hatcher, R. Planalp, J. Cho, F. M. Torti, and S. V. Torti. Curcumin: From ancient medicine to current clinical trials. *Cellular and Molecular Life Sciences*, 65(11):1631–1652, 2008.

[34] K. Miyazawa, I. Yajima, I. Kaneda, and T. Yanaki. Preparation of a new soft capsule for cosmetics. *Journal of cosmetic science*, 51(4):239–252, 2000.

[35] Marlene Jacquemond, Nicolas Jeckelmann, Lahoussine Ouali, and Olivier P. Haefliger. Perfume-Containing Polyurea Microcapsules with Undetectable Levels of Free Isocyanates Marle. *Journal ofAppliedPolymer Science*, 114:3074–3080, 2009.

[36] David Eladio Gorla, Roberto Vargas Ortiz, and Silvia Susana Catalá. Control of rural house infestation by Triatoma infestans in the Bolivian Chaco using a microencapsulated insecticide formulation. *Parasites & vectors*, 8(1):255, 2015.

[37] Hong Zhang, Ethan Tumarkin, Raheem Peerani, Zhihong Nie, Ruby May A. Sullan, Gilbert C. Walker, and Eugenia Kumacheva. Microfluidic production of biopolymer microcapsules with controlled morphology. *Journal of the American Chemical Society*, 128(37):12205–12210, 2006.

[38] M Ficheux, L Bonakdar, and J Bibette. Some Stability Criteria for Double Emulsions. *Langmuir*, 14(11):2702–2706, 1998.

[39] Sujit S. Datta, Alireza Abbaspourrad, Esther Amstad, Jing Fan, Shin Hyun Kim, Mark Romanowsky, Ho Cheung Shum, Bingjie Sun, Andrew S. Utada, Maike Windbergs, Shaobing Zhou, and David a. Weitz. 25th anniversary article: Double emulsion templated solid microcapsules: Mechanics and controlled release. *Advanced Materials*, 26(14):2205–2218, 2014.

[40] Sung-Wook Choi, Yu Zhang, and Younan Xia. Fabrication of Microbeads with a Controllable Hollow Interior and Porous Wall Using a Capillary Fluidic Device. *Advanced Functional Materials*, 19(18):2943–2949, 2009.

[41] Daeyeon Lee and David A. Weitz. Double emulsion-templated nanoparticle colloidosomes with selective permeability. *Advanced Materials*, 20(18):3498–3503, 2008.

[42] Elise Lorenceau, Andrew S. Utada, Darren R. Link, Galder Cristobal, Mathieu Joanicot, and D. A. Weitz. Generation of polymerosomes from double-emulsions. *Langmuir*, 21(20):9183–9186, 2005.

[43] Yves Hennequin, Nicolas Pannacci, Concepción Pulido De Torres, Georgios Tetradis-Meris, Stephane Chapuliot, Elisabeth Bouchaud, and Patrick Tabeling. Synthesizing microcapsules with controlled geometrical and mechanical properties with microfluidic double emulsion technology. *Langmuir*, 25(14):7857–7861, 2009.

[44] Shin Hyun Kim, Gi Ra Yi, Kyu Han Kim, and Seung Man Yang. Photocurable pickering emulsion for colloidal particles with structural complexity. *Langmuir*, 24(6):2365–2371, 2008.

[45] Zhihong Nie, Shengqing Xu, Minseok Seo, Patrick C. Lewis, and Eugenia Kumacheva. Polymer particles with various shapes and morphologies produced in continuous microfluidic reactors. *Journal of the American Chemical Society*, 127(22):8058–8063, 2005.

[46] Ryan C. Hayward, Andrew S. Utada, Nily Dan, and David a. Weitz. Dewetting instability during the formation of polymersomes from block-copolymer-stabilized double emulsions. *Langmuir*, 22(10):4457–4461, 2006.

[47] Alireza Abbaspourrad, Nick J. Carroll, Shin Hyun Kim, and David A. Weitz. Polymer microcapsules with programmable active release. *Journal of the American Chemical Society*, 135(20):7744–7750, 2013.

[48] Bruno F.B. Silva, Carlos Rodrguez-Abreu, and Neus Vilanova. Recent advances in multiple emulsions and their application as templates. *Current Opinion in Colloid and Interface Science*, 25:98–108, 2016.

[49] Shin-hyun Kim, Seog-jin Jeon, and Seung-man Yang. Optofluidic Encapsulation of Crystalline Colloidal Arrays into Spherical Membrane. *Journal of the American Chemical Society*, 130(8):6040–6046, 2008.

[50] Maike Windbergs, Yuanjin Zhao, John Heyman, and David A. Weitz. Biodegradable core-shell carriers for simultaneous encapsulation of synergistic actives. *Journal of the American Chemical Society*, 135(21):7933–7937, 2013.

[51] Alberto. Fernandez-Nieves and Wiley InterScience (Online Service). Microgel suspensions : fundamentals and applications, 2011.

[52] Esther Amstad, Shin Hyun Kim, and David A. Weitz. Photo- and thermoresponsive polymersomes for triggered release. *Angewandte Chemie - International Edition*, 51(50):12499–12503, 2012.

[53] Anthony M. Dilauro, Alireza Abbaspourrad, David A. Weitz, and Scott T. Phillips. Stimuli-responsive core-shell microcapsules with tunable rates of release by using a depolymerizable poly(phthalaldehyde) membrane. *Macromolecules*, 46(9):3309–3313, 2013.

[54] Alireza Abbaspourrad, Sujit S. Datta, and David A. Weitz. Controlling release from pH-responsive microcapsules. *Langmuir*, 29(41):12697–12702, 2013.

[55] Mary Anne White. The chemistry behind carbonless copy paper. *Journal of Chemical Education*, 75(9):1119–1120, 1998.

[56] Débora F. Do Nascimento, Jorge A. Avendaño, Ana Mehl, Maria J.B. Moura, Marcio S. Carvalho, and Wynter J. Duncanson. Flow of Tunable Elastic Microcapsules through Constrictions. *Scientific Reports*, 7(1):1–7, 2017.

[57] David A. McIlroy, Benjamin J. Blaiszik, Mary M. Caruso, Scott R. White, Jeffrey S. Moore, and Nancy R. Sottos. Microencapsulation of a reactive liquid-phase amine for self-healing Epoxy composites. *Macromolecules*, 43(4):1855–1859, 2010.

[58] Philipp W. Chen, Randall M. Erb, and André R. Studart. Designer polymer-based microcapsules made using microfluidics. *Langmuir*, 28(1):144–152, 2012.

[59] Sam Neuser, Philipp W. Chen, Andr?? R. Studart, and V??ronique Michaud. Fracture toughness healing in epoxy containing both epoxy and amine loaded capsules. *Advanced Engineering Materials*, 16(5):581–587, 2014.

[60] George M Whitesides. The origins and the future of microfluidics. *Nature*, 442(7101):368–373, 2006.

[61] Xiaole Mao, John Robert Waldeisen, and Tony Jun Huang. "Microfluidic drifting" - Implementing three-dimensional hydrodynamic focusing with a single-layer planar microfluidic device. *Lab on a Chip*, 7(10):1260–1262, 2007.

[62] Hyewon Kim, Randy P. Carney, Javier Reguera, Quy K. Ong, Xiang Liu, and Francesco Stellacci. Synthesis and characterization of Janus gold nanoparticles. *Advanced Materials*, 24(28):3857–3863, 2012.

[63] Douglas B. Weibel, Maarten Kruithof, Scott Potenta, Samuel K. Sia, Andrew Lee, and George M. Whitesides. Torque-actuated valves for microfluidics. *Analytical Chemistry*, 77(15):4726–4733, 2005.

[64] Henrik Bruus. *Theoretical Microfluidics*. Oxford University Press, first edition, jan 2008.

[65] Kwang W. Oh, Kangsun Lee, Byungwook Ahn, and Edward P. Furlani. Design of pressure-driven microfluidic networks using electric circuit analogy. *Lab on a Chip*, 12(3):515–545, 2012.

[66] Todd Thorsen, Richard W. Roberts, Frances H. Arnold, and Stephen R. Quake. Dynamic pattern formation in a vesicle-generating microfluidic device. *Physical Review Letters*, 86(18):4163–4166, 2001.

[67] Jean Christophe Baret, Oliver J. Miller, Valerie Taly, Michaël Ryckelynck, Abdeslam El-Harrak, Lucas Frenz, Christian Rick, Michael L. Samuels, J. Brian Hutchison, Jeremy J. Agresti, Darren R. Link, David A. Weitz, and Andrew D. Griffiths. Fluorescence-activated droplet sorting (FADS): Efficient microfluidic cell sorting based on enzymatic activity. *Lab on a Chip*, 9(13):1850–1858, 2009.

[68] B. E. Debs, R. Utharala, I. V. Balyasnikova, A. D. Griffiths, and C. A. Merten. Functional single-cell hybridoma screening using droplet-based microfluidics. *Proceedings of the National Academy of Sciences*, 109(29):11570–11575, 2012.

[69] J. J. Agresti, E. Antipov, A. R. Abate, K. Ahn, A. C. Rowat, J.-C. Baret, M. Marquez, A. M. Klibanov, A. D. Griffiths, and D. A. Weitz. Ultrahigh-throughput screening in

drop-based microfluidics for directed evolution. *Proceedings of the National Academy of Sciences*, 107(9):4004–4009, 2010.

[70] Benjamin L. Wang, Adel Ghaderi, Hang Zhou, Jeremy Agresti, David A. Weitz, Gerald R. Fink, and Gregory Stephanopoulos. Microfluidic high-throughput culturing of single cells for selection based on extracellular metabolite production or consumption. *Nature Biotechnology*, 32(5):473–478, 2014.

[71] Allon M. Klein, Linas Mazutis, Ilke Akartuna, Naren Tallapragada, Adrian Veres, Victor Li, Leonid Peshkin, David A. Weitz, and Marc W. Kirschner. Droplet barcoding for single-cell transcriptomics applied to embryonic stem cells. *Cell*, 161(5):1187–1201, 2015.

[72] Evan Z. Macosko, Anindita Basu, Rahul Satija, James Nemesh, Karthik Shekhar, Melissa Goldman, Itay Tirosh, Allison R. Bialas, Nolan Kamitaki, Emily M. Martersteck, John J. Trombetta, David A. Weitz, Joshua R. Sanes, Alex K. Shalek, Aviv Regev, and Steven A. McCarroll. Highly parallel genome-wide expression profiling of individual cells using nanoliter droplets. *Cell*, 161(5):1202–1214, 2015.

[73] Jean Christophe Baret, Yannick Beck, Isabelle Billas-Massobrio, Dino Moras, and Andrew D. Griffiths. Quantitative cell-based reporter gene assays using droplet-based microfluidics. *Chemistry and Biology*, 17(5):528–536, 2010.

[74] Oliver J Miller, Abdeslam El, Thomas Mangeat, Jean-christophe Baret, Lucas Frenz, Bachir El, Estelle Mayot, Michael L Samuels, Eamonn K Rooney, Pierre Dieu, Martin Galvan, Darren R Link, and Andrew D Griffiths. High-resolution dose – response screening using droplet-based microfluidics. *Proceedings of the National Academy of Sciences*, 109(2):378–83, 2012.

[75] Deniz Pekin, Yousr Skhiri, Jean Christophe Baret, Delphine Le Corre, Linas Mazutis, Chaouki Ben Salem, Florian Millot, Abdeslam El Harrak, J. Brian Hutchison, Jonathan W. Larson, Darren R. Link, Pierre Laurent-Puig, Andrew D. Griffiths, and Valérie Taly. Quantitative and sensitive detection of rare mutations using droplet-based microfluidics. *Lab on a Chip*, 11(13):2156–2166, 2011.

[76] Valerie Taly, Deniz Pekin, Leonor Benhaim, Steve K. Kotsopoulos, Delphine Le Corre, Xinyu Li, Ivan Atochin, Darren R. Link, Andrew D. Griffiths, Karine Pallier, Hélène Blons, Olivier Bouché, Bruno Landi, J. Brian Hutchison, and Pierre Laurent-Puig. Multiplex picodroplet digital PCR to detect KRAS mutations in circulating DNA from the plasma of colorectal cancer patients. *Clinical Chemistry*, 59(12):1722–1731, 2013.

[77] Audrey Didelot, Steve K. Kotsopoulos, Audrey Lupo, Deniz Pekin, Xinyu Li, Ivan Atochin, Preethi Srinivasan, Qun Zhong, Jeff Olson, Darren R. Link, Pierre Laurent-Puig, Hélène Blons, J. Brian Hutchison, and Valerie Taly. Multiplex picoliter-droplet digital PCR

for quantitative assessment of DNA integrity in clinical samples. *Clinical Chemistry*, 59(5):815–823, 2013.

[78] Adam R Abate, Keunho Ahn, Amy C Rowat, Christophe Baret, Manuel Marquez, Alexander M Klibanov, Andrew D Grif, David A Weitz, and G A L Aga. Correction for Agresti et al., Ultrahigh-throughput screening in drop-based microfluidics for directed evolution. *Proceedings of the National Academy of Sciences*, 107(14):6550–6550, 2010.

[79] Shelley L. Anna, Nathalie Bontoux, and Howard A. Stone. Formation of dispersions using "flow focusing" in microchannels. *Applied Physics Letters*, 82(3):364–366, 2003.

[80] A. S. Utada, L.-Y. Chu, A. Fernandez-Nieves, D. R. Link, C. Holtze, and D. A. Weitz. Dripping, jetting, drops, and wetting: The magic of microfluidics. *MRS Bulletin*, 32(9):702–708, 2007.

[81] Takasi Nisisako and T. Torii. Microfluidic large-scale integration on a chip for mass production of monodisperse droplets and particles. *Lab on a Chip*, 8(2):287–293, 2008.

[82] Rémi Dangla, Etienne Fradet, Yonatan Lopez, and Charles N Baroud. The physical mechanisms of step emulsification. *Journal of Physics D: Applied Physics*, 46:114003, 2013.

[83] Esther Amstad, Michael Chemama, Maximilian Eggersdorfer, Laura Rodriguez Arriaga, Michael P. Brenner, and David A. Weitz. Robust scalable high throughput production of monodisperse drops. *Lab Chip*, 16(21):138–155, 2016.

[84] A. S. Utada, E. Lorenceau, D. R. Link, P. D. Kaplan, H. A. Stone, and D.A. Weitz. Monodisperse Double Emulsions generated from a microcapillary device. *Science*, 308(5721):537–541, 2005.

[85] Y N Xia and G M Whitesides. Soft lithography. *Annual Review Of Materials Science*, 37(5):551–575, 1998.

[86] J. Cooper McDonald, David C. Duffy, Janelle R. Anderson, Daniel T. Chiu, Hongkai Wu, Olivier J. A. Schueller, and George M. Whitesides. Fabrication of microfluidic systems in poly(dimethylsiloxane). *ELECTROPHORESIS*, 21(1):27–40, 2000.

[87] Jessamine Ng Lee, Cheolmin Park, and George M Whitesides. Solvent Compatibility of Poly(dimethylsiloxane)-Based Microfluidic Devices. *Analytical Chemistry*, 75(23):6544–6554, 2003.

[88] Jonas Flueckiger, Vahid Bazargan, Boris Stoeber, and Karen C. Cheung. Characterization of postfabricated parylene C coatings inside PDMS microdevices. *Sensors and Actuators B: Chemical*, 160(1):864–874, dec 2011.

[89] Douglas B. Weibel, Willow R. DiLuzio, and George M. Whitesides. Microfabrication meets microbiology. *Nature Reviews Microbiology*, 5(3):209–218, 2007.

[90] Goran T Vladisavljević, Ho Cheung Shum, and David A Weitz. Control over the Shell Thickness of Core/Shell Drops in Three-Phase Glass Capillary Devices BT - UK Colloids 2011. pages 115–118, Berlin, Heidelberg, 2012. Springer Berlin Heidelberg.

[91] L. R. Arriaga, E. Amstad, and D. a. Weitz. Scalable single-step microfluidic production of single-core double emulsions with ultra-thin shells. *Lab Chip*, 15(August):3335–3340, 2015.

[92] A. Fernandez-Nieves, V. Vitelli, A. S. Utada, D. R. Link, M. M??rquez, D. R. Nelson, and D. A. Weitz. Novel defect structures in nematic liquid crystal shells. *Physical Review Letters*, 99(15):1–4, 2007.

[93] Sujit S. Datta, Shin Hyun Kim, Jayson Paulose, Alireza Abbaspourrad, David R. Nelson, and David A. Weitz. Delayed buckling and guided folding of inhomogeneous capsules. *Physical Review Letters*, 109(13):1–5, 2012.

[94] Lawrence S. Mok and Kyekyoon Kim. Motion of a gas bubble inside a spherical liquid container with a vertical temperature gradient. *Journal of Fluid Mechanics*, 176(1959):521–531, 1987.

[95] Shin-Hyun Kim, Jin Woong Kim, Jun-Cheol Cho, and David a Weitz. Double-emulsion drops with ultra-thin shells for capsule templates. *Lab on a chip*, 11(18):3162–3166, 2011.

[96] C Holtze, A C Rowat, J J Agresti, J B Hutchison, F E Angile, C H J Schmitz, S Koster, H Duan, K J Humphry, R A Scanga, J S Johnson, D Pisignano, D a Weitz, F E Angilè, C H J Schmitz, S Köster, H Duan, K J Humphry, R A Scanga, J S Johnson, D Pisignano, and D a Weitz. Biocompatible surfactants for water-in-fluorocarbon emulsions. *Lab on a Chip*, 8(10):1632–1639, 2008.

[97] Gianluca Etienne, Michael Kessler, and Esther Amstad. Influence of Fluorinated Surfactant Composition on the Stability of Emulsion Drops. *Macromolecular Chemistry and Physics*, 218(2):1–10, 2017.

[98] Wei Wang, Rui Xie, Xiao-Jie Ju, Tao Luo, Li Liu, David a Weitz, and Liang-Yin Chu. Controllable microfluidic production of multicomponent multiple emulsions. *Lab on a chip*, 11(9):1587–1592, 2011.

[99] Jian-Hong Xu, Xue-Hui Ge, Ran Chen, and Guang-Sheng Luo. Microfluidic preparation and structure evolution of double emulsions with two-phase cores. *RSC Advances*, 4(4):1900, 2014.

[100] a. R. Abate and D. a. Weitz. High-order multiple emulsions formed in poly(dimethylsiloxane) microfluidics. *Small*, 5(18):2030–2032, 2009.

[101] X H Ge, J P Huang, J H Xu, and G S Luo. Controlled stimulation-burst targeted release by smart decentered core-shell microcapsules in gravity and magnetic field. *Lab on a Chip*, 14(23):4451–4454, 2014.

[102] Melikhan Tanyeri, Mikhil Ranka, Natawan Sittipolkul, and Charles M. Schroeder. A microfluidic-based hydrodynamic trap: design and implementation. *Lab on a Chip*, 11(10):1786, 2011.

[103] Sang Seok Lee, Alireza Abbaspourrad, and Shin Hyun Kim. Nonspherical double emulsions with multiple distinct cores enveloped by ultrathin shells. *ACS Applied Materials and Interfaces*, 6(2):1294–1300, 2014.

[104] Ankur S. Chaurasia, Dimitris N. Josephides, and Shahriar Sajjadi. Large ultrathin shelled drops produced via non-confined microfluidics. *ChemPhysChem*, 16(2):403–411, 2015.

[105] Laura R. Arriaga, Sujit S. Datta, Shin Hyun Kim, Esther Amstad, Thomas E. Kodger, Francisco Monroy, and David a. Weitz. Ultrathin shell double emulsion templated giant unilamellar lipid vesicles with controlled microdomain formation. *Small*, 10(5):950–956, 2014.

[106] Ho Cheung Shum, Jin-Woong Kim, and David a Weitz. Microfluidic fabrication of monodisperse biocompatible and biodegradable polymersomes with controlled permeability. *Journal of the American Chemical Society*, 130(29):9543–9, jul 2008.

[107] Julian Thiele, Venkatachalam Chokkalingam, Shaohua Ma, Daniela a. Wilson, and Wilhelm T. S. Huck. Vesicle budding from polymersomes templated by microfluidically prepared double emulsions. *Materials Horizons*, 1(1):96, 2014.

[108] Siddharth Deshpande, Yaron Caspi, Anna Meijering, and Cees Dekker. Octanol-assisted liposome assembly on chip. *Nature communications*, accepted:1–9, 2015.

[109] P. Sajeesh, M. Doble, and a. K. Sen. Hydrodynamic resistance and mobility of deformable objects in microfluidic channels. *Biomicrofluidics*, 8(5):054112, 2014.

[110] Nan-Nan Deng, Wei Wang, Xiao-Jie Ju, Rui Xie, David a Weitz, and Liang-Yin Chu. Wetting-induced formation of controllable monodisperse multiple emulsions in microfluidics. *Lab on a chip*, 13(20):4047–52, 2013.

[111] Quentin Brosseau, Jérémy Vrignon, and Jean-Christophe Baret. Microfluidic Dynamic Interfacial Tensiometry (μDIT). *Soft matter*, 10:3066–76, 2014.

[112] Haruyuki Kinoshita, Shohei Kaneda, Teruo Fujii, and Marie Oshima. Three-dimensional measurement and visualization of internal flow of a moving droplet using confocal micro-PIV. *Lab Chip*, 7(3):338–346, 2007.

[113] Shaohua Ma, Joseph M Sherwood, Wilhelm T. S. Huck, and Stavroula Balabani. On the flow topology inside droplets moving in rectangular microchannels. *Lab on a Chip*, 14(18):3611, 2014.

[114] Andrew J. DeMello. Control and detection of chemical reactions in microfluidic systems. *Nature*, 442(7101):394–402, 2006.

[115] Raphaël Tomasi, Jean-Marc Noël, Aymen Zenati, Sandra Ristori, Federico Rossi, Valérie Cabuil, Frédéric Kanoufi, and Ali Abou-Hassan. Chemical communication between liposomes encapsulating a chemical oscillatory reaction. *Chem. Sci.*, 5(5):1854–1859, 2014.

[116] Helen Song and Rustem F. Ismagilov. Millisecond Kinetics on a Microfluidic Chip Using Nanoliters of Reagents. *Journal of the American Chemical Society*, 125(47):14613–14619, 2003.

[117] Gabriel Amselem, Cyprien Guermonprez, B. Drogue, S. Michelin, and Charles N. Baroud. Universal microfluidic platform for bioassays in anchored droplets Lab on a Chip. *Lab on a Chip*, 2016.

[118] Fuqiang Ma, Michael Fischer, Yunbin Han, Stephen G. Withers, Yan Feng, and Guang Yu Yang. Substrate Engineering Enabling Fluorescence Droplet Entrapment for IVC-FACS-Based Ultrahigh-Throughput Screening. *Analytical Chemistry*, 88(17):8587–8595, 2016.

[119] H. F. Chan, S. Ma, J. Tian, and K. W. Leong. High-throughput screening of microchip-synthesized genes in programmable double-emulsion droplets. *Nanoscale*, 9(10):3485–3495, 2017.

[120] Anastasia Zinchenko, Sean R A Devenish, Balint Kintses, Pierre Yves Colin, Martin Fischlechner, and Florian Hollfelder. One in a million: Flow cytometric sorting of single cell-lysate assays in monodisperse picolitre double emulsion droplets for directed evolution. *Analytical Chemistry*, 86(5):2526–2533, 2014.

[121] Armend Gazmeno Håti, Tomasz Szymborski, Mathias Steinacher, and Esther Amstad. Production of monodisperse drops from viscous fluids. *Lab on a Chip*, 18:648–654, 2018.

[122] Mark B. Romanowsky, Adam R. Abate, Assaf Rotem, Christian Holtze, and David A. Weitz. High throughput production of single core double emulsions in a parallelized microfluidic device. *Lab on a Chip*, 12(4):802, 2012.

[123] J. Zhang, R. J. Coulston, S. T. Jones, J. Geng, O. a. Scherman, and C. Abell. One-Step Fabrication of Supramolecular Microcapsules from Microfluidic Droplets. *Science*, 335(6069):690–694, 2012.

[124] Shaun W. Lim and Adam R. Abate. Ultrahigh-throughput sorting of microfluidic drops with flow cytometry. *Lab on a Chip*, 13(23):4563, 2013.

[125] Shin-Hyun Kim, Jin Woong Kim, Jun-Cheol Cho, and David A. Weitz. Correction: Double-emulsion drops with ultra-thin shells for capsule templates. *Lab on a Chip*, 17(3):567–567, 2017.

[126] Chun Xia Zhao, Dong Chen, Yue Hui, David A. Weitz, and Anton P.J. Middelberg. Controlled Generation of Ultrathin-Shell Double Emulsions and Studies on Their Stability. *ChemPhysChem*, 18(10):1393–1399, 2017.

[127] Chun-Xia Zhao, Dong Chen, Yue Hui, David A. Weitz, and Anton P. J. Middelberg. Stable ultrathin-shell double emulsions for controlled release. *ChemPhysChem*, 17(11):1553–1556, 2016.

[128] Rhutesh K. Shah, Ho Cheung Shum, Amy C. Rowat, Daeyeon Lee, Jeremy J. Agresti, Andrew S. Utada, Liang Yin Chu, Jin Woong Kim, Alberto Fernandez-Nieves, Carlos J. Martinez, and David A. Weitz. Designer emulsions using microfluidics. *Materials Today*, 11(4):18–27, 2008.

[129] Esther Amstad. Microfluidics: A Tool to Control the Size and Composition of Particles. *CHIMIA International Journal for Chemistry*, 71(6):334–341, 2017.

[130] Shin-Hyun Kim and David a. Weitz. One-Step Emulsification of Multiple Concentric Shells with Capillary Microfluidic Devices. *Angewandte Chemie*, 123(37):8890–8893, 2011.

[131] Ho Cheung Shum, Daeyeon Lee, Insun Yoon, Tom Kodger, and David A Weitz. Double Emulsion Templated Monodisperse Phospholipid Vesicles Double Emulsion Templated Monodisperse Phospholipid Vesicles. *Langmuir*, 24(July):7651–7653, 2008.

[132] Shin Hyun Kim, Jin Woong Kim, Do Hoon Kim, Sang Hoon Han, and David A. Weitz. Enhanced-throughput production of polymersomes using a parallelized capillary microfluidic device. *Microfluidics and Nanofluidics*, 14(3-4):509–514, 2013.

[133] Shin-Hyun Kim, Jin Nam, Jin Woong Kim, Do-Hoon Kim, Sang-Hoon Han, and David A. Weitz. Formation of polymersomes with double bilayers templated by quadruple emulsions. *Lab on a Chip*, 13(7):1351, 2013.

[134] M. J. Hope, M. B. Bally, G. Webb, and P. R. Cullis. Production of large unilamellar vesicles by a rapid extrusion procedure. Characterization of size distribution, trapped volume and ability to maintain a membrane potential. *BBA - Biomembranes*, 812(1):55–65, 1985.

[135] Valerie Taly, Bernard T. Kelly, and Andrew D. Griffiths. Droplets as microreactors for high-throughput biology. *ChemBioChem*, 8(3):263–272, 2007.

[136] Sarah Köster, Francesco E. Angilè, Honey Duan, Jeremy J. Agresti, Anton Wintner, Christian Schmitz, Amy C. Rowat, Christoph A. Merten, Dario Pisignano, Andrew D. Griffiths, and David A. Weitz. Drop-based microfluidic devices for encapsulation of single cells. *Lab on a Chip*, 8(7):1110–1115, 2008.

[137] Ashleigh B. Theberge, Fabienne Courtois, Yolanda Schaerli, Martin Fischlechner, Chris Abell, Florian Hollfelder, and Wilhelm T S Huck. Microdroplets in microfluidics: An evolving platform for discoveries in chemistry and biology. *Angewandte Chemie - International Edition*, 49(34):5846–5868, 2010.

[138] Mira T. Guo, Assaf Rotem, John A. Heyman, and David A. Weitz. Droplet microfluidics for high-throughput biological assays. *Lab Chip*, 12(12):2146–2155, 2012.

[139] Nachiket Shembekar, Chawaree Chaipan, Ramesh Utharala, and Christoph A. Merten. Droplet-based microfluidics in drug discovery, transcriptomics and high-throughput molecular genetics. *Lab Chip*, 16(8):1314–1331, 2016.

[140] Kenneth C. Lowe. Perfluorochemical respiratory gas carriers: Benefits to cell culture systems. *Journal of Fluorine Chemistry*, 118(1-2):19–26, 2002.

[141] L. Spencer Roach, Helen Song, and Rustem F. Ismagilov. Controlling nonspecific protein adsorption in a plug-based microfluidic system by controlling interfacial chemistry using fluorous-phase surfactants. *Analytical Chemistry*, 77(3):785–796, 2005.

[142] Helen Song, Delai L. Chen, and Rustem F. Ismagilov. Reactions in droplets in microfluidic channels. *Angewandte Chemie International Edition*, 45(44):7336–7356, 2006.

[143] K. C. Lowe. Fluorinated blood substitutes and oxygen carriers. *Journal of Fluorine Chemistry*, 109(1):59–65, 2001.

[144] Jean-Christophe Baret. Surfactants in droplet-based microfluidics. *Lab Chip*, 12(3):422–433, feb 2012.

[145] Fabienne Courtois, Luis F. Olguin, Graeme Whyte, Ashleigh B. Theberge, Wilhelm T S Huck, Florian Hollfelder, and Chris Abell. Controlling the retention of small molecules in emulsion microdroplets for use in cell-based assays. *Analytical Chemistry*, 81(8):3008–3016, 2009.

[146] Linas Mazutis, Jean-Christophe Baret, Patrick Treacy, Yousr Skhiri, Ali Fallah Araghi, Michael Ryckelynck, Valérie Taly, and Andrew D. Griffiths. Multi-step microfluidic droplet processing: kinetic analysis of an in vitro translated enzyme. *Lab Chip*, 9(20):2902–2908, 2009.

[147] James A. Stapleton and James R. Swartz. Development of an in vitro compartmentalization screen for high-throughput directed evolution of [FeFe] hydrogenases. *PLoS ONE*, 5(12), 2010.

[148] Pierre R. Marcoux, Mathieu Dupoy, Raphael Mathey, Armelle Novelli-Rousseau, Virginie Heran, Sophie Morales, Florence Rivera, Pierre L. Joly, Jean Pierre Moy, and Frédéric Mallard. Micro-confinement of bacteria into w/o emulsion droplets for rapid detection and enumeration. *Colloids and Surfaces A: Physicochemical and Engineering Aspects*, 377:54–62, 2011.

[149] Gabrielle Woronoff, Abdeslam El Harrak, Estelle Mayot, Olivier Schicke, Oliver J. Miller, Patrice Soumillion, Andrew D. Griffiths, and Michael Ryckelynck. New generation of amino coumarin methyl sulfonate-based fluorogenic substrates for amidase assays in droplet-based microfluidic applications. *Analytical Chemistry*, 83(8):2852–2857, 2011.

[150] Yousr Skhiri, Philipp Gruner, Benoît Semin, Quentin Brosseau, Deniz Pekin, Linas Mazutis, Victoire Goust, Felix Kleinschmidt, Abdeslam El Harrak, J. Brian Hutchison, Estelle Mayot, Jean-François Bartolo, Andrew D. Griffiths, Valérie Taly, and Jean-Christophe Baret. Dynamics of molecular transport by surfactants in emulsions. *Soft Matter*, 8(41):10618, 2012.

[151] Philipp Gruner, Birte Riechers, Benoît Semin, Jiseok Lim, Abigail Johnston, Kathleen Short, and Jean Christophe Baret. Controlling molecular transport in minimal emulsions. *Nature Communications*, 7:910392, 2016.

[152] Majdi Najah, Estelle Mayot, I. Putu Mahendra-Wijaya, Andrew D. Griffiths, Sylvain Ladame, and Antoine Drevelle. New glycosidase substrates for droplet-based microfluidic screening. *Analytical Chemistry*, 85(20):9807–9814, 2013.

[153] Jan-Willi Janiesch, Marian Weiss, Gerri Kannenberg, Jonathon Hannabuss, Thomas Surrey, Ilia Platzman, and Joachim P. Spatz. Key factors for stable retention of fluorophores and labeled biomolecules in droplet-based microfluidics. *Analytical Chemistry*, 87(4):2063–2067, 2015.

[154] Ott Scheler, Tomasz S. Kaminski, Artur Ruszczak, and Piotr Garstecki. Dodecylresorufin (C12R) outperforms resorufin in microdroplet bacterial assays. *ACS Applied Materials and Interfaces*, 8(18):11318–11325, 2016.

[155] Patrick A. Sandoz, Aram J. Chung, Westbrook M. Weaver, and Dino Di Carlo. Sugar additives improve signal fidelity for implementing two-phase resorufin-based enzyme immunoassays. *Langmuir*, 30(23):6637–6643, 2014.

[156] Lixiong Wen and Kyriakos D. Papadopoulos. Visualization of water transport in W1/O/W2 emulsions. *Colloids and Surfaces A: Physicochemical and Engineering Aspects*, 174(1-2):159–167, 2000.

[157] Jana Bahtz, Deniz Z. Gunes, Eric Hughes, Lea Pokorny, Francesca Riesch, Axel Syrbe, Peter Fischer, and Erich J. Windhab. Decoupling of mass transport mechanisms in the stagewise swelling of multiple emulsions. *Langmuir*, 31(19):5265–5273, 2015.

[158] Jana Bahtz, Deniz Z. Gunes, Axel Syrbe, Nicola Mosca, Peter Fischer, and Erich J. Windhab. Quantification of spontaneous w/o emulsification and its impact on the swelling kinetics of multiple w/o/w emulsions. *Langmuir*, 32(23):5787–5795, 2016.

[159] Simone Bochner De Araujo, Maria Merola, Dimitris Vlassopoulos, and Gerald G. Fuller. Droplet Coalescence and Spontaneous Emulsification in the Presence of Asphaltene Adsorption. *Langmuir*, 33(40):10501–10510, 2017.

[160] Linge Wang, Luca Chierico, Daniel Little, Nisa Patikarnmonthon, Zhou Yang, Mimoun Azzouz, Jeppe Madsen, Steven P. Armes, and Giuseppe Battaglia. Encapsulation of biomacromolecules within polymersomes by electroporation. *Angewandte Chemie - International Edition*, 51(44):11122–11125, 2012.

[161] Ji-Hwan Kang and Elsa Reichmanis. Low-Threshold Photon Upconversion Capsules Obtained by Photoinduced Interfacial Polymerization. *Angewandte Chemie*, 124(47):12011–12014, 2012.

[162] Ke Feng Xiao, Zhi Wang, Lei Lei Wang, Bao Hua Zhang, and Xiu Guang Feng. Screening of Additives for 1% Abamectin Microcapsules Suspension. *Advanced Materials Research*, 641-642:939–942, 2013.

[163] Rui Yang, Yan Zhang, Xin Wang, Yinping Zhang, and Qingwu Zhang. Preparation of n-tetradecane-containing microcapsules with different shell materials by phase separation method. *Solar Energy Materials and Solar Cells*, 93(10):1817–1822, 2009.

[164] Laurence Canaple, Annemie Rehor, and David Hunkeler. Improving cell encapsulation through size control. *Journal of Biomaterials Science, Polymer Edition*, 13(7):783–796, 2002.

[165] Huai Nyin Yow, Xiao Wu, Alexander F. Routh, and Richard H. Guy. Dye diffusion from microcapsules with different shell thickness into mammalian skin. *European Journal of Pharmaceutics and Biopharmaceutics*, 72(1):62–68, 2009.

[166] Erik Reimhult. Nanoparticle-triggered release from lipid membrane vesicles. *New Biotechnology*, 32(6):665–672, 2015.

[167] Behzad Shirmardi Shaghasemi, Mudassar Mumtaz Virk, and Erik Reimhult. Optimization of Magneto-thermally Controlled Release Kinetics by Tuning of Magnetoliposome Composition and Structure. *Scientific Reports*, 7(1):1–10, 2017.

[168] Bomi Kim, Sangmin Lee, and Shin-Hyun Kim. Double-Emulsion-Templated Anisotropic Microcapsules for pH-Triggered Release. *Advanced Materials Interfaces*, 1701472:1701472, 2018.

[169] Maximilian A. Zieringer, Nick J. Carroll, Alireza Abbaspourrad, Stephan A. Koehler, and David A. Weitz. Microcapsules for Enhanced Cargo Retention and Diversity. *Small*, 11(24):2903–2909, 2015.

[170] Neus Vilanova, Carlos Rodríguez-Abreu, Alberto Fernández-Nieves, and Conxita Solans. Fabrication of novel silicone capsules with tunable mechanical properties by microfluidic techniques. *ACS Applied Materials and Interfaces*, 5(11):5247–5252, 2013.

[171] Alessandra Vitale, Marzia Quaglio, Matteo Cocuzza, Candido Fabrizio Pirri, and Roberta Bongiovanni. Photopolymerization of a perfluoropolyether oligomer and photolithographic processes for the fabrication of microfluidic devices. *European Polymer Journal*, 48(6):1118–1126, 2012.

[172] Andreas Fery and Richard Weinkamer. Mechanical properties of micro- and nanocapsules: Single-capsule measurements. *Polymer*, 48(25):7221–7235, 2007.

[173] Guohui Wu, Alexander Mikhailovsky, Htet a. Khant, Caroline Fu, Wah Chiu, and Joseph a. Zasadzinski. Remotely triggered liposome release by near-infrared light absorption via hollow gold nanoshells. *Journal of the American Chemical Society*, 130(26):8175–8177, 2008.

[174] Guoting Qin, Zheng Li, Rongmin Xia, Feng Li, Brian E O Neill, Jessica T Goodwin, Htet a Khant, Wah Chiu, and King C Li. Partially polymerized liposomes: stable against leakeage yet capable of instantaneous release for remote controlled drug delivery. *NIH Public Access*, 22(15), 2012.

[175] Kannan M. Krishnan. Biomedical nanomagnetics: A spin through possibilities in imaging, diagnostics, and therapy. *IEEE Transactions on Magnetics*, 46(7):2523–2558, 2010.

[176] Jean Paul Fortin, Claire Wilhelm, Jacques Servais, Christine Ménager, Jean Claude Bacri, and Florence Gazeau. Size-sorted anionic iron oxide nanomagnets as colloidal mediators for magnetic hyperthermia. *Journal of the American Chemical Society*, 129(9):2628–2635, 2007.

[177] R.E. E Rosensweig. Heating magnetic fluid with alternating magnetic field. *Journal of Magnetism and Magnetic Materials*, 252(0):370–374, 2002.

[178] Eve Loiseau, Aymar Quarré de Boiry, Fabian Niedermair, Gerhard Albrecht, Patrick A. Rühs, and André R. Studart. Explosive Raspberries: Controlled Magnetically Triggered Bursting of Microcapsules. *Advanced Functional Materials*, 26(22):4007–4015, 2016.

[179] Omar Rifaie-Graham, Nikolas F B Galensowske, Charlie Dean, Jonas Pollard, Sandor Balog, Mohamed Chami, Antoine Vian, Esther Amstad, Marco Lattuada, and Nico Bruns. Force-responsive polymersomes inspired by the marine bioluminescence of dinoflagellates. *In reviewing process*, 2018.

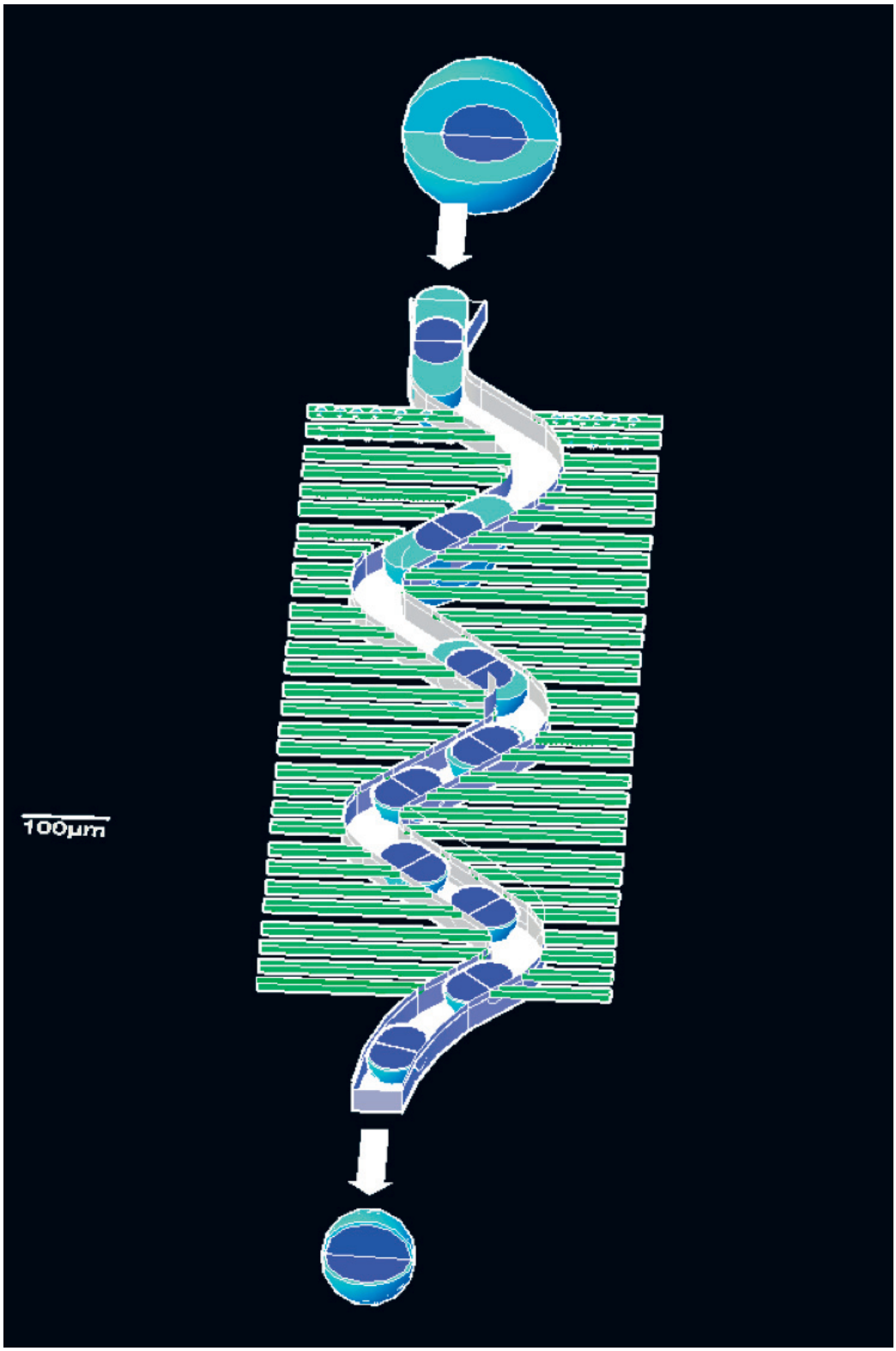
100µm